

## Roadmap

# The 2020 UV emitter roadmap

Hiroshi Amano<sup>1,2</sup>, Ramón Collazo<sup>3</sup>, Carlo De Santi<sup>4</sup>, Sven Einfeldt<sup>5</sup>, Mitsuru Funato<sup>6</sup>, Johannes Glaab<sup>5</sup>, Sylvia Hagedorn<sup>5</sup>, Akira Hirano<sup>7</sup>, Hideki Hirayama<sup>8</sup>, Ryota Ishii<sup>6</sup>, Yukio Kashima<sup>8,9</sup>, Yoichi Kawakami<sup>6</sup>, Ronny Kirste<sup>3</sup>, Michael Kneissl<sup>5,10</sup>, Robert Martin<sup>11,27</sup>, Frank Mehnke<sup>12</sup>, Matteo Meneghini<sup>4</sup>, Abdallah Ougazzaden<sup>13</sup>, Peter J Parbrook<sup>14</sup>, Siddharth Rajan<sup>15,16</sup>, Pramod Reddy<sup>17</sup>, Friedhard Römer<sup>18</sup>, Jan Ruschel<sup>5</sup>, Biplab Sarkar<sup>3,19</sup>, Ferdinand Scholz<sup>20</sup>, Leo J Schowalter<sup>21,22</sup>, Philip Shields<sup>23</sup>, Zlatko Sitar<sup>3</sup>, Luca Sulmoni<sup>10</sup>, Tao Wang<sup>24</sup>, Tim Wernicke<sup>10,27</sup>, Markus Weyers<sup>5</sup>, Bernd Witzigmann<sup>18</sup>, Yuh-Renn Wu<sup>25</sup>, Thomas Wunderer<sup>26</sup> and Yuewei Zhang<sup>15</sup>

<sup>1</sup> IMaSS, Nagoya University, Nagoya, 464-8603, Japan

<sup>2</sup> Nagoya University, Nagoya, 464-8601, Japan

<sup>3</sup> Department of Materials Science and Engineering, North Carolina State University, Raleigh, NC, 27695, United States of America

<sup>4</sup> Department of Information Engineering, University of Padova, via Gradenigo 6/b 35131, Padova, Italy

<sup>5</sup> Ferdinand-Braun-Institut, Leibniz-Institut für Höchstfrequenztechnik, Gustav-Kirchhoff-Str. 4 12489, Berlin, Germany

<sup>6</sup> Department of Electronic Science and Engineering, Kyoto University, Katsura Campus, Nishikyo-ku, Kyoto 615-8510, Japan

<sup>7</sup> UV Craftory Co., Ltd., Nagoya 464-0015, Japan

<sup>8</sup> RIKEN, 2-1 Hirosawa Wako, Saitama 351-0198, Japan

<sup>9</sup> Marubun Corporation, 8-1 Oodenma-cho, Nihonbashi, Chuo Ward, Tokyo 109-8577, Japan

<sup>10</sup> Technische Universität Berlin, Institute of Solid State Physics, Hardenbergstr. 36, 10623 Berlin, Germany

<sup>11</sup> Department of Physics, SUPA, University of Strathclyde, Glasgow G4 0NG, United Kingdom

<sup>12</sup> Georgia Institute of Technology, School of Electrical and Computer Engineering, 777 Atlantic Drive, Atlanta, GA 30332, United States of America

<sup>13</sup> Georgia Institute of Technology, School of Electrical and Computer Engineering, Georgia Tech-CNRS, UMI 2958 57070, Metz, France

<sup>14</sup> Tyndall National Institute and School of Engineering, University College Cork, Cork, Ireland

<sup>15</sup> Department of Electrical and Computer Engineering, The Ohio State University, Columbus, OH 43210, United States of America

<sup>16</sup> Department of Materials Science and Engineering, The Ohio State University, Columbus, OH 43210, United States of America

<sup>17</sup> Adroit Materials, Inc., 2054 Kildaire Farm Rd, Suite 205, Cary, NC 27518, United States of America

<sup>18</sup> Department of Electrical Engineering/Computer Science and CINSaT, University of Kassel, Wilhelmshoher Allee 71 D-34121, Kassel, Germany

<sup>19</sup> Department of Electronics and Communication Engineering, Indian Institute of Technology, Roorkee, Uttarakhand 247667 India

<sup>20</sup> Institute of Functional Nanosystems, Ulm University 89069, Ulm, Germany

<sup>21</sup> Crystal IS Inc., 70 Cohoes Ave., Green Island, NY 12183, United States of America

<sup>22</sup> Asahi Kasei Corporation, Fuji 416-8501, Japan

<sup>23</sup> Department of Electrical and Electronic Engineering, University of Bath, Bath BA2 7AY, United Kingdom



Original content from this work may be used under the terms of the [Creative Commons Attribution 4.0 licence](https://creativecommons.org/licenses/by/4.0/). Any further distribution of this work must maintain attribution to the author(s) and the title of the work, journal citation and DOI.

<sup>24</sup> Department of Electronic and Electrical Engineering, University of Sheffield, Sheffield S1 3JD, United Kingdom

<sup>25</sup> National Taiwan University, Institute of Photonics and Optoelectronics and Department of Electrical Engineering

<sup>26</sup> Electronics Materials and Devices Laboratory, PARC, a Xerox Company, 3333 Coyote Hill Road, Palo Alto, CA 94304, United States of America

<sup>27</sup> Authors to whom any correspondence should be addressed.

E-mail: [r.w.martin@strath.ac.uk](mailto:r.w.martin@strath.ac.uk) and [tim.wernicke@physik.tu-berlin.de](mailto:tim.wernicke@physik.tu-berlin.de)

Received 16 October 2019, revised 29 June 2020

Accepted for publication 15 July 2020

Published 15 September 2020



CrossMark

## Abstract

Solid state UV emitters have many advantages over conventional UV sources. The (Al,In,Ga)N material system is best suited to produce LEDs and laser diodes from 400 nm down to 210 nm—due to its large and tuneable direct band gap, n- and p-doping capability up to the largest bandgap material AlN and a growth and fabrication technology compatible with the current visible InGaN-based LED production. However AlGaIn based UV-emitters still suffer from numerous challenges compared to their visible counterparts that become most obvious by consideration of their light output power, operation voltage and long term stability. Most of these challenges are related to the large bandgap of the materials. However, the development since the first realization of UV electroluminescence in the 1970s shows that an improvement in understanding and technology allows the performance of UV emitters to be pushed far beyond the current state. One example is the very recent realization of edge emitting laser diodes emitting in the UVC at 271.8 nm and in the UVB spectral range at 298 nm. This roadmap summarizes the current state of the art for the most important aspects of UV emitters, their challenges and provides an outlook for future developments.

Keywords: ultraviolet, light emitting diodes, InGaIn, UV-LED, AlGaIn

(Some figures may appear in colour only in the online journal)

## Contents

1. UV-LEDs: state-of-the-art and applications	4
2. AlN on sapphire	7
3. The growth of bulk AlN and fabrication of AlN wafers	9
4. Radiative recombination efficiency of AlGaIn quantum wells: do we estimate it accurately in a proper way?	12
5. Point defects	14
6. Toward ohmic n-contacts on n-AlGaIn with high Al mole fraction	17
7. Doping of AlGaIn	19
8. Boron-containing (Al, Ga)N heterostructures	22
9. Development of UV-A LEDs	24
10. UVB-LEDs	26
11. UVC LEDs	28
12. UVC LEDs with emission below 250 nm	31
13. Light extraction efficiency of UVC LEDs	34
14. Nanostructuring for UV emitters	36
15. Simulation of UV-light emitting diodes and lasers	39
16. Reliability of UV LEDs	41
17. Tunnel junction-based UV LEDs	44
18. E-beam pumped emitters	47
19. UV laser diodes	50
References	52

**List of terms and acronyms**

AFM	atomic force microscopy—section 3	MOVPE	metal-organic vapour phase epitaxy, same method as MOCVD—section 2
CL	cathodoluminescence—section 4	MQW	multi-quantum well—section 12
C-DLTS and O-DLTS	capacitance-/optical-deep level transient spectroscopy—section 16	NRC	nonradiative recombination centres—section 4
DBR	distributed Bragg reflector—section 7	PL	photoluminescence—section 4
DFB	distributed feedback—section 19	pss	patterned sapphire substrate—section 2
DFT	density functional theory—section 5	PVT	physical vapour transport (growth of AlN)—section 3
DUV	deep ultra violet—section 4	PDD	point defect density—section 11
EQE	external quantum efficiency—section 1	QW	quantum well—section 4
EBL	electron blocking layer—section 10	RMS	root mean square roughness—section 3
ELO	epitaxial lateral overgrowth—section 2	roughness	
$\eta_{\text{rad}}$	radiative recombination efficiency—section 1	SIMS	secondary ion mass spectrometry—section 5
$\eta_{\text{inj}}$	current injection efficiency—section 1	SNOM	scanning near-field optical microscopy—section 4
$\eta_{\text{el}}$	electrical efficiency—section 1	TDD	threading dislocation density—section 2
FC	flip chip—section 13	TEM	transmission electron microscopy—section 7
FDTD	finite-difference time-domain—section 13	TJ	tunnel junction—section 7
LEE	$\eta_{\text{ext}}$ light extraction efficiency—section 1	TE	transverse electric—section 12
IQE	$\eta_{\text{IQE}}$ internal quantum efficiency—section 1	TM	transverse magnetic—section 12
HR-PhC	highly reflective photonic crystal—section 13	UV	ultra violet
HTA	high temperature annealing (of AlN)—section 2	UVA	315–400 nm, according to ISO 21348
HVPE	hydride vapour phase epitaxy—section 3	UVB	280–315 nm, according to ISO 21348
$I_{\text{f}}$	forward current—section 13	UVC	100–280 nm, according to ISO 21348
LED	light emitting diode—section 1	VCSEL	vertical cavity surface emitting laser—section 7
MBE	molecular beam epitaxy—section 7	$V_{\text{f}}$	forward voltage—section 13
		WPE	wall plug efficiency—section 1
		XRD	x-ray diffraction—section 7

# 1. UV-LEDs: state-of-the-art and applications

Michael Kneissl<sup>1,2</sup>

<sup>1</sup> Ferdinand-Braun-Institut, Leibniz-Institut für Höchstfrequenztechnik

<sup>2</sup> Technische Universität Berlin, Institute of Solid State Physics

## 1.1. Status

Driven by the wide range of applications the development of group III-nitride based ultraviolet emitters has gained considerable momentum since the early 2000s [1, 2]. In the UVA spectral band (400–315 nm) key applications include UV curing of polymers, inks, coatings, resins, and adhesives [3]. UVA emitters are also employed for sensing applications, e.g. the detection of blankophores and fluorescent labels as well as blood gas analysis and light therapy. Phototherapy, in particular the treatment of skin diseases like vitiligo and psoriasis, is one of the key applications for LEDs in the UVB wavelength range (315–280 nm). UVB-LEDs are also of great interest for the curing of surfaces since the penetration depth of UVB light in polymers is much smaller than that of UVA emitters. In addition, plant growth lighting constitutes a large scale application for UVB-LEDs. Here UVB-LEDs are employed to enhance the production of secondary metabolites in vegetables, which carry a number of health benefits for the consumer or to control the morphology and shapes of flowers [3]. Disinfection of drinking water and wastewater treatment are certainly the highest volume applications for LEDs emitting in the UVC spectral band (100–280 nm). In addition, sterilization of medical equipment, home appliances (e.g. refrigerators, washing machines), and various surfaces (e.g. in the food industry), would also benefit from UVC-LEDs. Sensing applications require specific emission wavelengths, depending on the absorption band of the gases or biomolecules of interest, and therefore cover the entire UV spectral range. Figure 1 presents some of the key applications for UV-LEDs. As can be seen, the wavelength and power requirements vary greatly for these applications. Whereas sensing applications entail low power but spectrally pure LEDs, for UV curing and disinfection LED modules delivering many Watts of UV light are crucial.

Since UVA-LEDs with emission wavelength above 315 nm have already reached excellent performance levels with output powers of several watts per LED chip, UV curing has evolved as the first large scale application for UV-LEDs. Compared to conventional UV sources, like low and medium pressure mercury lamps, UV-LEDs provide a number of advantages. Besides a freely selectable single wavelength emission, UV-LEDs require no warm-up time, are electronically dimmable, exhibit no forward heat radiation, are highly temperature stable, and exhibit long lifetimes. Due to their small form factors, UV-LEDs provide a much greater design flexibility for UV modules and are also environmentally friendly, since they contain no mercury or produce ozone. Even though the output

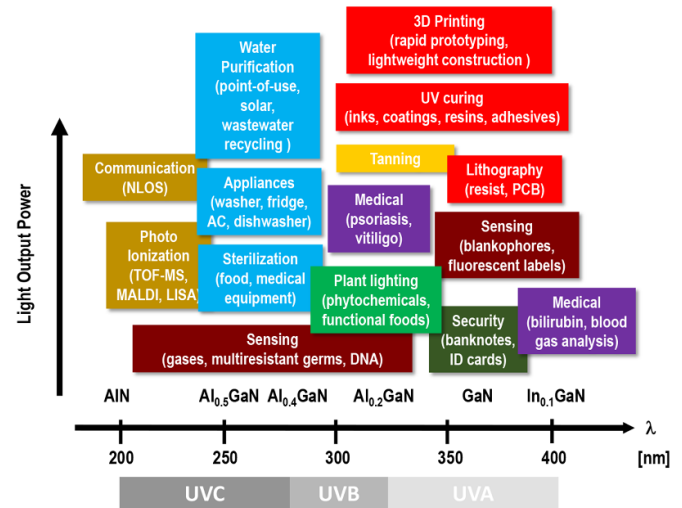


**Figure 1.** Key applications for UVA, UVB, and UVC LEDs. Reprinted by permission from Springer Nature Customer Service Centre GmbH: Springer [3] (2016).

power levels of UVB- and UVC-LEDs are currently only in the 1–100 mW range, these shorter wavelength UV-LEDs have already found entry in first applications, especially in areas where solution with conventional UV sources are impossible or significantly more complex.

## 1.2. Current and future challenges

As can be seen from figure 2 the external quantum efficiencies (EQE) of UV-LEDs vary greatly with the emission wavelength. Whereas UVA-LEDs with emission longer than 315 nm exhibit EQEs exceeding 50%, LEDs in the UVB and UVC band lag significantly behind. Although record EQEs of more than 20% for LEDs emitting near 275 nm have been reported [4], the performance levels of commercial devices in these wavelength bands are still in the single digit percentage range.

In order to analyse the shortcomings it is useful to take a look at the key parameters that describe the performance of UV-LEDs, i.e. the external quantum efficiency (EQE) and wall-plug efficiency (WPE). Both are related through the following equation

$$WPE = \frac{P_{out}}{I \cdot V} = EQE \frac{\hbar\omega}{e \cdot V} = EQE \cdot \eta_{el}$$

where  $P_{out}$ ,  $I$ , and  $V$  represent the output power, operating current, and operating voltage of the UV-LED, respectively,  $\hbar\omega$  the emitted photon energy, and  $\eta_{el}$  the electrical efficiency [3]. The EQE in turn is dependent on the radiative recombination efficiency  $\eta_{rad}$ , the carrier injection efficiency  $\eta_{inj}$ , and the light extraction efficiency  $\eta_{ext}$ . Accordingly, the EQE can be described as

$$EQE = \eta_{rad} \cdot \eta_{inj} \cdot \eta_{ext} = \eta_{IQE} \cdot \eta_{ext}$$

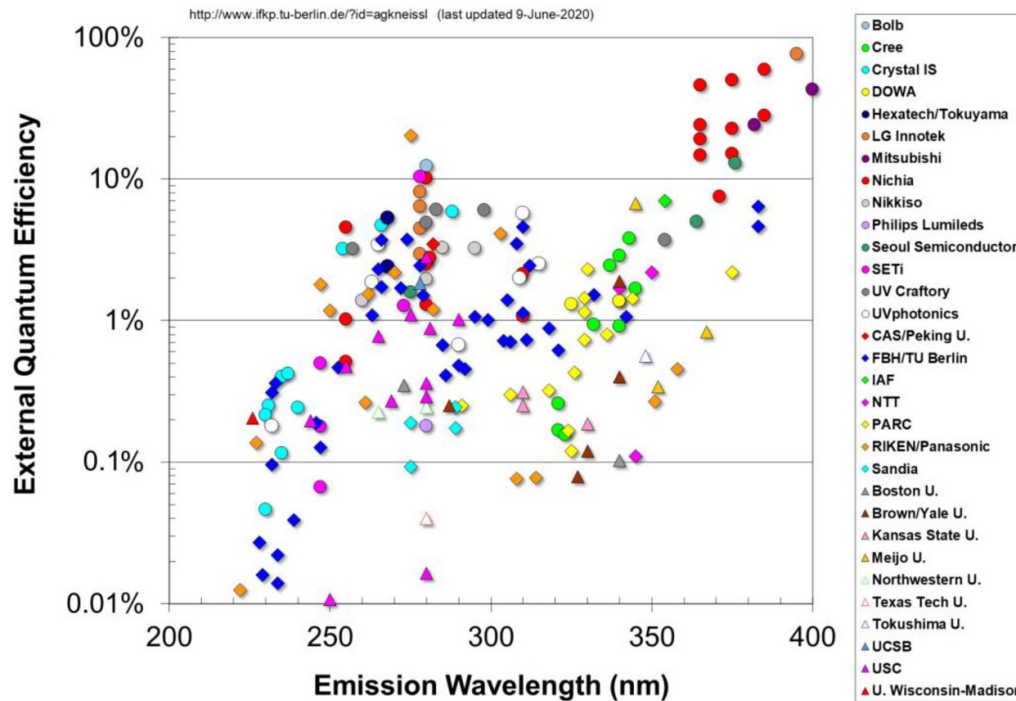


**Figure 2.** External quantum efficiencies of UV-LEDs in the spectral range between 200 and 400 nm. Reprinted by permission from Springer Nature Customer Service Centre GmbH: Springer [3] (2016).

where the product of the radiative recombination efficiency  $\eta_{rad}$  and the carrier injection efficiency  $\eta_{inj}$  is typically referred to as the internal quantum efficiency  $\eta_{IQE}$ . For example, record EQE and WPE for commercially available 280 nm LEDs are currently around 6.4% and 4.1% [5, 6]. Although it is difficult to precisely determine the different contributions to the overall efficiencies, from the description of the material properties and device structure one would estimate the radiative efficiency to be around 40%, an extraction efficiency around 20%, and an electrical efficiency of 64%. Consequently, progress in all of the contributing factors will be required in order to improve the EQE, wallplug efficiency, and output power of UV-LEDs.

### 1.3. Advances in science and technology to meet challenges

There are a number of different possible solutions in order to improve each of the parameters that govern the overall UV-LED performance, i.e.  $\eta_{rad}$ ,  $\eta_{inj}$ , and  $\eta_{ext}$ . For example, the extraction efficiency  $\eta_{ext}$  can be greatly enhanced by encapsulating the LED chips with a UV-transparent high refractive index material. A key challenge here is to find suitable materials, that are UV-transparent and also do not degrade under UV exposure. This is not a trivial task, but first candidates have emerged, e.g. fluoropolymers like CYTOP® [7]. Other approaches to enhance light extraction include the utilization of UV-reflective metal contacts together with a UV-transparent p-AlGaIn heterostructure. However, finding suitable metal layers that are highly reflective in the UVB and UVC spectral range and at the same time enable low resistance ohmic

contacts is not straightforward. Therefore, in many cases a trade-off between enhancing light extraction and degrading other parameters like operating voltages and electrical efficiency has to be made. Another key parameter is the radiative recombination efficiency  $\eta_{rad}$  which is strongly affected by the defect density in the semiconductor materials [8]. As most UV-LEDs are grown on sapphire substrates a large number of threading dislocations are generated at the AlN/sapphire interface. Even with advanced growth technologies in order to reduce the defect density, the threading dislocation density (TDD) in AlGaIn heterostructures is typically between  $10^{10} \text{ cm}^{-2}$  and  $10^8 \text{ cm}^{-2}$  [9, 10], which corresponds to IQEs ranging from a few percent to over 60% [8]. Therefore, reducing the TDD is paramount to improving the radiative recombination efficiency and IQE of UV-LEDs. We have just provided these examples to illustrate the issues and refer to the discussion in the following articles describing in more detail the recent developments in materials and device technologies.

### 1.4. Concluding remarks

Even though the large scale application of UV-LEDs will require substantial advances in the performance levels of UVB- and UVC-LEDs, it is clear that in the not too distant future group III-nitride based UV emitters will replace most conventional UV sources like mercury lamps. UV-LED and blue LED technologies share the basis of III-nitride material and device technologies. Although the technological solutions

are very different there seem to be no fundamental roadblocks that would inhibit a steady improvement in UV-LED performance. How quickly these advances will be realized, will also depend on the magnitude of the research efforts in the field, but based on the trajectory of the performance improvements of the past decade one can anticipate that UVB and UVC LEDs with WPE of more than 10% should become commercially available by 2022 [2].

#### *Acknowledgements*

M K gratefully acknowledges support by the German Research Foundation (DFG) within the Collaborative Research Center ‘Semiconductor Nanophotonics’ (CRC 787) as well as funding by the Federal Ministry of Education and Research (BMBF) of Germany within the ‘Zwanzig20’ consortium ‘Advanced UV for Life’.



## 2. AlN on sapphire

Sylvia Hagedorn and Markus Weyers

Ferdinand-Braun-Institut, Leibniz-Institut für Höchstfrequenztechnik

### 2.1. Status

UV LEDs are nearly exclusively bottom emitters, since p-GaN and contact materials are not transparent in the UV. Sapphire (or rather the pure corundum) is transparent and mass-produced for GaN LEDs. For UV transparency the semiconductor layer stacks have to start with AlN, which creates much bigger challenges in MOVPE (metalorganic vapour phase epitaxy) growth than GaN. The target is to obtain a low density of threading dislocations (TDD). Such dislocations form at the sapphire—AlN hetero-interface by coalescence of small nuclei and are non-radiative recombination pathways. A low TDD thus is prerequisite for high internal quantum efficiency [11]. While growth of thick layers is effective in reducing the TDD by mutual annihilation of dislocations, the high strain resulting from lattice mismatch and mismatch in the thermal expansion coefficients leads to strong wafer bow or even cracking of thicker layers. Strong bow makes processing of the wafers difficult, crack formation renders them useless for devices. Total internal reflection at the AlN-sapphire interface limits light extraction, which is especially low at short wavelengths. Patterned sapphire substrates (pss) are used for blue LEDs to enhance light extraction and to reduce TDD (or the layer thickness at which a low TDD is obtained). For UV LEDs this is still being developed. While UV LEDs have made tremendous progress in recent years, there is still plenty of room to improve their performance towards that achieved by blue LEDs which already approach the theoretical limits. The AlN-sapphire buffer layers are the basis for this further development. As yet, there is no completely satisfying solution that is proven by device performance and widely adopted.

### 2.2. Current and future challenges

Due to the high bond strength of AlN, high growth temperatures are preferred. On the other hand, high temperatures in an MOVPE reactor may result in surface reactions between the sapphire substrate and the gas phase. This does not only contain the injected process gases but also species stemming from parasitic deposits within the reactor. As one result of such pre-reactions, islands with N-polarity may form, which later are buried by the matrix with Al-polarity aided by the formation of AlON [12]. So mastering the growth start is a challenge with strong impact on TDD. After coalescence of the initial nuclei, the TDD needs to be further reduced. A rough growth front with a high density of steps can help in this (by bending dislocations away from the +c surface normal). However, for the growth of the AlGaIn device layers, high steps are detrimental since they can result in compositional modulation by a higher Ga incorporation rate at such steps [13]. To reproducibly manage the transition to a rough growth front and back

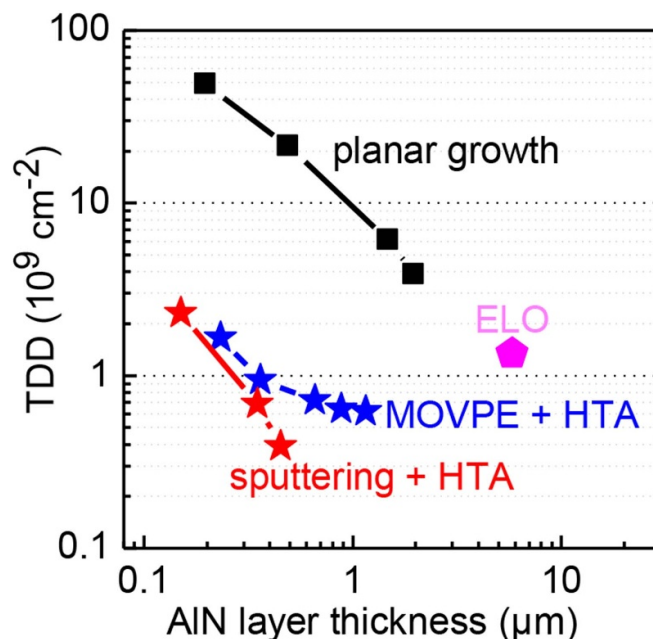


**Figure 3.** Reduction of threading dislocation density with grown AlN layer thickness. For planar growth, cracking limits the thickness that can be achieved. Epitaxial lateral overgrowth (ELO) patterning allows thicker layers and thus lower TDD but is not very economic [10]. High temperature annealing (HTA) achieves low TDD already for much thinner layers. (S Hagedorn *et al*, Ferdinand-Braun-Institut, unpublished results.)

to a smooth final AlN surface is a challenge. The pss approach for enhanced light extraction is hampered by the low surface mobility of Al. Thus the patterns (holes in the c-plane surface or pillars with c-plane top facet) need to be on the sub-micron scale (nano-pss). Also, AlN tends to nucleate in misoriented crystallites on non-c-plane sidewalls of such patterns. The c-oriented grains are difficult to coalesce if they are bounded by m-plane facets. So it remains a challenge to obtain smooth, fully coalesced AlN buffers on such nano-pss. Wafer bow results in an inhomogeneous temperature over the wafer making it a challenge to obtain homogeneous layer properties, especially when wafer size is being scaled up.

### 2.3. Advances in science and technology to meet challenges

There are a number of approaches towards reducing TDD. These include specific growth schemes for example by multistep growth with variation of the growth temperature, the ratio of TMAI and NH<sub>3</sub> flow, the total pressure or by pulsed supply of the precursors. Although different growth recipes have been published as being successful, discussion with many groups active in the field indicates that reproducibility and homogeneity are issues that are being faced (but usually not discussed in scientific papers). A better understanding of the reasons for these limitations is required to optimize the production of AlN-sapphire templates.

A relatively new approach is the reduction of the TDD by annealing of thin AlN layers at high temperature (HTA) [14]. This approach allows TDD in the range of  $5 \times 10^8 \text{ cm}^{-2}$

already for layer thicknesses of less than 1  $\mu\text{m}$  reducing problems with wafer bow and cracks. It also works if sputtered layers of initially low quality (high TDD) are subjected to HTA (figure 3). In addition to being a relatively cheap process, sputtering also removes the issue of chemical attack on sapphire during heating up in an MOVPE environment. While a proof of principle has been given [15], further studies of process reproducibility and resulting device lifetime are necessary before this approach can be considered as validated.

To address the issue of light extraction, growth on nano-pss needs to be developed further [16]. This includes finding the right patterns (which are different from those used for GaN not only in pitch but also in shape). Also the patterning of sapphire on this nanoscale needs to be optimized towards homogeneous and reproducible shape. The right growth parameters to obtain smooth and fully coalesced layers without misoriented crystallites need to be found. While the better understanding being developed in studies of planar growth provides guidelines, the presence of different orientations of sapphire and AlN will require modifications to the growth processes on nano-pss.

While work currently is mainly on 2 inch sapphire substrates, higher volumes will require the transition to larger diameters. To cope with wafer bow this will probably require

thicker substrates which as a consequence may require another round of growth process optimization.

#### 2.4. Concluding remarks

While a low TDD and a smooth surface and not too big wafer bow are necessary requirements for AlN templates for UV LEDs, their suitability needs to be verified by growing device layer sequences, processing devices and studying their performance including reliability. Thus this topic will remain on the agenda for the foreseeable future. A combination of nano-patterning with defect reduction by HTA promises high crystalline perfection, acceptable wafer bow and improved light extraction and is worthwhile being studied more in detail [17, 18].

#### Acknowledgements

Work at Ferdinand-Braun-Institut on AlN templates for UV emitters is funded by the German Ministry of Research and Education (BMBF) within the ‘Advanced UV for life’ consortium and the German Research Foundation (DFG) within the Collaborative Research Center 787 ‘Nanophotonics’. The authors thank all coworkers at FBH and TU Berlin for their input and the jointly obtained results.



### 3. The growth of bulk AlN and fabrication of AlN wafers

Ronny Kirste and Zlatko Sitar

North Carolina State University

#### 3.1. Status

For most semiconductor technologies, like Si, Ge, III-arsenides, single crystalline substrates obtained from bulk growth provide for highest epitaxial layer quality and devices with optimum efficiency and lifetime. With the progress in hydride vapour phase epitaxy (HVPE) and ammonothermal growth of GaN crystals, these substrates are also entering InGaN and GaN device development. For Al-rich AlGaIn epitaxial layers desired for UV laser diodes, LEDs, next generation power diodes, and sensors, single crystal AlN substrates are fabricated either via HVPE or sublimation growth/physical vapour transport (PVT) [11, 19–21]. In PVT growth, an AlN-powder source is sublimed at temperatures exceeding 2200 °C in a nitrogen atmosphere. On the opposite side of the crucible, a seed is positioned and heated to temperatures slightly lower than the source. Due to the thermal gradient, the sublimed source molecules diffuse to the seed where they form AlN via a reverse reaction. The structural quality of the grown AlN crystals depends strongly on the type and quality of seed crystals, which are needed to provide structural information for the condensing Al and N atoms. Next to the control of thermal fields in PVT growth the use of native AlN seeds is essential to achieve high-quality crystalline boules and wafers. These seeds are typically obtained by spontaneous nucleation and growth of Lely-like, c-oriented platelets close to the equilibrium conditions. The first results of bulk growth of AlN on native seeds were presented in 2002; this process later became a basis for the development of an iterative boule expansion process and increase of the diameter of the native seeds over time.

Over the past two decades, PVT growth of AlN has been pursued by various laboratories around the world [19, 20, 22, 23]. Despite all these efforts, commercial availability of these substrates is still limited. Available PVT grown substrates typically have a dislocation density  $<10^3 \text{ cm}^{-2}$  and are available in diameters up to 2". Figure 4 shows a typical AlN boule (a) and a wafer cut from such a boule (b); an x-ray topograph (c) from a high quality AlN wafer confirms the low dislocation density that can be achieved.

AFM imaging of polished AlN wafers reveals  $c/2$  steps and an RMS roughness  $<0.1 \text{ nm}$ . Using these AlN wafers, epitaxial growth via metalorganic vapour phase epitaxy (MOVPE) has been developed and doped and undoped AlGaIn layers with up to 40% Ga-content can be grown pseudomorphically [24, 25]. Optically pumped UV lasers on AlN substrates have been demonstrated by various groups and the lowest threshold of  $6 \text{ kW cm}^{-2}$  was achieved [21, 26, 27].

#### 3.2. Challenges and future development

While the crystal quality of PVT grown AlN substrates and epitaxial films grown on them is excellent, a few challenges need to be addressed in the near future before a widespread commercial adoption can be anticipated.

First, availability of 2" AlN wafers was limited up until recently. This hindered a possible entry even for fundamental epitaxy and device growth for many research facilities since many fabrication lines are designed for at least 2" wafers, with many foundries even moving further to 4". Although there is no fundamental limit for large-size AlN boules, the expansion process is relatively slow and will require significant long-term investment to achieve production of 4" or even larger boules.

Second, for UV light emitting diode (LED) applications, AlN substrates need to be transparent in the targeted emission window. PVT-grown AlN contains relatively high concentrations of C, Si, and O, which results in reduced thermal conductivity and various absorption centres that negatively impact the performance of any LEDs grown on them by absorbing the emitted UV light [28]. While the impact on UV laser diodes is not as significant, any leakage of the optical mode into the substrate will negatively impact the laser diode threshold. The most impactful absorption centre for AlN is located at 4.7 eV or 265 nm, which is at the desired UVC LED emission wavelength for disinfection applications. Absorption coefficients exceeding  $1000 \text{ cm}^{-1}$  are commonly observed at this wavelength. This absorption band has been associated with the luminescence emissions around 2.7 eV and 3.9 eV. It has recently been discussed that the absorption is related to the  $C_N^-$  point defect and the emission is related to the transition between the  $V_N$  and  $C_N$  point defects [29]. Thus, controlling these two point defects is key to reducing the absorption coefficient. Indeed, AlN epi-ready wafers have been deployed that have reasonable absorption coefficients  $<100 \text{ cm}^{-1}$ , which was achieved by compensation with Si (figure 5(a)) [28]. While this approach significantly reduces the 265 nm absorption, the growth conditions to achieve the desired transparency may result in the formation of low angle grain boundaries in the PVT AlN crystals, which reduces the quality of the substrates up to the point that epitaxial layers show signs of relaxation and surface deterioration. Therefore, more efforts need to be made to reduce carbon and other point defects in PVT-grown AlN [30]. Alternatively, either the substrate could be removed during the LED fabrication or HVPE could be used to grow transparent AlN on PVT crystals to retain crystalline quality and obtain low point defect concentrations. Since the incorporation of C in HVPE and MOVPE can be controlled more efficiently, such substrates are excellent for UV LED and laser applications when the PVT seed is removed (figure 5(b)).

Third, conductive AlN substrates would be beneficial for UV laser diodes as they would allow for vertical devices with more homogenous carrier injection, simplified laser design, and simpler fabrication. In addition, AlN and Al-rich AlGaIn could potentially be used for high power Schottky diodes due to their high breakdown fields. AlN has a figure of merit that

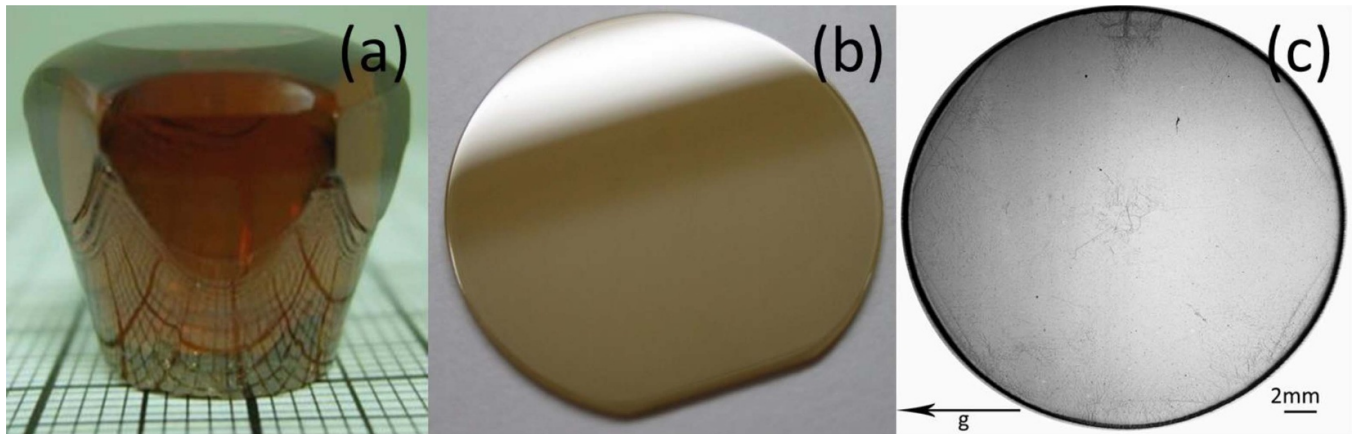


**Figure 4.** (a) Photograph of an AlN boule grown via the PVT method (mm-grid); (b) image of a 1'' AlN wafer after mechanical and chemo-mechanical polishing; (c) x-ray topograph confirming that most of the wafer area is dislocation free.

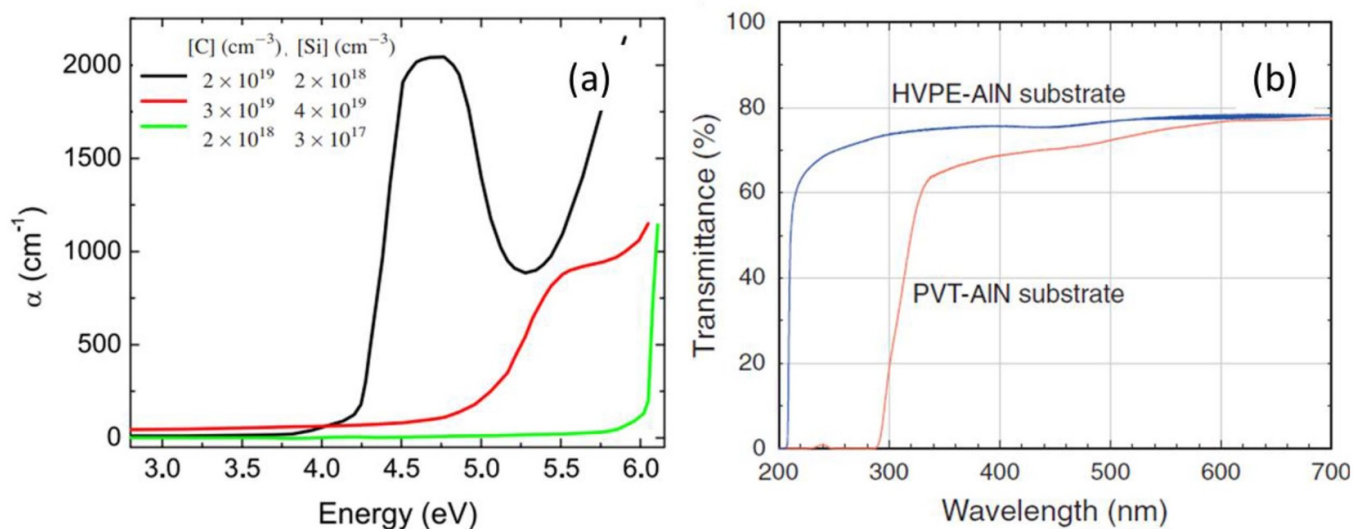


**Figure 5.** (a) 265 nm absorption can be reduced by orders of magnitude by controlling the carbon concentration in AlN; (b) using PVT substrates as seeds for HVPE and subsequent PVT seed removal results in transparency down to the fundamental bandedge.

is nearly 200 times higher than that of SiC and 35 times higher than that of GaN. The main obstacle in using AlN substrates for power devices is their lack of conductivity—all AlN substrates are highly insulating. While the most promising n-dopant in AlGa<sub>0.5</sub>N is Si, it forms DX-centre and suffers from high activation energy and compensation for Al-content >85% [31]. Therefore, significant efforts are needed to better understand the effect of compensation and DX-centre formation and increase doping efficiency [24, 32, 33].

Fourth, the AlN surface and epitaxy of AlGa<sub>0.5</sub>N films on AlN substrates needs to be addressed beyond simple trial-and-error approaches. This includes surface preparation, growth initiation, control of the surface morphology during growth, as well as engineering of possible relaxation schemes for thick AlGa<sub>0.5</sub>N films. So far, optically pumped laser structures and fully fabricated laser diodes for electrical injection have been successfully grown on AlN substrates by a few groups

[21, 26]. While significant efforts have been made to explain the epitaxial growth of AlGa<sub>0.5</sub>N and the impact of various process parameters on the growth in general terms to allow for process transfer between different reactors, the reported results are not always optimal; in the worst case, epitaxy of AlGa<sub>0.5</sub>N on AlN may lead to re-nucleation and the associated high dislocation density, thus nullifying the use of AlN substrates.

Lastly, it should be mentioned that, despite high current prices, substrate cost is not a major challenge for future application of AlN substrates. The price per device will significantly drop for larger substrate areas (2'', 4'', ...) and, even at the current price levels, the substrate contributes only 10–20% of the overall cost of a UV laser diode or LED. In addition, since the input cost of AlN crystal growth is not significantly different to that of SiC, the AlN substrate prices are expected to follow those of SiC in high volume production.

### 3.3. Concluding remarks

Device growth on native substrates is always more desirable than the growth on non-native substrates, since it allows for better crystal quality, resulting in more efficient and more robust devices. Although commercially available AlN substrates have improved greatly in quality and size over the years, a widespread penetration has not been achieved. This is mostly due to the challenges discussed above and lack of

a demonstration of a vastly superior device grown on AlN. However, in order to advance AlN PVT and HVPE crystal growth, and consequently also AlN-based device technology, significant investments need to be made not only in further research and development of the AlN crystal growth, but also in AlGaN epitaxy, property control, and development of associated devices. Only the development of all these components in unison will ultimately justify the AlN-based technology.

#### 4. Radiative recombination efficiency of AlGaIn quantum wells: do we estimate it accurately in a proper way?

Yoichi Kawakami, Mitsuru Funato and Ryota Ishii

Kyoto University

##### 4.1. Status

Recent progress on the research of nitride semiconductors has led to the realization of highly efficient blue LEDs, active layers of which are composed of InGaIn-based quantum wells (QWs). Currently, the improvement of efficiencies in Al-rich AlGaIn-QWs based LEDs is a challenging subject for the development of deep ultraviolet (DUV) emitters. The external quantum efficiency (EQE) is expressed by the product of three terms, carrier injection efficiency, radiative recombination efficiency ( $\eta_{rad}$ ) and light extraction efficiency. Although EQEs are directly measurable values, it is difficult to resolve them accurately into the three terms.

The  $\eta_{rad}$  has generally been estimated by the temperature dependence of photoluminescence (PL) intensities. However, it should be noted that these values are overestimated in many cases if they were based on the assumption that the  $\eta_{rad}$  is 100% at cryogenic temperatures. Precise PL measurements dependent on photo-excitation intensity [34], and rate equation analysis on time-resolved PL data [35], have revealed the failure of such an assumption. Moreover, one should be aware that  $\eta_{rad}$  is dependent on carrier density in the active layers. Carrier densities can be estimated precisely if the selective photo-excitation is made in the PL measurement, but it is not the case for the non-selective excitation.

In recent years, various experimental techniques have been reported for the estimation of  $\eta_{rad}$ . One approach is to detect the absolute emission intensities by means of the omnidirectional PL measurements using an integration sphere [36]. The second approach is to detect the heat generation induced by the non-radiative recombination processes, by employing techniques such as transient lens spectroscopy [37] or photo-acoustic spectroscopy [38]. In the former approach, estimation not only of light extraction efficiency but also of photon-recycling-effect is the key for the exact estimation of  $\eta_{rad}$ . In the latter approach, the quantification of the heat signal is the subject for the accuracy in determining  $\eta_{rad}$ .

##### 4.2. Current and future challenges

If we aim at the improvement of  $\eta_{rad}$ , it is very important to understand the carrier recombination processes as initially discussed in the Shockley–Read–Hall model. The carrier recombination rate ( $R$ ) can be divided into (1) nonradiative recombination rates due to defects and/or dislocations ( $R_{nr}$ ), (2) radiative recombination rate ( $R_r$ ) and (3) nonradiative recombination rate due to Auger process ( $R_{au}$ ), so that  $R = R_{nr} + R_r + R_{au}$ . In the so-called ABC model, the term of  $R_{nr}$ ,  $R_r$  and  $R_{au}$  is assumed to be proportional to injected carrier density ( $n$ ), to

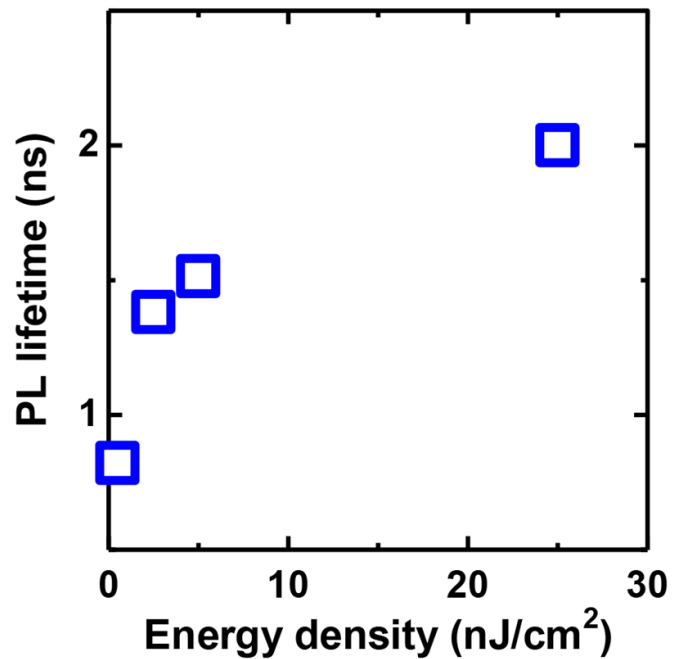


**Figure 6.** PL lifetimes of an AlGaIn/AlN QW emitting at 245 nm under various photo-excitation energy densities which are taken at room temperature.

the square of  $n$ , and to the cube of  $n$ , respectively if the background carrier density in the active layers is negligibly small. Consequently,  $R$  can be expressed as  $R = An + Bn^2 + Cn^3$ , and we can derive  $\eta_{rad} = R_r/R = Bn^2/(An + Bn^2 + Cn^3)$ . This model gives us apparently good results on the fitting of optical powers as a function of injected currents, by choosing proper parameters of  $A$ ,  $B$  and  $C$ . Therefore, a lot of research groups have reported their fitting results based on this model. However, there has been no direct verification of such power laws in the ABC model, and there exists the risk not only for misunderstanding the physics of recombination processes but also for misinterpreting the  $\eta_{rad}$  estimation.

We have performed photoluminescence (PL) measurements on Al-rich AlGaIn QWs in a wide range of photo-excited carrier densities, and carrier recombination processes have been analysed with a model based on rate equations. This has led to the quantitative estimation of  $\eta_{rad}$  values. Our finding was that radiative recombination processes are exciton recombination under relatively small carrier densities which correspond to the operating conditions of LEDs [35]. Since exciton recombination has to be treated as monomolecular process, its radiative recombination should show single exponential decay which is independent on exciton density. Moreover, the probability of carriers/excitons to be captured by nonradiative recombination centres (NRCs) is not constant but decreases with increasing carrier/exciton densities because of the effect of saturation induced by the filling of NRCs. Figure 6 shows the PL lifetimes of an AlGaIn/AlN QW emitting at 245 nm at room temperature which are increased with increasing photo-excited carrier densities due probably

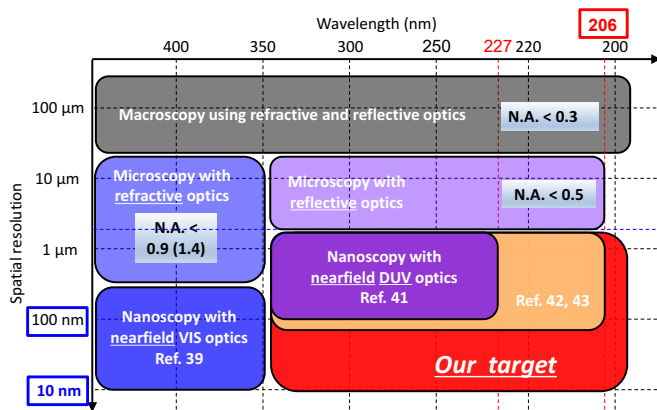


**Figure 7.** Current status and future prospect of PL-mapping technology.

to the saturation of NRCs. These results indicate the failure of the conventional ABC model.

#### 4.3. Advances in science and technology to meet challenges

The visualization of radiative and nonradiative recombination centres is the key to reveal the recombination mechanisms in semiconductors. Cathodoluminescence (CL) is a useful technique to map CL intensities in AlGaIn-based DUV emission. However, the spatial resolution is affected not only by the spread of the incident electron beam in the sample but also by the diffusion length of the excitons/carriers. Scanning near-field optical microscopy (SNOM) has various merits for assessing the detailed recombination dynamics. We can choose the optical mode in the PL mapping with SNOM. In the illumination collection mode (IC-mode), both photo-excitation and the PL detection are performed through an optical fibre probe with small aperture. In the IC-mode, the spatial resolution is only limited by the diameter of aperture. The best spatial resolution achieved is down to about 10 nm in the visible spectral detection [39]. In the illumination mode (I-mode), the optical excitation is made through an optical fibre probe while the PL detection is made with a lens in the

far-field configuration. In this mode the spatial resolution may be limited by the diffusion length like in the case of CL mapping. In the collection mode (C-mode), photo-excitation or electrical injection is done on large areas while the detection is through an optical fibre probe. Careful comparison of PL mapping images taken at the same area in between IC-mode, I mode and C-mode (we named it as multi-mode SNOM) gives us useful information on the carrier/exciton diffusion processes [40].

However, there have been existing technological difficulties in developing the SNOM in the DUV region. The shortest wavelength reported was 227 nm in the excitation, and longer than 240 nm in the detection with a spatial resolution of about 100 nm [41]. We have recently achieved an excitation with 206 nm, and the detection down to 220 nm with a spatial resolution better than 100 nm [42, 43]. As illustrated in figure 7, one target is to reach the detection wavelength down to 200 nm with an improved spatial resolution.

#### 4.4. Concluding remarks

In this contribution, we have reviewed the issue in estimating  $\eta_{rad}$  of UV-emitting AlGaIn QWs. The role of excitons in the emission mechanism has already been reported for InGaIn QWs [44]. Since the exciton binding energies of AlGaIn QWs are much larger than those of InGaIn QWs, one should bear in mind the importance of excitons in discussing the recombination model. As for the origins of NRCs in Al-rich AlGaIn QWs, point defects play more important role than in InGaIn based QWs [45]. Development of characterization techniques such as DUV SNOM that visualizes the capture process of excitons or carriers to such NRCs and establishment of estimation scheme of  $\eta_{rad}$  may contribute to drastic improvement of EQE of UV LEDs.

#### Acknowledgements

This work is partially supported by JSPS KAKENHI (Grant Nos. JP15H05732, JP16H02332, and JP16H06426).



## 5. Point defects

Pramod Reddy<sup>1</sup> and Ramón Collazo<sup>2</sup>

<sup>1</sup> Adroit Materials Inc.

<sup>2</sup> North Carolina State University

### 5.1. Status

There exists a ‘point defect problem’ in Al rich  $\text{Al}_x\text{Ga}_{1-x}\text{N}$  ( $x > 0.5$ ) that has presented a major challenge to implementing AlGaIn-based deep-UV optoelectronics. An increased incorporation of impurities and generation of native defects such as vacancies has been observed with increase in Al content (necessary for a technological push into deep-UV regimes) and is likely a consequence of the dependence of the defect formation energy on the Fermi energy whose range increases from GaN (3.4 eV) to AlN (6.1 eV). The incorporated point defects vary with the growth method, growth facet, doping type and concentration, and the growth environment, i.e. temperature, metal/N chemical potentials, pressure, etc, and accordingly impact various optical and electronic properties of different regions in the optoelectronic device and hence the technological feasibility of ultra-wide bandgap-based deep UV emitters. Consequently, there are many point defect phenomena that are of high technological interest and we mention a few in the following: in metalorganic vapour phase epitaxy (MOVPE) grown AlGaIn, when doped with Si (n-type) at low to moderate levels ( $< 1 \times 10^{19} \text{ cm}^{-3}$ ), and in unintentionally doped regions, carbon and vacancy-oxygen complexes are reported to be the major compensating impurities and are a major constraint in designing active regions in optoelectronics including quantum wells [46, 47]. At higher concentrations, Si itself forms an acceptor complex with an Al/Ga-vacancy resulting in a self-compensation mechanism [48]. Further, at Al content  $> 80\%$ , Si relaxes from a donor type III-substitutional site to an acceptor type DX configuration and results in a monotonically increasing activation energy from 20 to 50 meV for  $x < 0.8$  to around 300 meV for  $x = 1$  [31]. In p-type AlGaIn, doping itself is less understood with reports of both very low and very high dopant (Mg) activation energies [49, 50]. Nevertheless, the hydrogen passivation and self-compensation by nitrogen vacancies have also been reported in Al-rich AlGaIn similar to GaN. With recent availability of single crystal AlN substrates and very low dislocation density ( $< 10^3 \text{ cm}^{-2}$ ) AlGaIn epitaxy on them [24], interesting phenomena have been observed. They include: the crucial balance between carbon, silicon and oxygen impurities in PVT-grown AlN single crystals whose ratios control the optical properties of the substrate [51], and the observed dependence of the compensating point defect (vacancy-silicon complex) formation and hence electronic performance on the extended defect (threading dislocation) density [24].

### 5.2. Current and future challenges

The various point defect phenomena mentioned in the previous section manifest very important technological challenges

to the implementation of Al-rich AlGaIn-based optoelectronics: The strong dependence of internal quantum efficiency (IQE) and associated non-radiative recombination coefficient in the quantum wells and active regions of UV emitters on the impurity concentrations demonstrates that point defects act as recombination centres thereby greatly reducing device performance [52, 53]. Hence, low doped or ‘intrinsic’ regions such as quantum wells require low point defect density for high IQEs. This is evidenced by the low IQE shown in figure 8(a) for AlGaIn/AlN multi-quantum well structures at low ammonia flows where incorporation of impurities such as carbon and oxygen is energetically favourable. Further, generation of native defects ( $V_{\text{III}}$  and  $V_{\text{N}}$ ) and formation of defect complexes have also been demonstrated to be energetically favourable under various growth conditions. The point defects have been identified by density functional theory (DFT) analysis in corroboration with thermodynamic analysis and electrical characterization, secondary ion mass spectrometry and photoluminescence characterizations in III-nitrides especially at high Al content [46, 47, 54]. At higher doping concentrations (n- or p-type) required in charge injection layers, conductivity exhibits a ‘knee behaviour’ due to self-compensation (vacancy-silicon complexes in n-type and nitrogen vacancies in p-type) [24]. Hence, an upper doping limit exists that lowers the maximum conductivity resulting in increased ohmic losses and large contact resistances. Finally, the relaxation of Si from donor configuration to a DX centre configuration has precluded AlN and  $\text{Al}_x\text{Ga}_{1-x}\text{N}$  ( $x > 0.8$ ) from being employed in deep-UV optoelectronics [31]. Consequently, DX control is one of the most important technological challenges for implementing LEDs and lasers operating at wavelengths  $< 240 \text{ nm}$ . A summary of the Si behaviour in AlGaIn is shown in figure 8(b) showing the ‘knee behaviour’ due to self-compensation and the abrupt decrease in carrier concentrations for Al content  $> 80\%$ . So far, we have mentioned the point defect issues within the active regions of the device structure. However, point defects have also played a major role in substrate suitability. Specifically, in the development of physical vapour transport (PVT) AlN single crystals with dislocation densities  $< 10^3 \text{ cm}^{-2}$  which promised highly efficient AlGaIn-based optoelectronics, excessive carbon has led to absorption in the deep-UV region and has posed the most significant challenge to implementing UV emitters directly on PVT AlN substrates [29].

### 5.3. Advances in science and technology to meet challenges

The difficulty in overcoming the point defect challenge arises from the dependence of the type and concentration of these defects on a large number of factors including growth technique, the precursors, growth mode, temperature, doping, etc. Developing specific experimental optimizations for each point defect may not be feasible due to the high iterative costs and the likely conflicting requirements of different point defects and other aspects of crystal quality that affect device performance. A general solution would be a predictive point defect control scheme that may be employed to determine the optimal growth conditions within predefined constraints determined



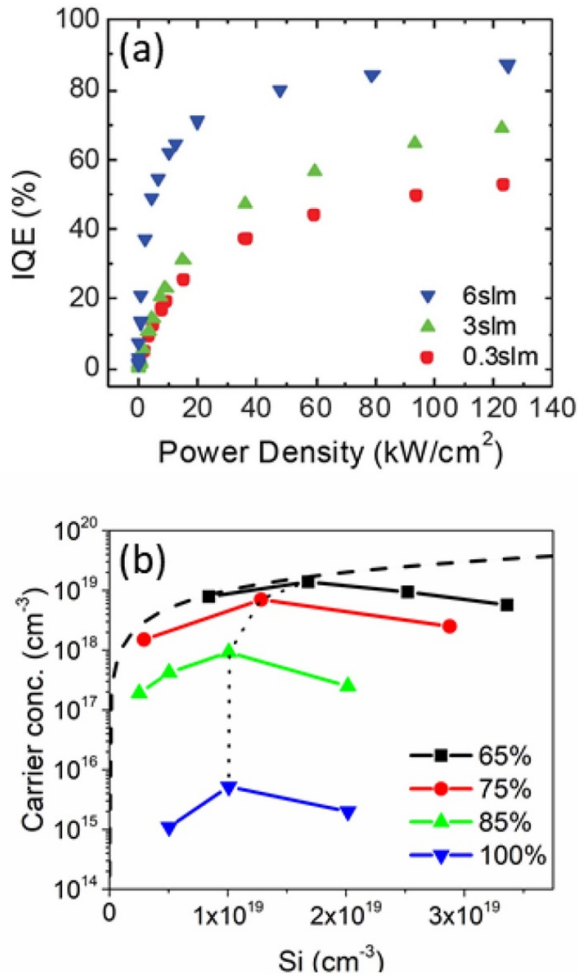


**Figure 8.** (a) The IQE for AlGaIn MQW structures on single crystal AlN substrates as a function of excitation power density shown for different point defect concentrations (here, higher ammonia flow corresponds to lower non-radiative recombination defect centre concentrations). (b) The dependence of carrier concentration as a function of doping concentration for different Al compositions in the alloy AlGaIn. The black dashed line assumes the carrier concentration to be same as silicon concentration.

by other factors including growth rates, crystal quality and system limitations. Such a point defect scheme would employ (a) DFT analysis in corroboration with characterization techniques such as secondary ion mass spectroscopy (SIMS) and photoluminescence (PL) to identify the point defect responsible for a particular challenge and (b) dependence of thermodynamic and reaction kinetics describing the growth process on practical growth knobs and (c) finally understanding the relationship between the point defects and the thermodynamics and reaction kinetics describing the growth process. This would require a highly synergistic collaboration requiring the development and extension of DFT from typical zero kelvin and standard states to experimentally employed growth temperatures and supersaturated states determined from the developed thermodynamic and reaction models. In this direction, recent developments of a point defect control model directly providing a quantitative relationship between point defect formation energies and growth knobs has allowed for

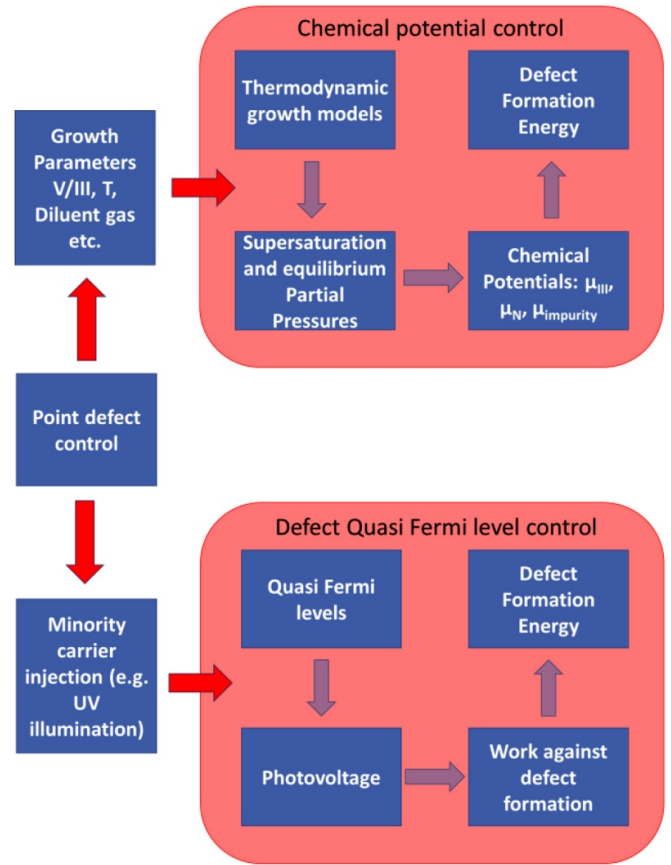


**Figure 9.** A schematic of targeted and predictable point defect control via chemical potential control and defect quasi Fermi level control.

quantitative predictions of carbon as a function of growth conditions [33]. Finally, using the dependence of point defects on the chemical potentials (metal rich versus N rich), and employing single crystal AlN substrates, record high IQEs ( $>80\%$ ) and low lasing thresholds ( $<10 \text{ kW cm}^{-2}$ ) have been achieved [21, 52]. An illustration is seen in figure 8(a) where a shift towards N rich chemical potential via increased ammonia flow results in lower non-radiative recombination centre concentrations and a significant improvement in IQE. However, significant research efforts are necessary to generalize the scheme to different materials and growth techniques by including reaction kinetics and transients into the theoretical models so that for a given growth technique and practical constraints, the optimal growth conditions for a given application can be determined theoretically without the requirements for expensive experimental iterations. Further, point defects form when they are energetically favourable at equilibrium. Hence non-equilibrium doping techniques such as implantation need to be investigated in Al-rich AlGaIn and AlN. Another solution would be to develop a point defect control scheme that targets a class of point defects having a common character where the exact identification is unnecessary. In this direction, manipulation of the Fermi level or electron chemical potential is another useful tool to control the defect formation energy of a particular class of defects, i.e. charged compensating defects. Hence,

defect quasi Fermi level (dQFL) control-based point defect reduction has been employed to improve the performance in different material systems such as nitrides and arsenides, with both n-type and p-type doping, with very different defect configurations, but with one common characteristic, i.e. all the defects were of compensating type and charged [55, 56]. Here, a significant advantage would be applying the point defect control scheme by external mechanism (in this case, an above bandgap light source) without altering the growth conditions. A summary of the developed point defect control frameworks is shown in figure 9.

#### 5.4. Concluding remarks

In conclusion, the ‘point defect problem’ in Al-rich  $\text{Al}_x\text{Ga}_{1-x}\text{N}$  ( $x > 0.5$ ) requires a comprehensive solution for high performance deep-UV optoelectronics. Although experimental iterative approach towards low defect densities may be feasible in the short term, a long-term solution requires an understanding of point defect incorporation and ‘known and controlled’ growth environments. In this direction, the energy of formation of the defects may present a general solu-

tion where the reaction constituent chemical potentials and electron chemical potential may be appropriately tuned within predefined constraints to obtain minimum defect incorporation and maximum efficiencies. This approach requires extending the DFT analysis beyond the current 0 K and standard state calculations towards practical growth environment to understand point defect incorporation and developing and utilizing developed thermodynamic and reaction kinetic models that theoretically describe the growth environment which can then be controlled by internal knobs (e.g. gas flows, temperature, etc) and external knobs (e.g. illumination).

#### Acknowledgements

The authors acknowledge funding in part from NSF (ECCS-1508854, ECCS-1610992, DMR-1508191, ECCS-1653383, ECCS-1916800), ARO (W911NF-15-2-0068, W911NF-16-C-0101), AFOSR (FA9550-17-1-0225), DOE (DE-SC0011883), and ONRG NICOP (N62909-17-1-2004). We also acknowledge fruitful discussions with Zlatko Sitar, Douglas Irving, Jonathon Baker, Ronny Kirste, Seiji Mita, James Tweedie and Shun Washiyama.

## 6. Toward ohmic n-contacts on n-AlGa<sub>1-x</sub>N with high Al mole fraction

Luca Sulmoni

Technische Universität Berlin, Institute of Solid State Physics

### 6.1. Status

Ohmic contact formation on n-type III-nitrides is well established, at least for n-GaN. The basic mechanism responsible for ohmic behaviour involves N extraction by the contact metal upon thermal annealing and the formation of a heavily n-doped thin layer in the proximity of the interface [57, 58]. In fact, N vacancies act as donors in GaN thus enhancing the probability of tunnelling for carriers through the thinner Schottky barrier [59, 60]. Typically, the metal stack consists of four metals divided in two bilayers [58]. The first bilayer is responsible for the contact formation whereas the second one, usually referred to as capping layer, prevents the oxidation and the out-diffusion ('ball up') of the underlying metal stack. The most widely employed contact scheme is Ti/Al/Ni/Au. In many publications, the onset of the ohmic behaviour was attributed to the formation of a crystalline TiN layer (~5–20 nm thick) at the metal/semiconductor interface, indicating the reaction between Ti and GaN [57, 58, 60, 61]. While investigating the n-contact formation for higher Al mole fractions, the most common approach has been to transfer the already established metallization scheme for n-GaN to the n-AlGa<sub>1-x</sub>N material system. Unfortunately, Ti-based electrodes have shown to form ohmic contacts with n-AlGa<sub>1-x</sub>N only up to an AlN molar fraction of 0.58 [62]. Typically, the best reported values of contact resistivities are lower than  $10^{-6} \Omega \text{ cm}^2$  on n-GaN. However, due to the need of a transparent current spreading layer, UV light emitters utilize n-Al<sub>x</sub>Ga<sub>1-x</sub>N [63]. Up to an Al mole fraction of  $x = 0.7$ , contact resistivities on n-Al<sub>x</sub>Ga<sub>1-x</sub>N are similar to n-GaN but increase drastically to  $1 \Omega \text{ cm}^2$  on n-AlN (figure 10) [64], which goes hand in hand with the observed increase in n-sheet resistance [65]. In terms of wall-plug efficiency (WPE), devices emitting in the UV still exhibit significantly lower efficiencies than blue LEDs: >80% at 450 nm, >4% at 280 nm and >0.01% at 230 nm [5, 63, 66]. As discussed in sections 10 and 11, the reduced external quantum efficiency (EQE) at shorter wavelength is responsible to a significant extent for this efficiency drop. Nevertheless, minimizing the contact resistivities of p- and n-layers in deep UV LEDs and lasers is essential for improving WPE, reducing operating voltages and avoiding resistive Joule heating.

### 6.2. Current and future challenges

The causes for the non-ohmic characteristics of Ti-based contacts on n-AlGa<sub>1-x</sub>N with high Al mole fractions are twofold. Firstly, the Schottky barrier increases due to the lower electron affinity of AlGa<sub>1-x</sub>N with increasing Al mole fraction as well as the lack of appropriate low work-function metals [57]. The lack of metals with work-functions lower than 4 eV is a fundamental physical limitation. Therefore, the main strategy in order to achieve ohmic contacts on n-AlGa<sub>1-x</sub>N is to reduce

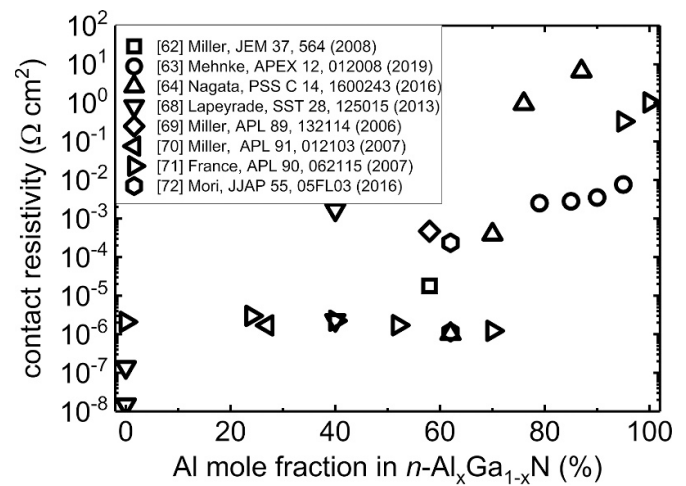


**Figure 10.** Contact resistivity as a function of the Al mole fraction for n-contacts on n-Al<sub>x</sub>Ga<sub>1-x</sub>N in the entire alloy composition.

the Schottky barrier width and therefore enhance tunnelling probabilities. Unfortunately, N extraction by Ti will become less energetically favourable as the AlN bond in the n-AlGa<sub>1-x</sub>N layer is stronger than for GaN (lower formation enthalpy) [58]. During the annealing process, Ti substitutionally replaces Ga in the alloy leading to the formation of voids, highly defective Al + Ti + N phases and TiN protrusion islands, preferentially formed along dislocations, at the metal/nitride interface thus hindering the development of an uniform contact area [58, 61]. Due to the higher resistivity of n-AlGa<sub>1-x</sub>N layers and of n-contacts in comparison to n-GaN, an interdigitated n-electrode is usually implemented during the microfabrication process in order to improve the current uniformity in the emitting area.

Nonetheless, a careful adjustment of the metal stack and the thermal annealing conditions is not the only challenge in order to form low resistance and ohmic n-contacts to n-AlGa<sub>1-x</sub>N at high Al mole fractions. Other important parameters play a critical role, such as the doping concentration in the underlying n-AlGa<sub>1-x</sub>N layer and the dry etching conditions. Since UV LEDs are fabricated on a non-conductive substrate such as sapphire, the buried n-AlGa<sub>1-x</sub>N contact layer must be exposed using plasma etching. Plasma-induced damage often results in an etched surface of poor quality thus undermining significantly the optical and electronic properties of n-AlGa<sub>1-x</sub>N. Cao *et al* reported that when increasing the Al mole fraction the plasma-induced defects act as deep-level centres, pinning the Fermi level and increasing the Schottky barrier height [67]. It is thus mandatory to carefully adjust the dry etching conditions and to introduce an adequate surface treatment in order to minimize the plasma damages and to assist the n-contact formation.

### 6.3. Advances in science and technology to meet challenges

In order to reduce the aggressive Ti-GaN reaction occurring in Ti-based n-contacts, different strategies have been suggested such as an Al layer with an adequate thickness on top of Ti

(optimal Ti/Al ratio), the implementation of diffusion barriers between Ti and AlGa<sub>N</sub> (e.g. Cr, Zr, Nb, ...) or the substitution of Ti by V. In the latter case, the generation of a heavily n-doped thin layer at the AlGa<sub>N</sub> interface is driven by the Al in the metal scheme while V acts as an indiffusion barrier [68]. Circumstantial evidence reported by several authors of the N extraction from the n-AlGa<sub>N</sub> layer and the consequent low n-contact resistance was the formation of a continuous thin AlN layer (~2–5 nm thick) at the interface [62, 68]. Nevertheless, the driving force for the reaction metal/AlGa<sub>N</sub> weakens as AlGa<sub>N</sub> becomes more energetically stable with the increase in Al mole fraction: N atoms create a more stable compound with Al than with Ga due to the lower formation enthalpy of AlN (−318.1 kJ mol<sup>−1</sup>) in comparison to GaN (−110.9 kJ mol<sup>−1</sup>) [58, 61]. In fact, it was possible to obtain ohmic V-based n-contacts only up to an AlN mole fraction of 0.7 [64]. The challenge is to find or develop a material (preferably highly conductive as a metal) able to form more stable nitrides than TiN or AlN on n-AlGa<sub>N</sub> layers with high Al content.

The high crystal quality with TDD lower than 10<sup>4</sup> cm<sup>−2</sup> of AlN bulk substrates is expected to improve the IQE of deep UV devices (see section 3). Unfortunately, due to the high ionization energy of donors in n-AlGa<sub>N</sub> layers with very high Al mole fraction, conductive AlN bulk substrates are not expected to be utilized in near future. In fact, the practical use of such substrates would be beneficial especially for UV lasers to circumvent the need of exposing the buried n-AlGa<sub>N</sub> with

plasma etching as mentioned before (current fabrication techniques typically involve substrate removal followed by a flip-chip process) thus allowing for a more homogeneous vertical carrier injection.

#### 6.4. Concluding remarks

Ohmic n-contacts on wide-bandgap semiconductors such as n-AlGa<sub>N</sub> with high Al content are challenging given several material limitations. First of all, the self-compensation of the Si dopant sets an upper limit on the amount of available donors in the n-AlGa<sub>N</sub> layer thus frustrating any effort in thinning the depletion region of the Schottky metal/semiconductor contact. Secondly, metals with sufficiently low work-function are not available. Finally, the N vacancy formation is hindered as the AlN bond in n-AlGa<sub>N</sub> becomes more and more energetically stable with decreasing Ga content and obstructs the formation of a heavily n-doped layer at the interface upon electrode annealing. Therefore, breakthroughs in terms of n-conductivity are expected to occur by new material concepts.

#### Acknowledgements

Funding by the German Federal Ministry of Education and Research (BMBF) within the ‘Advanced UV for Life’ project is acknowledged.



## 7. Doping of AlGaIn

Biplab Sarkar<sup>1,2</sup> and Ramón Collazo<sup>2</sup>

<sup>1</sup> Indian Institute of Technology Roorkee

<sup>2</sup> North Carolina State University

### 7.1. Status

A high electrical conductivity in n- and p-type AlGaIn is necessary to minimize the resistive losses in the epitaxial layers of UV light emitters. Furthermore, a high free carrier density also leads to low-resistance contacts. Thus, effective doping of AlGaIn has been under serious investigation for more than two decades. N-type dopants (Si, Ge, etc) can readily be incorporated in GaN and Al-rich AlGaIn epitaxial layers during growth. These dopants provide a relatively low ionization energy ( $E_A$ ) and high free electron density ( $>10^{19} \text{ cm}^{-3}$ ) in AlGaIn films. However, Mg is the only dopant that so far can be considered viable for p-type GaN and AlGaIn epitaxial films. Mg shows a high  $E_A$  ( $>120 \text{ meV}$ ) in metalorganic vapour phase epitaxy (MOVPE) grown p-GaN films, resulting in a free hole density that is only a fraction of the doping density. This becomes worse as the Al mole fraction increases in the AlGaIn films, as  $E_A$  is expected to increase monotonically to  $>500 \text{ meV}$  for AlN films. As mentioned in the previous chapter, increasing the Al-mole fraction in AlGaIn results in several point defects and charge compensators. Accordingly, several methods have been developed recently to achieve a high electrical conductivity in both n-type and p-type AlGaIn epitaxial layers. This chapter is dedicated to highlight the advances in the doping of AlGaIn to achieve a low  $E_A$  and high electrical conductivity.

**7.1.1. N-type doping of (Al)GaIn.** A low  $E_A$  of Si donors in (Al)GaIn yields a free electron density in the range of  $\sim 10^{19} \text{ cm}^{-3}$  and conductivity of  $<10 \text{ m}\Omega \text{ cm}$  in  $n\text{-Al}_x\text{Ga}_{1-x}\text{N}$  films ( $x < 0.8$ ) [73, 74]. Availability of native substrates is a bonus for achieving a higher conductivity in Al-rich AlGaIn films [75]. However, the donor  $E_A$  undergoes a steady rise in Al-rich AlGaIn films when the Al mole fraction goes above 80%, as shown in figure 11. This sharp increase in  $E_A$  is attributed to the formation of Si-DX centres acting as acceptor-type compensating point defects. Furthermore, the Si doping in AlGaIn is also responsible for a ‘knee-behaviour’ in resistivity with increase in the doping density [73, 74]. While the low Si doping density is responsible for the formation of carbon and vacancy-oxygen complexes, a high Si doping leads to self-compensation and vacancy related complexes (e.g.  $V_{\text{III}} + \text{Si}$ ) [48, 76]. All these acceptor type point defects compensate the free electron density in Al-rich AlGaIn films.

Apart from Si, germanium and oxygen have also been attempted to dope n-AlGaIn films. Ge typically shows a donor  $E_A$  of  $\sim 30 \text{ meV}$  in GaN, and is predicted to allow a doping density beyond the Mott transition [77]. However, the onset of DX centre formation is predicted to arise at an Al mole fraction of 52%, much lower than the Si counterpart. Therefore, a very high doping density can be achieved in  $\text{Al}_x\text{Ga}_{1-x}\text{N}$  films ( $x < 0.52$ ) using Ge doping. Similarly, oxygen can also

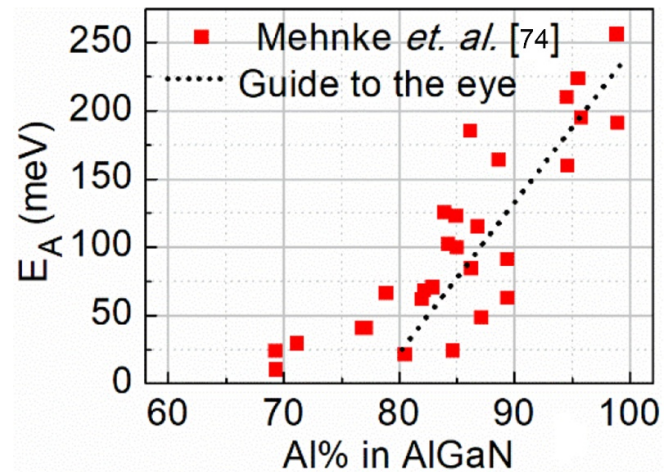


**Figure 11.** Donor  $E_A$  of Si in Al-rich AlGaIn epitaxial films [74]. Si donor  $E_A$  in n-GaN is  $\sim 15 \text{ meV}$ , which increases to  $\sim 50 \text{ meV}$  in  $n\text{-Al}_x\text{Ga}_{1-x}\text{N}$  ( $x < 0.8$ ) epitaxial films [73]. Thus, nearly full ionization of free carriers at room temperature is typically observed in  $n\text{-Al}_x\text{Ga}_{1-x}\text{N}$  ( $x < 0.8$ ) epitaxial films.

be incorporated in AlGaIn epitaxial films, and gets incorporated during the growth due to the presence of residual oxygen in the growth chamber. However, oxygen donors show a much higher  $E_A$  than Si, and the onset of DX centres also occurs at a lower Al mole fraction ( $\sim 61\%$  Al mole fraction) in AlGaIn [78]. All these issues make Si the preferred choice for n-type doping of AlGaIn epitaxial films.

**7.1.2. P-type doping of AlGaIn.** Achieving a free hole density of the order of  $10^{18} \text{ cm}^{-3}$  in GaN and AlGaIn films has been a major challenge for decades. Mg is the only known viable acceptor doping source that can occupy a substitutional site in (Al)GaIn epitaxial films. A free hole density in the order of  $10^{17} \text{ cm}^{-3}$  is achievable in p-GaN films grown on foreign substrates using high temperature growth techniques (e.g. MOVPE). Although relatively lower temperature growth (e.g. molecular beam epitaxy) results in a higher free hole density due to lower hydrogen incorporation, the subsequent device processing incurs very high temperature process steps raising several reliability issues. Native AlN substrates offer a suitable alternative for high temperature p-GaN growth having free hole density nearly an order of magnitude higher than the foreign substrates [79]. The lower dislocation density of single crystal AlN substrates minimizes the incorporation of donor-type nitrogen vacancies in p-GaN. An  $E_A < 100 \text{ meV}$  is thus achievable in p-GaN films grown on single crystal AlN substrates using MOVPE.

For AlGaIn, the Mg acceptor  $E_A$  is believed to increase monotonically from 120 to 200 meV in GaN to 500 meV in AlN [49]. Alongside, compensating nitrogen vacancies are also expected to exhibit a significant reduction in formation energy in p-AlGaIn w.r.t. increase in the Al mole fraction [59]. However, recent studies reported a significantly lower acceptor  $E_A$  in Al-rich p-AlGaIn films, as shown in figure 12.

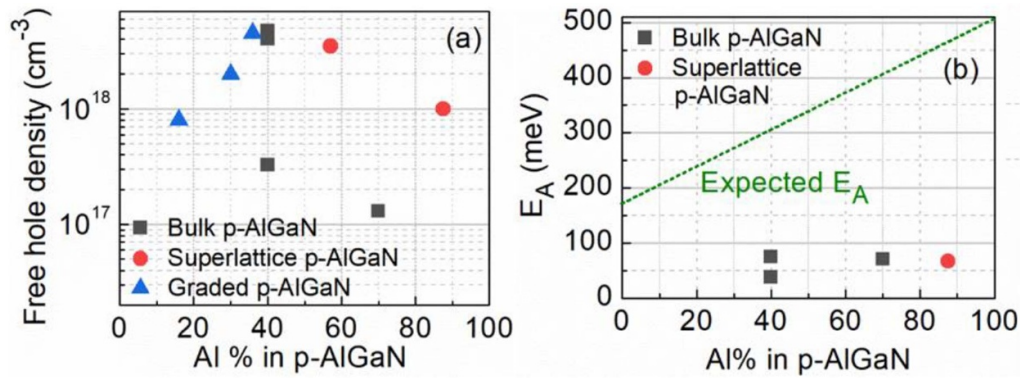


**Figure 12.** Recent reports on Mg-doping of AlGa<sub>N</sub>; (a) free hole density ( $p$ ), and (b) acceptor  $E_A$  for bulk and superlattice p-AlGa<sub>N</sub> films. Reproduced with permission from [75].

Kinoshita *et al* has reported an  $E_A$  of <72 meV in bulk p-Al<sub>0.7</sub>Ga<sub>0.3</sub>N films grown on sapphire substrate [49]. Similarly, Chen *et al* reported a free hole density of  $\sim 4.75 \times 10^{18} \text{ cm}^{-3}$  in p-Al<sub>0.4</sub>Ga<sub>0.6</sub>N by using In-surfactants and a Mg delta-doping scheme [80]. Along with improvement in bulk doping, alternative approaches such as superlattice structures and polarization doping schemes have also been developed to achieve a high free hole density in p-AlGa<sub>N</sub> (figure 12). Short-period superlattice structures consisting of several thin p-AlGa<sub>N</sub> films with alternating Al mole fractions allow periodic oscillations of the valence band of p-AlGa<sub>N</sub> layers. This technique results in regions where the Mg energy level is much closer to the Fermi-level. The effective acceptor  $E_A$  is thus reduced, and a free hole density in the order of  $10^{18} \text{ cm}^{-3}$  can be achieved in p-AlGa<sub>N</sub> superlattice structures [81]. Similarly, a graded p-AlGa<sub>N</sub> film (polarization doping scheme) results in the presence of polarization induced 3D charges, and hence the film is degenerate of free carriers. A free hole density of the order of  $10^{18} \text{ cm}^{-3}$  has also been reported from polarization doped p-AlGa<sub>N</sub> films grown on foreign as well as native AlN substrates [82].

## 7.2. Current and future challenges

Doping all III-nitride epitaxial films will remain a major focus of the community for the coming years. Si doping of AlGa<sub>N</sub> up to 70% Al mole fraction can be considered to be matured enough. However, several scattering mechanisms limit the carrier mobility thereby increasing the sheet resistance of the epitaxial films. Thus, a major effort will be required to increase not only the free carrier density, but also the carrier mobility in Al-rich AlGa<sub>N</sub>. Crystal growth technique has to be optimized to minimize the point defect incorporation and produce smooth high quality epitaxial films. A lower dislocation density in the epitaxial films minimizes the point defect incorporation, and provides a better internal quantum efficiency. Thus, AlGa<sub>N</sub> growth optimization on low dislocation density templates will require a major effort. Recent reports on AlGa<sub>N</sub> growth on native substrates and high temperature annealed templates are promising [75, 83]. Moreover, contact mechanism in n-type Al-rich

AlGa<sub>N</sub> films is still unknown for Al-rich AlGa<sub>N</sub> films. Unlike GaN and Ga-rich AlGa<sub>N</sub> films, obtaining a low resistance ohmic contact is a challenge. Ti/Al based contacts typically show a non-linear current-voltage characteristic when applied to Al-rich n-AlGa<sub>N</sub> films. Moreover, current conduction in Al-rich AlGa<sub>N</sub> films is dominated by different tunnelling mechanisms such as trap-assisted tunnelling. A major effort will thus be required to understand the contact formation mechanisms to enhance the contact performance and mitigate the reliability issues of future III-nitride deep-UV emitters.

Similarly, Mg doping of AlGa<sub>N</sub> will remain a major focus for the coming years. The role of dislocation density, point defects, vapour supersaturation, etc, are yet to be well understood for p-(Al)Ga<sub>N</sub> films. Alternative methods such as polarization doping and superlattice structures will be required to attain maturity before these technologies can be commercialized. Apart from free carriers, contacting the p-side of the III-nitride light emitters remains a major challenge. Standard Ni/Au contact metallization scheme to p-GaN results in highly resistive ohmic contacts with a contact resistance of  $> 10^{-3} \Omega \text{ cm}^2$  in most of the reported literature. Alternatively, the tunnel junction concept has been developed to achieve low resistance ohmic contacts to the p-side of the III-nitride light emitters. In this scheme, the contact is applied to a highly doped n-GaN film grown on p-GaN. When bias is applied, electrons are drawn from the valence band of p-GaN into the n-GaN due to the inter-band tunnelling. Similarly, free holes from the valence band of p-GaN are injected into the light emitter's active region. Thus, low resistance ohmic contacts can be formed in the p-side of the III-nitride light emitter by contacting the highly doped n-GaN instead of the p-GaN film. Note that an additional applied voltage (hence power loss) is required for the tunnel junction to allow holes to be injected into the light emitter's active region. Moreover, growth of subsequent n-GaN films on Mg-doped GaN at high temperatures result in 'memory effect' where Mg incorporates into the n-GaN. Thus, excellent doping control is mandatory to ensure a sharp and thin depletion region across the highly doped tunnel junctions. All these open challenges simply indicate the quantum of efforts



required to fully explore the potential of all III-nitride based devices.

### 7.3. *Advances in science and technology to meet challenges*

Recent advances in growth, characterization and measurement techniques for III-nitride emitters have been a remarkable achievement. Several research groups have developed point defect control schemes (such as defect quasi fermi-level control, chemical potential control, vapour supersaturation, high quality templates, etc) resulting in very high free carrier density in Al-rich AlGa<sub>N</sub> epitaxial films. Formation of DX centres in Si-doped Al-rich AlGa<sub>N</sub> films during growth is a physics limited issue. However, recent reports indicate that high energy implantation (a non-equilibrium process) of Si into Al-rich AlGa<sub>N</sub> and AlN films may provide pathway to mitigate the DX centre formation. A significantly lower  $E_A$  in ion-implanted n-AlN film grown on AlN substrate has been demonstrated recently [84]. Therefore, a paradigm shift of the doping scheme can be looked into to mitigate some of the critical doping issues in Al-rich AlGa<sub>N</sub> films.

Talking about the active region of the III-nitride light emitters, nearly defect-free quantum wells providing >80% internal quantum efficiency have been developed for both foreign and native substrates. Similarly, for laser diodes, doped waveguides and reflecting mirrors has been optimized to provide excellent wave confinement. However, to achieve lasing in deep-UV spectrum, resistive losses in the p-type cladding region must be minimized. Bulk Mg-doping and alternate doping schemes seems promising to provide low resistance p-

AlGa<sub>N</sub> cladding regions. So far, most of the III-nitride emitters have been designed having p-GaN as the contact layer. However, p-GaN absorbs the deep-UV light emitted by the active region of the emitter. Thus, recent reports on low  $E_A$  and high free hole density in Al-rich p-AlGa<sub>N</sub> seem promising to directly apply contact metallization to the p-AlGa<sub>N</sub> cladding layer. Moreover, standard Ni/Au contacts used in the p-side of laser diode are also known to absorb the deep-UV light. To overcome this absorption, reflective contact metallization schemes to replace the Ni/Au contact have been developed. Takano *et al* have even demonstrated improved light extraction efficiency in deep-UV flip-chip LEDs (275 nm) by using transparent p-AlGa<sub>N</sub> contact layer and Rh mirror contact [4]. All these reports indicate the importance of developing cutting-edge epitaxial film growth and contact metallization schemes to realize highly efficient deep-UV emitters.

### 7.4. *Concluding remarks*

This chapter provides a brief review of current status of n- and p-type doping in Al-rich AlGa<sub>N</sub> films for future highly efficient III-nitride light emitters. Identification of different point defects is necessary to understand the charge compensators responsible for compensating the free carriers in Al-rich AlGa<sub>N</sub> films. Epitaxial films grown on low threading dislocation density templates seems promising in many aspects. Recent reports on Mg doping in Al-rich p-AlGa<sub>N</sub> films is very promising for deep-UV emitters. With advancement in growth techniques for both foreign and native substrates, high performance Al-rich AlGa<sub>N</sub> based devices like LEDs and laser diodes can be realized in the near future.

## 8. Boron-containing (Al, Ga)N heterostructures

Ferdinand Scholz<sup>1</sup> and Abdallah Ougazzaden<sup>2</sup>

<sup>1</sup> Institute of Functional Nanosystems, Ulm University

<sup>2</sup> Georgia Institute of Technology, Georgia Tech-CNRS

### 8.1. Status

Boron (B) is the topmost and thus smallest element of the 3rd column of the periodic system of elements, being placed right above aluminium (Al) and gallium (Ga). Hence, one can expect a substantially smaller lattice constant and a larger band gap of B-containing nitrides (e.g.  $\text{Al}_{1-x}\text{B}_x\text{N}$ ) as compared to their B-free equivalents (i.e. AlN in this example). Typically, the lattice constant of such alloys follows Vegard's law being a linear relation between the composition  $x$  and the lattice constants of the binary end members (here AlN and BN), if both binaries crystallize in the same lattice type. However, while AlN and its Ga- and In-containing alloys crystallize in the hexagonal wurtzite structure, the thermodynamically most stable structure of BN is a hexagonal layered structure similar to graphite, whereas a wurtzitic phase can only be realized under specific boundary conditions. Anyway, by considering the data which are known for wurtzitic BN (w-BN), a variation of the lattice constants of  $\text{Al}_{1-x}\text{B}_x\text{N}$  by about 10% when varying  $x$  can be expected with B incorporation into AlN leading to smaller lattice constants, while mixing Ga into AlN would lead to larger lattice constants. Therefore, B is a prospective candidate to manage lattice mismatch and strain in AlBGaN heterostructures.

The bandgap of such alloys typically follows a quadratic correlation described by a bowing parameter  $b$  besides the bandgaps of the binary end members. The band gap of w-BN is still heavily discussed (see e.g. [85, 86]); it was calculated to be about 6.8 eV with indirect character (figure 13), while the direct band gap is estimated to be around 10 eV [85]. Similarly, only sparse data are known about the bowing parameters. Calculated bandgap data for AIBN presented in [85] may be best described with a bowing parameter of 7 eV for the direct bandgap and of 4 eV for the indirect transition.

Of course, essentially all other material characteristics are also functions of the respective ternary or quaternary composition. Particularly the variation of the refractive index when mixing B to Al(Ga)N alloys seems very promising for the realization of Bragg mirrors made of virtually strain-free AlGa<sub>1-x</sub>N-AlB<sub>y</sub> superlattices [87]. Moreover, alloying with B creates new degrees of freedom for managing both, the spontaneous and the piezo-electric polarization in respective heterostructures [87–89]. Therefore, optical and electronic devices could benefit from the development of this material system.

### 8.2. Current and future challenges

These simple considerations lead to very promising properties of B containing group III nitride heterostructures. However, a closer look reveals a lot of challenges. The dominant problem is the controllable and reproducible synthesis of

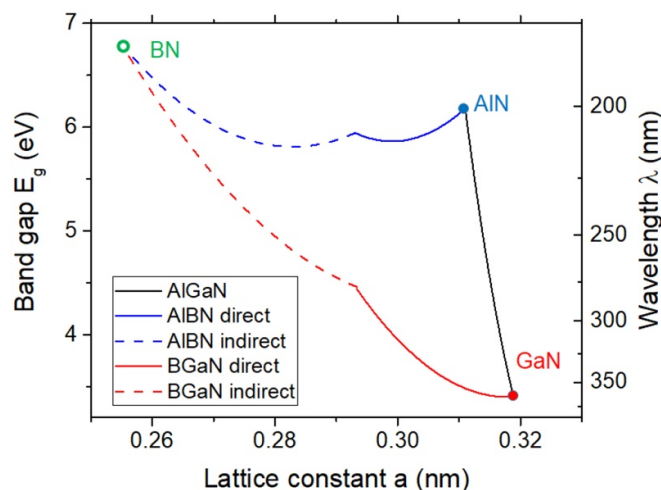


**Figure 13.** Bandgap versus lattice constant of the ternary alloys BGaN and AIBN. Notice the indirect band structure of w-BN. The connecting lines are plotted as a best compromise of unfortunately not yet fully consistent data from several sources. The direct band gap of w-BN is taken as 10.2 eV [85], whereas bowing parameters of 7 and 4 eV are assumed for the direct (full lines) and indirect transitions (broken lines), respectively, for both B-containing ternaries. For simplicity we assumed Vegard's law for the lattice constant. Any slight deviation (as sometimes discussed) would not change the major message of this diagram.

such alloys in high crystalline quality—being a major reason why their basic properties are still heavily debated. Calculations of their thermodynamic phase diagrams indicate that the AlBGaN material system exhibits a substantial miscibility gap at reasonable temperatures [90]. At temperatures around 1000 °C, only few percent of B are expected to be incorporated into Al(Ga)N, whereas full miscibility is only predicted for temperatures exceeding 9000 K [91]. On the other hand, particularly for strain management, only small amounts of B are needed: 6% of B lead to lattice matching between AlBGaN quantum wells and AlN barriers for an emission wavelength of 270 nm, whereas only 2% are required for a strain-free  $\text{Al}_x\text{Ga}_{1-x}\text{N}-\text{Al}_y\text{B}_z\text{Ga}_{1-y-z}\text{N}$  multi quantum well structure with the same target wavelength and reasonable barrier height ( $x \sim 0.55$ ,  $y \sim 0.7$ ).

Epitaxial growth results seem to confirm and even emphasize these problems. Very high B contents, mostly in the range of 10–15%, have been achieved by few groups by metalorganic vapor phase epitaxial growth at comparably low temperature of about 900–1000 °C (see e.g. [92, 93]). Such layers and heterostructures exhibit fair x-ray diffraction results and have been studied with respect to their refractive index data in AIBN-AlN Bragg mirrors. Best reflectivities of only about 80% at 311 nm have been measured [87], but no PL is reported from such structures which may be taken as a confirmation of their limited crystalline quality. When directly compared to GaN, BGaN layers show reasonable luminescence only for a B content below 1%, whereas larger B concentrations dramatically reduce the emitted light intensity (see e.g. [94]), although higher intensities are expected in strain-optimized structures [95]. By careful optimization

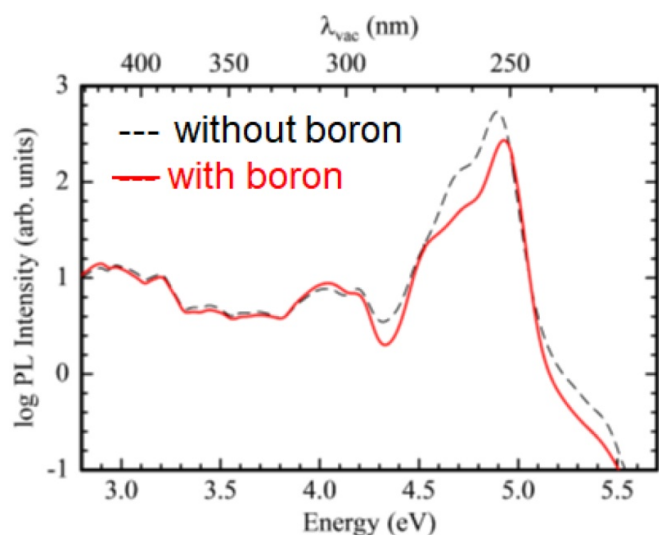


**Figure 14.** Low-temperature PL (10 K) of a thin AlGaIn layer and a similar AlBGaIn layer with about 1% B. Notice the comparable intensity of both samples. [96] John Wiley & Sons. © 2018 WILEY-VCH Verlag GmbH & Co. KGaA, Weinheim.

of the growth procedure, strong PL intensities in AlBGaIn layers containing 1–2% of B similar as in respective B-free AlGaIn layers (figure 14) have been recently reported [96]. Transmission electron microscopy (TEM) studies confirm the limited crystalline quality of essentially all AlBGaIn layers with boron concentrations larger than some tenths of a percent. In consequence, many material properties of B containing nitrides are still questionable strongly limiting the consistency of device simulation studies.

### 8.3. Advances in science and technology to meet challenges

The major challenge for benefitting from the above mentioned promising properties of B containing AlGaIn structures is the suppression of defect formation typically accompanied with the incorporation of major B amounts, e.g. by adopting nanoselective area growth [97]. To this end, a better understanding of the characteristics of B on the growing semiconductor surface is mandatory. Only scarce, if any data are available about its surface diffusion properties. Owing to the strong B–N bond, very high growth temperatures are recommended to enhance the B surface diffusion length. However, this may lead to strong parasitic gas phase reactions between the B precursor (typically tri-ethyl-boron TEB) and ammonia (NH<sub>3</sub>). The mobility of B on the growing surface can also be increased by modulating the precursor flows [93, 98], i.e. supply the group III and group V precursors sequentially, which also minimizes the risk of gas phase pre-reactions and hence may allow to use substantially higher growth temperatures. This approach, currently studied by many groups, needs further optimization. High resolution TEM may help

to get a better understanding about the interaction between boron incorporation and defect generation. Moreover, some groups report about the incorporation of parasitic impurities, in particular oxygen and carbon, together with boron [99]. The reason for this behaviour is not yet well understood. The fairly strong chemical binding of the ethyl groups to boron in TEB may be responsible for the latter. Hence other B precursor molecules need to be investigated. Few studies have been done with diborane (B<sub>2</sub>H<sub>6</sub>) and borazine (B<sub>3</sub>N<sub>3</sub>H<sub>6</sub>) as well with tri-isopropyl-boron (TiPB), but here more detailed studies are needed to evaluate their usefulness for the growth of AlBGaIn layers, particularly regarding the impurity problem. Such improved layer quality would also enable more elaborate determination of their structural and optoelectronic properties.

Obviously, the field is still at its infancy compared to the much more developed AlGaIn and GaInN fields. For instance, successful p- or n-doping of BAlN and BGaIn has not yet been reported. Similarly, high performance optical or electronic devices comprising AlBN and BGaIn have yet to be demonstrated.

### 8.4. Concluding remarks

The addition of boron to the group III nitride alloy components seems to open very promising solutions regarding strain, polarization and refractive index management in Al(B)GaIn heterostructures. They may find applications in both optoelectronic (deep UV LEDs, UV detectors, sensors, etc) as well as in novel electronic devices (high electron mobility transistors, Schottky diodes, etc). However, we are obviously faced with very heavy problems regarding the epitaxial growth of B containing layers as a consequence of the extraordinary chemical properties of boron as a member of the second row of the periodic system. Very thorough optimization of the epitaxial growth procedure may lead to substantially better AlBGaIn layer qualities as compared to today's situation, but it will remain a major challenge to achieve device performance data, e.g. UV emitters better than obtainable by relying on B-free AlGaIn structures.

### Acknowledgements

We thank Oliver Rettig (Inst. of Functional Nanosystems, Univ. of Ulm) and Suresh Sundaram (GT-Lorraine UMI GT-CNRS, 2958 Metz, France) for their great help in preparing this paper. Moreover, we gratefully acknowledge the financial support of our AlBGaIn research by the Deutsche Forschungsgemeinschaft (Uni Ulm) and by the French National Research Agency (ANR) to the UMI GT-Lorraine as a part of the projects: GABORE (BLAN07-1-203 576), BATGAN (ANR-11-BS09-0038), VESUVE (ANR-11-BS03-0012) and the GANEX Laboratory of Excellence (Labex).

## 9. Development of UV-A LEDs

Peter J Parbrook<sup>1</sup> and Tao Wang<sup>2</sup>

<sup>1</sup> Tyndall National Institute and School of Engineering,  
University College Cork

<sup>2</sup> University of Sheffield

### 9.1. Status

UVA covers the wavelength range 315–400 nm. Sources in this region have application in UV curing, photolithography, phototherapy (including melanoma treatment), security (bank-note verification), dentistry, crime scene investigation and as a pump source for general illumination [100]. As a result of the wide range of applications, the UV market is dominated by UVA, along with the growing UVB/UVC area mainly for water purification [101]. The GaN bandgap (~362 nm) is in the centre of this range, with longer/shorter wavelengths achieved via InGa<sub>N</sub>, AlGa<sub>N</sub> (or InAlGa<sub>N</sub>) alloys. From a technological perspective the bandgap of GaN splits UVA into two distinct parts. For longer (>365 nm) wavelengths, devices can use adapted technology from that used in visible LEDs. For shorter wavelengths (<365 nm) there is a performance collapse, which can be seen clearly in the device external quantum efficiency (EQE) against wavelength plot shown in figure 2 in section 1 of this Roadmap [11]. For most applications, the key parameter is raw optical power produced at the target wavelength. This correlates strongly to efficiency, due to the limits on the current density and heating that a device can tolerate, and hence the cost of ownership, running cost of the UV emission system. Improvements will lead to improved take up in systems using sources across this range.

Early reports of UVA-LEDs include: a 370 nm LED based on an AlGa<sub>N</sub>/Ga<sub>N</sub> double heterostructure (DH) in 1994 [102]; 350 nm UV-LEDs, using Ga<sub>N</sub>/AlGa<sub>N</sub> quantum wells (QWs) for the active region (output power of 13 μW at 20 mA) in 1998 [103]; and the use of InGa<sub>N</sub> QWs for 380 nm was demonstrated by Mukai and Nakamura [104]. A 1 mW 348 nm UV-LED using AlInGa<sub>N</sub> quaternary as an active region at 50 mA was reported in 2002 [105]. Using Ga<sub>N</sub> as a substrate, the crystal quality can be greatly improved, leading to 352 nm UV-LEDs producing 0.55 mW at 20 mA (estimated internal quantum efficiency (IQE) >80%) in 2001 [106]. These results are based on conventional Ga<sub>N</sub>-on-sapphire technology, or Ga<sub>N</sub> substrates. More recently, there have been significant improvements in the EQE of near UV-LEDs (NUV-LEDs), namely, the UVA-LEDs specifically in the spectral range from 365 to 400 nm, such as 30% EQE for 365 nm UVA-LEDs and 50% EQE for 385 nm UVA-LEDs. Properly packaged 365 nm UVA-LEDs with an output power of up to 12 W have been reported [100]. For 380 nm LEDs such technology can now provide commercial devices with powers exceeding 1 W in a suitably packaged envelope. However, this is not the case for shorter wavelength devices.

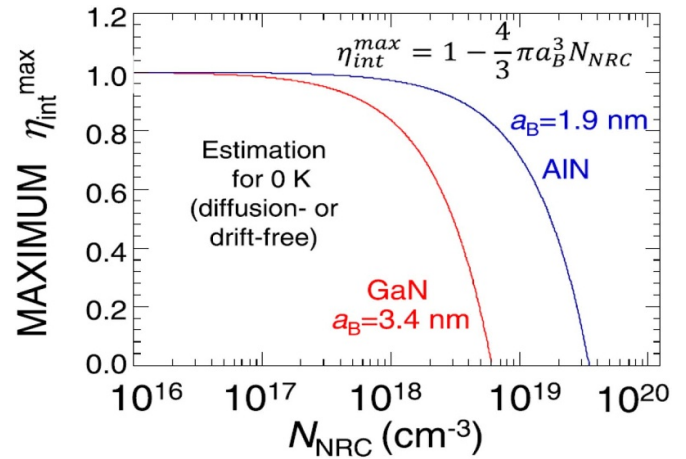


**Figure 15.** Maximum IQE as a function of point defect density. Reprinted with permission from [105], Copyright (2002), AIP Publishing LLC.

### 9.2. Current and future challenges

The major challenge in all LEDs is to maximize wall plug efficiency (light output over electrical input). This can be defined in terms of the product of IQE, light extraction efficiency (LEE)—giving EQE—and the electrical loss. As one targets shorter wavelengths these elements all become more challenging. LEE is the primary cause of the efficiency drop for wavelengths <365 nm. In all LED design a primary goal is to minimize all possible absorption losses in the device. For LEDs grown on Ga<sub>N</sub> operating >365 nm there is minimal optical absorption as Ga<sub>N</sub> is transparent. However, for wavelengths <365 nm optical absorption is harder to control as one generally is required to use a Ga<sub>N</sub> or AlN based template layer to ensure high structural quality to ensure a high IQE. If devices are grown on Ga<sub>N</sub> many of the photons produced do not escape the diode, and LEE values of a few percent are typical. The alternative is to apply a ‘Ga<sub>N</sub>-free technology’ to prepare such LEDs on AlN templates. AlN, however, has a ~3% mismatch to Ga<sub>N</sub> and UVA materials require high Ga<sub>N</sub> content alloys, leading to significant strain control issues. Furthermore, convincing technologies to make a low resistance ohmic p-contact directly to AlGa<sub>N</sub> (as opposed to Ga<sub>N</sub>) means that the vast majority of <360 nm LEDs still have absorption (hence LEE) issues.

IQE is affected by a number of factors in this region. For <360 nm point defects may become progressively more important at shorter wavelength as shown in figure 15 [107]. Typically, the V/III ratio for AlGa<sub>N</sub> growth is much less than (In)Ga<sub>N</sub> to enhance atomic diffusion, potentially leading to significant increase in vacancy point defect density. A further issue is the control of the polarization fields across the QWs. At longer wavelengths the need to include AlGa<sub>N</sub> to prevent carrier overflow, and the strain consequences to an otherwise Ga<sub>N</sub>-based structure can lead to an IQE drop. Finally for <365 nm LEDs n-AlGa<sub>N</sub> must be used, resulting in alloy



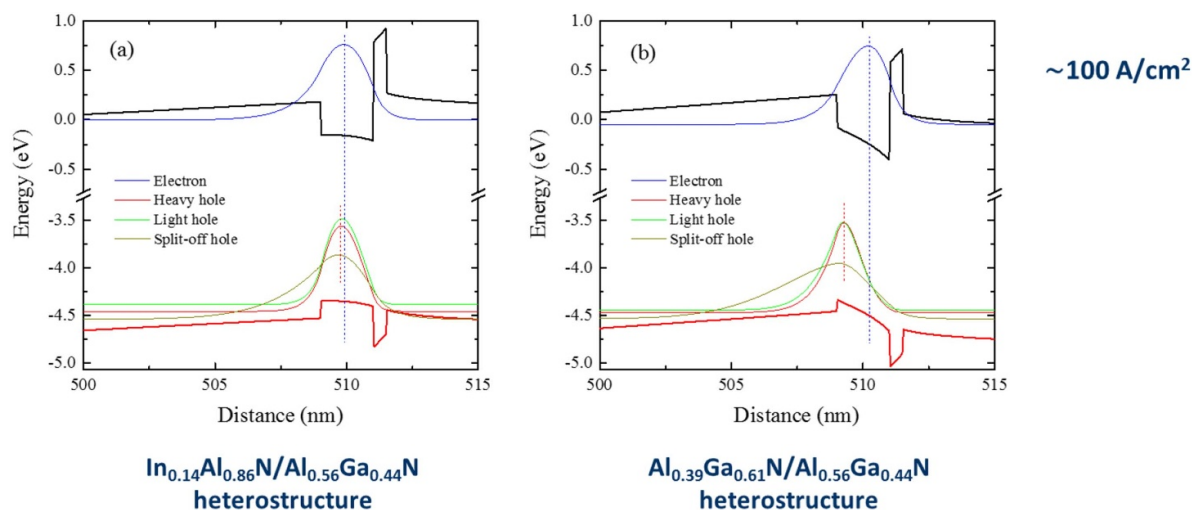


**Figure 16.** Improved electron–hole wavefunction overlap for InAlN–AlGaIn versus AlGaIn–AlGaIn quantum well UVA LEDs ( $\sim 340 \text{ nm}$ ). Reproduced from [109]. © 2019 The Japan Society of Applied Physics. All rights reserved.

scattering and consequently a large mobility drop [73], which coupled with the challenges in making n-AlGaIn thick (due to strain and roughening) leads to additional voltage losses. This is in addition to further challenges in optimizing the p- and n-electrical contact design.

### 9.3. Advances in science and technology to meet challenges

For UVA LEDs  $>365 \text{ nm}$  package design is likely to have the biggest future impact on device performance, utilizing best practice from those used in visible LEDs. This includes optimization of light extraction and heat from the chip. Further, the low In content in the QWs for these devices means that carriers can potentially move to extended defects more easily than in their visible counterparts, so the optimization of devices on lower defect GaN templates will be beneficial. This needs to be achieved either through obtaining best crystal quality cost effectively on sapphire (or Si with a substrate removal step and care to preventing cracking), or in finding routes to reuse expensive high quality templates with device lift off.

For devices operating  $<360 \text{ nm}$  routes to improve the LEE are critical. Ideally this means a GaN-free growth process, or route to removing GaN material in post growth fabrication. An ideal would be use of thick, high quality AlGaIn layers, which is an area but this is not easily achievable as the strain leads to cracking (GaN) or dislocation climb and layer roughening (AlN). There is developing research using such approaches (both for UVA and UVB LEDs) with improvements in emission quality and a more controlled roughening if a crystallographic miscut is introduced. However, this does lead to a step-bunched morphology with composition variations in the AlGaIn, and additionally quantum well thickness variations. The impacts on this on device performance still require further work [108]. Currently AlGaIn on AlN is more promising, despite the issues of strain for the n-AlGaIn buffer and high Ga content AlGaIn QWs (with polarization field control issues) that this presents. Improved routes to allow smooth, thick AlGaIn buffer growth of high crystal quality, for example

using patterning to allow strain control, would revolutionize the short wavelength UVA.

As for UVB and UVC LEDs, making direct contact to AlGaIn through doping and contact metal optimization is also required. Such routes have demonstrated promise, but need work to retain the benefits to LEE while minimizing electrical loss [4]. The high spontaneous polarization in AlGaIn means that polarization fields are always an issue in UV LEDs. Thus the potential of using semi- or non-polar materials, which might allow thicker AlGaIn as there is an easier route to strain relaxation, is worth investigating. In theory InAlN–AlGaIn QWs can create polarization-free active regions on c-plane for UVA, leading to improved electron–hole wavefunction overlap, as shown in figure 16. However, while LED operation has been demonstrated the challenges in material growth are high [109]. Small quantities of In in InAlGaIn QWs may have benefit for higher IQE, particularly in the  $340\text{--}365 \text{ nm}$  range.

### 9.4. Concluding remarks

In conclusion, UVA LEDs can be split into two distinct bands. At longer wavelengths devices show high efficiency and can generally use adapted forms of the mature technologies using to make state-of-the-art blue LEDs. Devices with high powers are commercially available and improvements in package and defect reduction may lead to improved future performance. For shorter wavelengths ( $315\text{--}365 \text{ nm}$ ) where GaN absorption is a major problem compromising LEE in particular, development of a true GaN-free technology for devices is critical if UV LEDs to be fully exploited as sources in this range.

### Acknowledgements

Peter Parbrook acknowledges Science Foundation Ireland support via 07/EN/E001A, 10/IN.1/I2993 and 12/RC/2276\_P2. Tao Wang is financially supported by the EPSRC Project No. EP/M015181/1 and EP/M003132/1

## 10. UVB-LEDs

Tim Wernicke

Technische Universität Berlin, Institute of Solid State Physics

### 10.1. Status

For the UVB spectral range, 280–315 nm, the external quantum efficiency (EQE) values achieved so far are lower than those record efficiencies of LEDs emitting around 275 nm and UVA LEDs (see section 1), i.e. there is a ‘UVB gap’ also extending into the UVA region especially in the 305–330 nm range with lower performance in comparison to shorter and longer emission wavelengths. Nevertheless UVB LEDs emitting at 305 nm are commercially available with an emission power of 100 mW at a current of 350 mA (EQE 6%) with an operation voltage of 7 V [110]. This EQE is similar to currently available LEDs emitting around 280 nm and 340 nm [110]. This disparity in reported record values and available products has technological and economic reasons. Research efforts and number of publications for UVB-LEDs is much smaller compared to the UVA and UVC spectral range, most likely because there is currently no high volume application (see section 1) and combining all possible approaches to increase the light extraction efficiency (see section 13) have not been attempted yet. These novel approaches have a high potential for increasing the EQE of UVB LEDs as well but need to be tested for their impact on degradation behaviour before a general application. Nevertheless, UVB-LEDs have numerous applications, e.g. phototherapy, plant growth lighting and polymer curing (see section 1). Especially the first two require a peak wavelength at about 310 nm as light below 300 nm is harmful for these applications. From a technological point of view, the UVB-LEDs profit from most technological advances for UVC-LEDs but suffer from a lack of suitable substrates as they cannot be grown on defect reduced AlN—the large compressive strain leads to a formation of defects in UVB emitting quantum wells (QWs) [111, 112]. This can be mitigated by growing a relaxed  $\text{Al}_{0.5}\text{Ga}_{0.5}\text{N}$  buffer on AlN/sapphire template [113]. The relaxation process can be facilitated by introducing an AlN/GaN superlattice as indicated in figure 17 [113] and is only possible with a sufficiently high threading dislocation density (TDD)  $>3 \times 10^9 \text{ cm}^{-2}$  as the compressive strain is released by tilt of edge type dislocations [113]. However, in this way a further reduction of the TDD in UVB LEDs is not easily possible leading to a lower internal quantum efficiency (IQE).

The electrical efficiency  $\eta_{\text{el}}$  of UVB-LEDs, which describes the losses by Joule heating at contacts and in the semiconductor layers, still gives room for improvement: Even comparably low operation voltages of 6 V at 100 mA [114] or 7 V at 350 mA [110] are several volts higher than the physical limit being defined by the bandgap in the quantum wells, i.e. close to 4 V (see also section 1). In the UVA these issues are solved with 365 nm LEDs exhibiting a very high electrical efficiency and low voltage of 3.49 V at 20 mA [115] and

at 700 mA [110]. For UVB-LEDs ohmic n-contacts—Ti/Al-based as well as V/Al-based—with resistivities of  $10^{-5} \Omega \text{ cm}^2$  (see section 6) and AlGaIn layers with low resistivity have been realized. Therefore whole process needs to be optimized for lower voltages. Additionally, the operation voltage is increased if transparent p-doped AlGaIn layers are employed [116, 117].

The lifetime of UVB-LEDs can reach several thousand hours ([114] and see section 16) and even though their visible counterparts are much more stable, these values are sufficient for first applications.

In order to develop high efficiency and high power UVB-LEDs with EQEs exceeding 20% it is necessary to solve a number of challenges.

### 10.2. Current and future challenges

One of the main challenges to achieve UVB-LEDs with a higher light output power is reducing the threading dislocation density to allow for higher IQE values. Even though threading dislocations can be reduced by annihilation in a thick  $\text{Al}_{0.5}\text{Ga}_{0.5}\text{N}$  buffer layer the lowest threading dislocation density that could be achieved is still  $>10^9 \text{ cm}^{-2}$ . To further increase the internal quantum efficiency of UVB emitting quantum wells, the relaxation process needs to be decoupled from threading dislocations and/or the annihilation of dislocations has to be enhanced. One approach is the structuring of the AlN surface before AlGaIn overgrowth leading to relaxation and effective dislocation annihilation and TDD of  $2\text{--}5 \times 10^8 \text{ cm}^{-3}$  depending on the aluminium content in the layer [118]. A similar effect is achieved by introducing a 3D growth of  $\text{Al}_{0.55}\text{Ga}_{0.45}\text{N}$  and subsequent coalescence achieving TDD of  $7\text{--}9 \times 10^8 \text{ cm}^{-3}$  [112]. Another way to mitigate the effect of threading dislocations is growing UV-LEDs on highly miscut sapphire substrates of  $1^\circ$  with a step bunched surface leading to UVB-LEDs emitting at 300 nm with a record high EQE of 6% [114].

There are only few publications discussing the carrier injection efficiency  $\eta_{\text{inj}}$  mainly by a variation of the electron blocking layer (EBL) or by introducing an electron blocking heterostructure [111, 119] and the exact value of the injection efficiency is not clear, i.e. how much improvement of the external quantum efficiency can be achieved by further optimizing these layers. However, high efficiency LEDs require an almost perfect injection efficiency and the design of the electron blocking layer seems to have a crucial effect on the lifetime of the LEDs (see section 16).

The LEE has the highest potential for an EQE increase as current UVB LEDs do not incorporate techniques for increasing the LEE (see section 13). Successfully reducing the absorption in layers [111] and at interfaces as well as reducing the total internal reflection are the main tasks.

For the degradation of UVB LEDs the root cause seems to be deep levels at the pn-junction and within the quantum wells introduced by point defects leading to a reduction in output power (see section 16). The main challenge is to reduce these point defects by optimizing the growth parameters which will not only lead to longer lifetimes but also higher IQE and CIE.



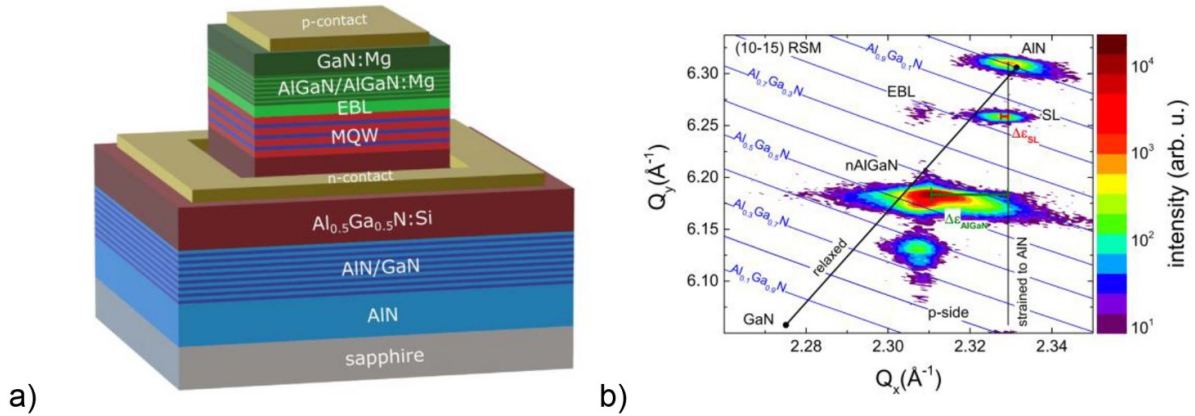


**Figure 17.** (a) Schematic of a typical UVB-LED heterostructure. For coherent growth of the MQW emitting at 305 nm a relaxed  $\text{Al}_{0.5}\text{Ga}_{0.5}\text{N}$  layer is grown (from Susilo *et al*, pssa). (b) XRD reciprocal space map around the AlN 105 reflection of a full UVB LED illustrating the strain relaxation process. The AlN/GaN superlattice is grown coherently strained on the AlN/sapphire template (nearly the same  $Q_x$  value). The  $\text{Al}_{0.5}\text{Ga}_{0.5}\text{N}$  starts to grow first strained but then relaxes during further overgrowth ( $Q_x$  shifting to lower values) thus forming a metamorphic quasi-substrate that allows to grow EBL and buffer layer with the new lattice constant. Reprinted from [113], Copyright (2017), with permission from Elsevier.

### 10.3. Advances in science and technology to meet challenges

To further increase the IQE, a further reduction of the TDD down to  $2 \times 10^8 \text{ cm}^{-2}$  would be desirable [8]. Here approaches involving lateral overgrowth or maybe even AlGaIn quasibuffers prepared by hydride vapour phase epitaxy (HVPE) or achieving high quality AlGaIn by high temperature annealing (see section 2) might be a necessary technological development. For the material of the QW novel indium or boron containing alloys might allow for a boost in IQE. Indium containing quaternary InAlGaIn or even ternary InAlN might allow for an increased IQE by introducing localization and maybe also a reduced point defect density, however recent UVB LEDs with record high quantum efficiency employ pure AlGaIn quantum wells [114, 117] suggesting that TDD and point defect density are most important. Boron containing quaternary AlBGaIn MQWs would allow to reduce the compressive strain (see section 8) and grow coherently strained on AlN making use of optimized AlN buffer layers or bulk substrates with much lower threading dislocation densities. However, the prerequisite for a successful implementation of such materials will be mastering their growth.

The LEE will be strongly increased by increasing the aluminium content in the p-doped AlGaIn layers so the emitted photons are not absorbed in this layer [116, 117], see also section 13. In comparison to UVC-LEDs, the necessary aluminium content to achieve transparency is much lower leading to a smaller increase of the operation voltage. However, very high LEEs will only be achieved in combination with reflective contacts leading to a significant improvement of LEE and EQE. Here the challenge is to find a highly reflective material that forms an ohmic contacts to p-doped AlGaIn or realize

photonic crystals (see section 13). The alternative approach to realize transparent LEDs is employing tunnel junctions as demonstrated for 326 nm LEDs (see section 17). To reduce internal reflections the substrate removal by laser lift off [120] or electrochemical etching [114] and/or roughening [121] will increase the light extraction efficiency. In parallel the encapsulation of UVB-LEDs will positively affect the LEE for transparent as well as non-transparent LEDs (see sections 11 and 13).

### 10.4. Concluding remarks

UVB LEDs will also in future exhibit lower external quantum efficiencies than UVA and UVC LEDs due to the lack in suitable substrates with a low threading dislocation density. In future several approaches might allow for an effective reduction in threading dislocation density even though most of them require considerable development effort. A strong increase in LEE can be expected for the near future as increasing the aluminium content on the p-side and incorporating tunnel junctions lead to a lower additional voltage in comparison to UVC-LEDs due to the smaller bandgap of the material allowing for a high efficiency operation as soon as these techniques can be implemented.

### Acknowledgements

The author thanks Sven Einfeldt and Akira Hirano for fruitful discussions. The author gratefully acknowledges support by the German Research Foundation (DFG) within the Collaborative Research Center ‘Semiconductor Nanophotonics’ (CRC 787) and the German Federal Ministry of Education and Research (BMBF) within the project ‘Advanced UV for Life’.

## 11. UVC LEDs

Akira Hirano<sup>1</sup> and Hiroshi Amano<sup>2,3</sup>

<sup>1</sup> UV Craftory Co., Ltd.

<sup>2</sup> IMASS, Nagoya University

<sup>3</sup> Nagoya University

### 11.1. Status

UVC LEDs with wavelengths between 250 and 280 nm are expected to be used as an alternative to low-pressure mercury lamps. In this section, UVC refers to this limited wavelength range. The main application of UVC light sources is sterilization, and the wavelength giving the peak disinfection efficiency is about 265 nm [122]. Low-pressure mercury lamps with an intense emission at the sterilization line (253.7 nm) have a high WPE of about 25% and a lifetime of 6000 h. Although AlGaIn-based deep UV-LEDs ( $\lambda < 300$  nm) in UVB have a potentiality of WPE of about 10% and the lifetime over 10,000 h [122], WPE of 265 nm LEDs is significantly less than 10%. The LED lifetime decreases as the wavelength decreases from 280 nm [122, 123]. With this background, at a wavelength of 275 nm, which is slightly shorter than 280 nm, higher initial EQEs over 10% were reported to be achievable by using a p-reflective contact and unknown encapsulation [124] and by integrating a p-reflective contact, patterned sapphire substrate, and lens [4], respectively. However, reliability tests have not yet been reported for the case of using a p-AlGaIn contact, and the devices with a p-reflective electrode also exhibited an increased forward voltage ( $V_f$ ). In the case of using a p-GaN contact layer, EQEs of 4.9% at 270 nm with encapsulation [125] and 5.5–6.0% at 265 nm with distinctive roughening [126] were obtained using an AlN bulk substrate. Also, the results of reliability tests have been reported for 265 nm UVC LEDs with a p-GaN contact layer on sapphire [113, 122]. Using a p-GaN layer, encapsulations using a fluoro-polymer [127] and a sapphire lens [123] were demonstrated to enhance the LEE 2.3-fold and 1.5-fold in UVC, respectively, which do not adversely affect the lifetime for UVC LEDs without increasing  $V_f$ . Figures 18(a) and (b) show the EQEs for bare dies of DUV-LEDs with a p-GaN layer grown on sapphire and the reported EQEs incorporating the techniques of enhancing LEE, respectively. Figure 18(b) includes the EQEs achievable from the results shown in figure 18(a).

### 11.2. Current and future challenges

Generally, the near-future tasks are considered to be best discussed under the premise of using a p-GaN layer because the LED lifetime is expected to be longer than that of a low-pressure mercury lamp. An improvement in IQE by reducing the TDD and point defect density (PDD) and an improvement in LEE are considered to be priorities.

To reduce the TDD to near  $10^8$  cm<sup>-2</sup>, a typical approach is to use bulk AlN substrates with a TDD of less than  $10^6$  cm<sup>-2</sup>. Also, the TDD can be reduced to  $5 \times 10^8$  cm<sup>-2</sup> by using a

1.0°-miscut sapphire substrate [113]. Figure 19(a) indicates the further improvement of TDD by using 1.5°-miscut sapphire [122], showing the possible improvement in IQE by reducing the TDD.

The possibility of increasing the IQE by reducing the PDD has been reported [52, 53]. A moderately Si-doped quantum well (QW) exhibited improved IQEs for AlGaIn QWs with a TDD of greater than  $10^9$  cm<sup>-2</sup> near 250 nm [53]. Also, control of the PDD was shown by increasing the V/III ratio when growing 258 nm QWs [52] using an AlN bulk substrate. These results indicate that the IQE of UVC LEDs can be improved by reducing the PDD.

For the LEE, it is necessary to discuss the packaging techniques for UVC LEDs ( $\lambda < 250$  nm). The molecular structure of the fluoro-resin used for encapsulating UVC-LEDs (265 nm) has been clarified to be polymerized perfluoro(4-vinylxy-1-butene) with end groups of  $-\text{CF}_3$  [127]. However, the low refractive index of 1.35 limits the improvement in LEE. The refractive index of fluoro-resin is difficult to increase. Thus, consideration of the shape effect is important for increasing LEE. It is desirable to fabricate hemispherical lenses on surface-mounted devices (SMDs) by forming a lens array on a large AlN sheet (e.g.  $4 \times 4$  inch<sup>2</sup>) followed by isolation to make small SMDs (e.g.  $3.5 \times 3.5$  mm<sup>2</sup>). Another successful approach to improve LEE is to use sapphire lenses with a refractive index of 1.8 [123].

### 11.3. Advances in science and technology to meet challenges

The utilization of EL emission from QWs penetrating p-contact layers is currently difficult in practice owing to the lack of both a low-resistivity p-contact and a conductive p-AlGaIn cladding layer. Aluminium (Al) is the only metal with reflectivity in UVC. Furthermore, when an Al-based contact on AlGaIn is annealed, the Al-based electrode loses its reflectivity in UVC. Thus, the development of an effective reflective structure above EB layers is considered to be a long-term challenge, which will be described in sections 13 and 17.

To date, mass-produced DUV-LEDs on sapphire have been grown on AlN with TDD of  $2\text{--}5 \times 10^8$  cm<sup>-2</sup> [113, 124] or greater. To reduce the TDD to near  $10^8$  cm<sup>-2</sup>, studies on the behaviour of AlN at around and above 1400 °C will also be beneficial as well as fabricating and evaluating LEDs. Also, AlN templates with a low TDD is considered to be useful for determining the possible improvement in IQE because the required TDD for fabricating DUV-LEDs are considered to be between  $10^8$  cm<sup>-2</sup> and  $10^9$  cm<sup>-2</sup> [113]. The behaviour of AlN is expected to be similar to that of GaN when the growth temperature is increased.

A detailed study on the decrease in EQE during reliability tests will be meaningful for achieving devices with comparable lifetime to those of low-pressure mercury lamps. In figure 19(b), the increased deterioration of the output of UVC-LEDs compared with that of UVB-LEDs is shown. The reliability test for 265 nm LEDs suggests two main mechanisms for the initial and subsequent decrease in the EL output. The decrease



#### 11.4. Concluding remarks

The initial EQEs of UVC-LEDs (265 nm) have been reported to be about 2/3 of those for UVB-LEDs (280–300 nm). Further reduction of the PDD and TDD is expected to increase the IQEs of UVC-LEDs. Also, the improvement in LEE by encapsulating dies was demonstrated. The utilization of light towards the p-side without increasing  $V_f$  and decreasing the lifetime of UVC-LEDs is also useful. The UVC-LEDs'

lifetime is expected to be much longer than 6000 h. To date, a decrease in EL output of about 50% for 265 nm LEDs during the reliability test was observed; thus, the deterioration of UVC-LEDs must be reduced.

The production of low-pressure mercury lamps is similar to that of fluorescent room lamps. To satisfy the Minamata Convention on Mercury by replacing low-pressure mercury lamps, an EL output of 100 mW for 2–3 US dollars must be targeted, keeping the cost-feasibility including the packaging in mind.



## 12. UVC LEDs with emission below 250 nm

Frank Mehnke<sup>1</sup>, Leo J Schowalter<sup>2,3</sup> and Tim Wernicke<sup>4</sup>

<sup>1</sup> Georgia Institute of Technology, School of Electrical and Computer Engineering

<sup>2</sup> Crystal IS Inc.

<sup>3</sup> Asahi Kasei Corporation

<sup>4</sup> Technische Universität Berlin, Institute of Solid State Physics

### 12.1. Status

Ultraviolet (UV) light emitting diodes (LEDs) in the UVC spectral region below 250 nm are of great interest as they, for example, enable *in-situ* sensing applications of diverse gases and liquids in industrial, medical, and automotive sectors. This includes the monitoring of nitrates in water, NO<sub>x</sub> and SO<sub>x</sub> in gas emissions, DNA purity analysis, and high-performance liquid chromatography.

Currently, such short wavelength LEDs are, in design and technology, similar to LEDs emitting around 270 nm grown on c-oriented AlN templates or substrates (see sections 2 and 3) but contain much higher aluminium mole fractions in the AlGa<sub>0.5</sub>N/AlGa<sub>0.5</sub>N multiple quantum wells (MQW) and n-side current spreading layers. The understanding of the n-type doping mechanisms of these high aluminium mole fraction layers enabled short wavelength LED emission down to the physical limit of AlN at 210 nm [128]. However, due to several material and heterostructure design challenges the external quantum efficiency (EQE) and wall plug efficiency (WPE) of such short emitting devices is exponentially dropping with decreasing emission wavelengths. As shown in figure 20 (left) one order of magnitude in EQE is lost for every 8 nm in reduced emission wavelength, i.e. 10<sup>-2</sup> at 242 nm, 10<sup>-3</sup> at 234 nm, 10<sup>-4</sup> at 226 nm, 10<sup>-5</sup> at 218 nm, and 10<sup>-6</sup> at 210 nm [63, 128–135]. This is attributed to a strongly decreasing radiative recombination efficiency ( $\eta_{\text{rad}}$ ), carrier injection efficiency ( $\eta_{\text{inj}}$ ), and light extraction efficiency ( $\eta_{\text{ext}}$ ) with decreasing emission wavelength and directly translates in reduced emission powers. In addition, the WPE is further reduced at short wavelengths since making contacts to high aluminium mole fraction AlGa<sub>0.5</sub>N is more difficult (see section 6). Another issue with these short wavelength devices is that their lifetime is often much shorter than their longer wavelength counterparts. A successful commercial product will need to address all of these issues.

Up to now there are only a few research reports on LEDs emitting below 250 nm [63, 128–135] and only a limited-release of LEDs at 235 nm is commercially available (see figure 20, right) [136]. In order to open the market for LEDs emitting below 250 nm which are considered to become much more cost-effective, small, robust, and persistent in comparison to discharge lamps both the efficiency and the emission power need to be improved. This will allow for applications such as gas sensing and enable new applications.

### 12.2. Current and future challenges

The main limiting mechanisms prohibiting higher emission powers and efficiencies of AlGa<sub>0.5</sub>N-based UV LEDs with emission below 250 nm are related to the low  $\eta_{\text{rad}}$ ,  $\eta_{\text{inj}}$ , and the low  $\eta_{\text{ext}}$  and to high operation voltages (leading to a limitation of the driving current and the WPE)—all of which need to be addressed in future research. Firstly,  $\eta_{\text{rad}}$  within the MQW active region is strongly connected to the threading dislocation density (TDD) favouring LEDs on low TDD monocrystalline AlN substrates. However,  $\eta_{\text{rad}}$  might also be reduced by an increasing point defect incorporation (see section 5) at these high aluminium mole fractions which is yet to be proven by measurements. Another potential issue is that  $\eta_{\text{inj}}$  into the MQWs decreases with decreasing emission wavelength as electron blocking becomes inefficient due to the smaller conduction band offset from the MQW to the AlN electron blocking layer (EBL). Furthermore, not only suppression of electron leakage but also supporting hole injection into the MQWs is a major challenge to the heterostructure design and the doping profile of the UV LEDs [134]. Finally,  $\eta_{\text{ext}}$  is reduced with decreasing wavelength due to the transition of the optical polarization of the emitted light from dominant transverse electric (TE) to dominant transverse magnetic (TM) [137, 138]. This is caused by valence band switching at an emission wavelength of around 240 nm and results in an emission pattern where photons tend to propagate parallel to the c-oriented surface. Consequently,  $\eta_{\text{ext}}$  through the substrate backside is reduced. Additional challenges arise by using monocrystalline AlN substrates as these may exhibit sub-bandgap absorption due to impurity incorporation during growth (see section 3) depending on the particular growth method employed [139]. Furthermore, the poor p-type doping of high aluminium mole fraction AlGa<sub>0.5</sub>N necessitates the usage of absorbing p-layers and p-contacts, which strongly reduces  $\eta_{\text{ext}}$ .

In order to further improve the WPE of UV LEDs with emission below 250 nm lower operation voltages are needed. In particular, a lower AlGa<sub>0.5</sub>N:Si layer resistivity and n-contact resistivity need to be achieved for high aluminium mole fraction layers. Both exhibit physical limitations due to the large bandgap of the material. The AlGa<sub>0.5</sub>N:Si layer resistivity is increasing with increasing aluminium mole fraction due to increasing donor ionization energy, DX-centre formation, and incorporation of compensating point defects (see section 7). The n-contact resistivity is increasing with increasing aluminium mole fraction due to a transition from Ohmic to Schottky behaviour due to the low electron affinity, a very stable oxide, a high probability of forming deep levels during plasma etching, and the difficulty in forming shallow donors during the contact formation process (see section 6).

Initial lifetime tests on sub-250 nm LEDs have suggested severely reduced lifetimes in comparison to longer wavelength UVC LEDs. In order to improve the lifetime of these device, the underlying mechanisms will need to be understood. However, an analysis of the degradation causes as well as a

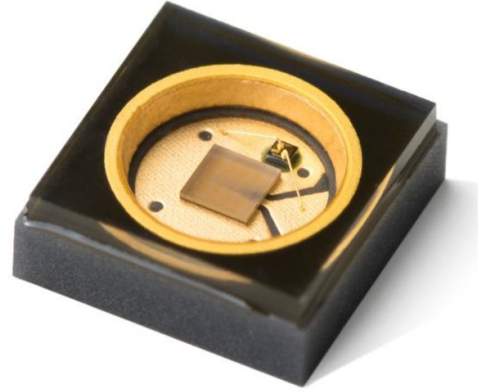
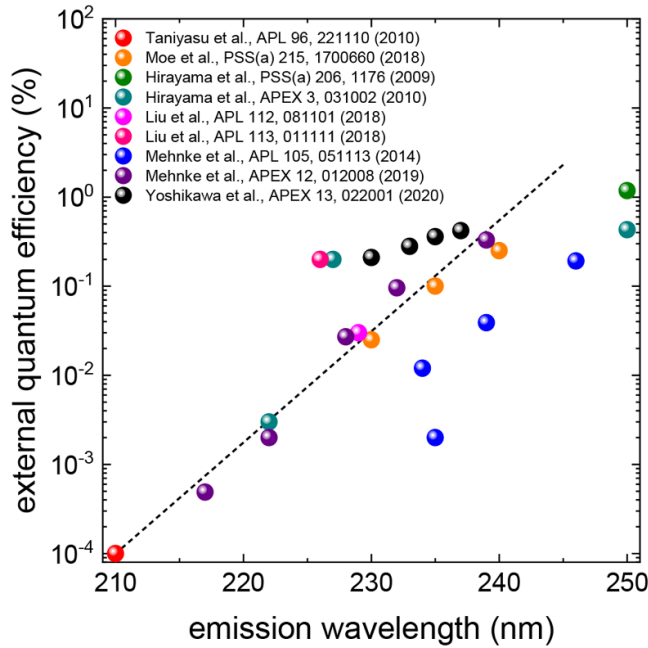


**Figure 20.** (Left) External quantum efficiency of state-of-the-art UVC LEDs indicating the exponential reduction for emission wavelengths below 250 nm [63, 128–135]. The wall plug efficiency of these short wavelength devices fall off even more sharply. (Right) Image of Optan™ 235 which is in limited release from Crystal IS [136]. The diode is  $3.5 \times 3.5 \text{ mm}^2$  in size with a  $0.8 \times 0.8 \text{ mm}^2$  size chip and is packaged in standard Optan™ SMD package. It is designed to be run at 20 mA at a forward voltage of 6 V with powers binned from  $50 \mu\text{W}$  to greater than  $500 \mu\text{W}$ . These devices are rated to have a lifetime over 1000 h.

variation of growth and fabrication processes parameters has only recently been initiated [140].

### 12.3. Advances in science and technology to meet challenges

In the future, higher emission powers with better WPE and lifetime are desired. Longer lifetimes can be expected with future heuristic and analytical studies as well as an improved point defect control. Additionally, lower TDD may also lead to longer lifetimes. However, there is only a limited amount of data currently available comparing devices grown on AlN templates with devices grown on monocrystalline AlN substrates. A reduction of the forward voltage requires further development of highly conductive n-AlGaIn layers by an improved control of the point defect density as well as low contact resistivity n- and p-electrodes especially by improved doping, novel contact metal stacks and improved surface treatments.

Future analysis of the LEDs will give insight to which portion the drop in EQE is related to  $\eta_{\text{rad}}$ ,  $\eta_{\text{inj}}$ , and  $\eta_{\text{ext}}$ , respectively, leading to a focus in the respective LED development. In order to improve  $\eta_{\text{rad}}$ , point defects resulting in nonradiative recombination in the active region can still result from the epitaxial growth conditions and further improvement is needed in this area. This measure will only be effective for growth on low TDD AlN, e.g. by growing LEDs pseudomorphically on monocrystalline AlN substrates with a TDD in the  $10^4 \text{ cm}^{-2}$  range [129]. The improvement of  $\eta_{\text{inj}}$  by a reduction of electron leakage needs to be obtained by clever heterostructure design, as the height of the EBL cannot be increased beyond the AlN bandgap and no larger bandgap semiconductor

material is currently known. This may be addressed by multiple quantum barrier EBLs [131] which can provide a larger conduction band offset in comparison to AlN and allow for hole tunnelling due to quantum interference. Advanced device simulations can provide the required design information, however, these calculations rely on several material parameters which are not well known and need to be further investigated. Furthermore, supporting the hole generation and injection needs to be mastered by heterostructure design and doping profile, e.g. the development of p-type polarization doping using aluminium mole fraction graded layers. It is also possible that new alloys such as AlBN (see section 8) may offer an advantageous band alignment allowing for improved  $\eta_{\text{inj}}$ . In any case, clever device designs will be needed to maximize both  $\eta_{\text{rad}}$  and  $\eta_{\text{inj}}$  simultaneously since improvement in one can also be made at the expense of the other.  $\eta_{\text{ext}}$  may be improved by shifting the optical polarization towards TE by tailoring the design of the MQW active region. The use of thin QWs and high aluminium mole fraction barriers has been demonstrated to increase TE emission at a given wavelength [137, 138]. Alternatively, growth of semi- and nonpolar MQWs might boost  $\eta_{\text{ext}}$  as the rotation of the crystal axis also leads to a rotation of the emission profiles [128], although currently the growth technology of such devices is much more immature compared to c-oriented ones. Nevertheless, the light extraction through the substrate can be improved for TE but especially for TM polarized light by one or multiple of the following approaches: (a) substrate removal, (b) substrate or bottom layer roughening, (c) pre- or post-epitaxial patterning of the buffer layers, i.e. epitaxial lateral overgrowth, patterned substrates, or photonic



crystals (see sections 13 and 14), as well as (d) encapsulation. A big boost in  $\eta_{\text{ext}}$  could be gained by the use of transparent p-doped short period superlattices combined with reflective p-electrodes especially if the penalty of higher forward voltage could be avoided. Also, new approaches such as p-Si nanomembranes [133] acting as reflective contact yielded excellent results and might push  $\eta_{\text{ext}}$  and  $\eta_{\text{inj}}$  to higher levels. Another promising approach to overcome the transparency-conductivity dilemma is the implementation of p-(i)-n tunnel junctions (see section 17). These offer the opportunity of using highly conductive and transparent AlGaIn:Si layers and n-electrodes, which overcomes several but not all challenges of p-AlGaIn.

#### 12.4. Concluding remarks

Improving the WPE, EQE and emission power of UV LEDs with emission below 250 nm cannot be performed by small single changes in the heterostructure design but requires manifold optimization and tradeoffs. These LEDs will benefit from technological improvements for longer wavelength LEDs, however, they will need additional development effort to solve

the specific challenges, additionally hampered by the smaller expected market size. The exponential decrease of the EQE with decreasing emission wavelength is fundamental and will persist in spite of strong improvements for each wavelength. Additionally, applications based on these LEDs can only be realized when the lifetimes of the devices can be guaranteed.

Major breakthroughs in device performance of UV LEDs emitting below 250 nm may be expected to occur by new design concepts. For example, the development of tunnel junctions or p-Si nanomembranes can resolve the transparency-conductivity dilemma, pushing the device performance of UV LEDs with emission below 250 nm to higher levels.

#### Acknowledgements

Funding by the German Federal Ministry of Education and Research (BMBF) within the ‘Advanced UV for Life’ project and by the Deutsche Forschungsgemeinschaft (DFG) within the Collaborative Research Center ‘Semiconductor Nanophotonics’ (SFB 787) is acknowledged. Crystal IS is a wholly owned subsidiary of the Asahi Kasei Corporation which provided funding for the ‘235 nm LED’ project.

### 13. Light extraction efficiency of UVC LEDs

Hideki Hirayama<sup>1</sup> and Yukio Kashima<sup>1,2</sup>

<sup>1</sup> RIKEN

<sup>2</sup> Marubun Company

#### 13.1. Status

High output power 265–280 nm commercially available UVC LEDs have flip-chip (FC) geometry, and UVC light is extracted through the sapphire or AlN single crystal substrate. The performance of a UVC LED with wavelength at 280 nm with 50 mW output power at a driving forward voltage ( $V_f$ ) of 5.5–7 V and a driving forward current ( $I_f$ ) of 350 mA exhibits an electrical power-to-light conversion efficiency (wall-plug efficiency; WPE) of about 2–3%. The detailed breakdown of the total WPE [2] is estimated to be approximately 60% for internal quantum efficiency (IQE) including injection efficiency ( $\eta_{inj}$ ), 80% for electrical efficiency ( $\eta_{el}$ ), and about 6–8% for light extraction efficiency (LEE) [2, 141].

For a deep-UV (DUV) LED, the fact that the LEE is particularly small compared to that of a blue LED is a very big problem. The main reasons for low LEE in a DUV LED are that DUV light is heavily absorbed by the p-GaN contact layer, and total internal reflection occurs at the interface between the LED body and air. Therefore, improving LEE is the most important subject and greatly contributes to the improvement of output power and WPE of DUV LEDs.

The LEE of a current DUV LED was calculated by the combination of the ray-tracing method and the finite-difference time-domain (FDTD) method [141]. Figure 21 shows the calculation models of flip-chip (FC) DUV-LEDs with Al reflector mounted on ceramic package for (a) a usual LED and (b) an LED with lens. The assumed layer structure for a current LED on the sapphire substrate consists of a 4- $\mu\text{m}$ -thick AlN, a 2  $\mu\text{m}$  thick n-AlGaIn buffer layer with emitting and electron blocking layers, a 1  $\mu\text{m}$  thick p-GaN contact layer and Ni/Au p-type electrode with a reflectivity of 30%. The polarization of the emitted light determining the radiation profile and LEE is influenced by the aluminium contents of well and barriers and the strain state of the material and dominated by transverse electric polarization for emission wavelengths >240 nm [142]. The reflectivity of the Al-coated reflector of the package is 90%. Using these conditions, the calculation result of LEE for a 280 nm UVC LED is 6.3% [141], which is in good agreement with the above estimated value.

#### 13.2. Current and future challenges

In order to achieve a significant increase of LEE, it is effective to introduce a p-AlGaIn transparent contact layer which is completely transparent to a wavelength of 270 nm instead of a p-GaN contact layer [4, 141, 143, 144]. It is also important to introduce a highly-reflective p-type

electrode [4, 143], e.g. p-type silicon [133], Pd(1 nm)/Al [145], Ni/Mg or rhodium [146] electrodes with reflectivity of >70%, instead of a Ni/Au electrode with reflectivity of 30% [141]. By introducing them, LEE improves more than twice and a calculated value of 13.1% was obtained [141]. However, since the hole concentration in the p-AlGaIn contact layer is  $1 \times 10^{14} \text{ cm}^{-3}$  or less and forward voltage ( $V_f$ ) rises by several volts [4], WPE cannot be greatly improved.

In order to improve LEE while maintaining WPE, thin p-GaN layers can be introduced. However, the LEE enhancement drops quickly already for thin GaN layers of 10–20 nm [115]. Therefore we propose forming a highly reflective photonic crystal (HR-PhC) in the p-GaN contact layer [141]. Figure 22 shows (a) a cross section of the schematic structure and (b) corresponding electric-field (E-field) mappings calculated by FDTD analysis and (c) the calculated results of LEE as a function of the distance from the quantum well (QW) emitting layer to a hole array PhC for 280 nm AlGaIn UVC LEDs with HR-PhC [141]. In addition, as a comparison, we also conducted the LEE enhancement simulation with a p-GaN-free structure, i.e. using a model of p-AlGaIn transparent contact layer with highly-reflective electrode [141]. In this case the radiation from the QW emitting layer does not penetrate into the PhC layer and reflected by the PhC, as confirmed from the cross-sectional E-field mappings shown in figure 22(b). In figure 22(c), we can confirm that with and without p-GaN the LEE is strongly enhanced especially when the vertical field resonant condition is satisfied. We found that the maximum increases in LEE enhanced by introducing the HR-PhC are by 2.8 and 1.8 times, respectively, for the p-GaN and p-AlGaIn contact layer UVC LEDs [141]. The maximum LEE of the p-GaN and p-AlGaIn contact layer 280 nm UVC LED with PhC were 18.0% and 23.8%, respectively.

#### 13.3. Advances in science and technology to meet challenges

As described above, when DUV light is emitted from the LED body into air, the DUV light is totally internally reflected at interfaces, and absorbed by a contact layer. Therefore, in order to increase the LEE of a DUV LED, it is quite important to use a low-absorption structure, e.g. by using a HR-PhC p-layer. When the absorption is low, the LEE is further enhanced by redirecting light into the light extraction cone within the semiconductor by p-side PhC [141], nanopatterned sapphire [4], structured AlN/sapphire [142, 147]. The total internal reflection at the substrate/air interface can be alleviated by directly bonding a hemispherical lens [123], encapsulation [4, 7] or hybrid nanostructuring [148]. In the model shown in figure 22(b), a quartz hemispherical lens is assumed to be directly bonded to the back surface of the sapphire substrate. The calculation results of LEEs of the 280 nm UVC LEDs with quartz hemispherical lenses are 13.1% and 28.3%, respectively, for the p-GaN and p-AlGaIn contact layer cases which is

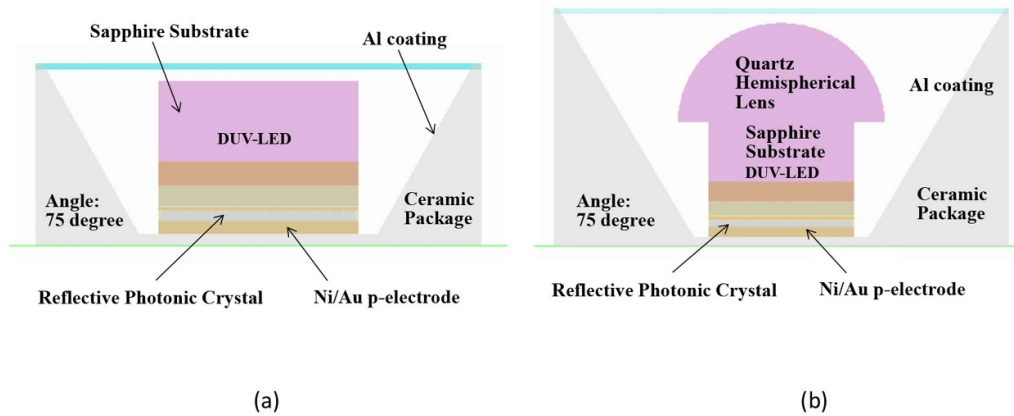


**Figure 21.** Calculation models of flip-chip (FC) DUV LEDs with Al reflector mounted on ceramic package for (a) a usual LED and (b) a LED with lens used for the analysis by the combination of ray-tracing and finite-difference time-domain (FDTD) methods.

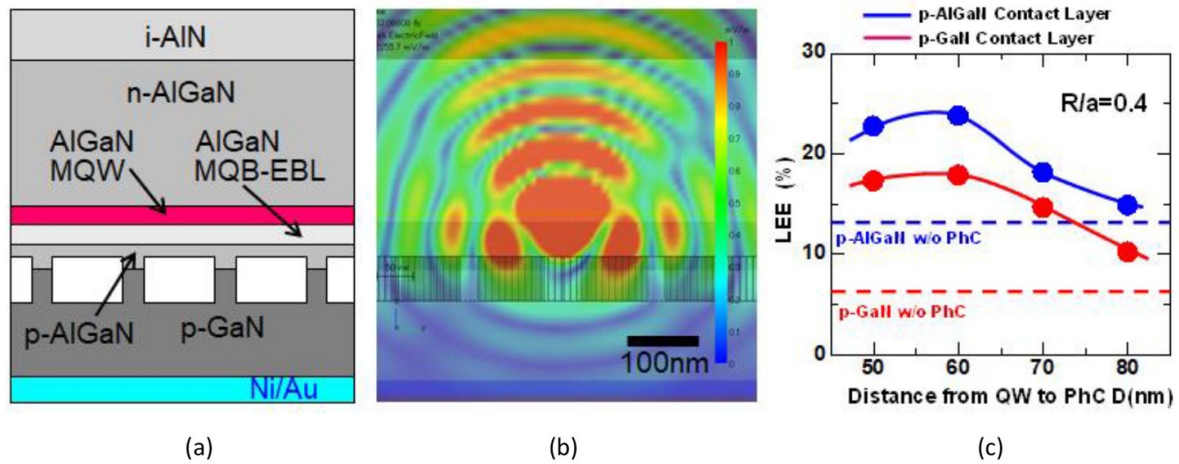


**Figure 22.** (a) Cross section of schematic structure and (b) corresponding electric-field (E-field) mappings calculated by FDTD analysis and (c) the calculated results of LEE as a function of the distance from the quantum well (QW) emitting layer to the PhC for 280 nm AlGaIn UVC LEDs with HR-PhC.

a strong enhancement compared to 6.3% and 13.1%, respectively. Indeed, a record high EQE of 20% was demonstrated for a 275 nm LED with transparent p-AlGaIn layer, reflective Rh contact and hemispherical encapsulation [4]. The main advancements which will lead to a widespread implementation of these light extraction techniques are reduction of the additional Voltage by improving the conductivity of p-AlGaIn (see section 7), demonstrating the reliability of such LEDs (methods described in section 16) and implementing low cost fabrication techniques.

#### 13.4. Concluding remarks

To date, the efficiency and the output-power of an AlGaIn DUV-LEDs are significantly limited by a low LEE, which is reduced by a strong absorption of a p-GaN contact layer. The LEE would be dramatically increased in near future by introducing an absorption-free contact layer, a highly-reflective p-type electrode, a reflective PhC fabricated on p-contact layer, by bonding lenses, by fabricating a vertical LED structure, and/or by combining these effects.

## 14. Nanostructuring for UV emitters

Philip Shields<sup>1</sup> and Robert Martin<sup>2</sup>

<sup>1</sup> University of Bath

<sup>2</sup> University of Strathclyde

### 14.1. Status

Reports of using nanostructures in UV-emitting devices have increased sharply over the past 5 years as they can potentially solve the existing obstacles for obtaining efficient nitride-based UV-LEDs [148–155]. They follow a longer and more substantial effort in the use of nanostructures to aid visible LEDs. We describe below some examples of how existing uses of nanostructures have overcome the following key issues: the influence of defects on the internal quantum efficiency (IQE); the poor light extraction efficiency (LEE) in planar UV-devices due to the emission of predominantly TM-polarized light from AlN-rich AlGa<sub>N</sub> and the high absorption in conventionally-used layers; and the difficulty in achieving efficient p-doping in AlGa<sub>N</sub> materials.

Firstly, annealing AlN nanostructures at high temperatures has been shown to improve the IQE in subsequent c-plane QWs by dramatically reducing the number of edge dislocations [150]. Laterally growing from these or other nanopatterned templates, such as sapphire or silicon, alongside the use of maskless techniques, permits the use of traditional epitaxial lateral overgrowth defect reduction techniques whilst coping with the poor mobility of Al species in the growth environment that traditionally leads to delayed coalescence and poor quality surfaces [151, 152].

Secondly, the presence of scattering interfaces in nano-ELOG structures also improves the LEE, which is especially important for AlN-rich AlGa<sub>N</sub> materials for which the valence band ordering enhances TM-polarization [153]. The nanoscale features can also promote strain relaxation, allowing strain engineering of the valence band to influence the dominant emission polarization as well as a potential improvement of the crystal quality.

Thirdly, the ability to manipulate strain and polarization in nanostructures has been employed to significantly increase the incorporation of the Mg p-dopant and enhance hole mobilities compared with Al(Ga)<sub>N</sub> planar films. For example, figure 23 shows nitrogen polar AlN nanowires grown directly on Si, which demonstrated increases in IQE and reductions in turn on voltage [154]. Highly conductive p-AlGa<sub>N</sub> can avoid the use of absorbing p-GaN, as in conventional UV LEDs, and increase both the electrical efficiency and reduce optical losses.

Finally, the nanostructuring of additional materials such as Al can lead to enhanced UV emission through the coupling of surface plasmons with the emitting dipoles [155]. Photonic crystal effects have also been incorporated into the nanopatterning of AlN surfaces to increase LEE in deep-UV LEDs, using nanoimprint lithography [148].

### 14.2. Current and future challenges

These examples show some different ways that nanostructuring can improve UV-emitting devices. However, simultaneously improving the IQE, LEE and electrical efficiency without introducing further detrimental effects remains a challenge. Following work in the visible regime, an ultimate goal might be the use of a regular and organized array of dislocation-free nanostructures as a scaffold for high-aspect-ratio core-shell nanorods arranged to ensure maximum light scattering from both TE and TM emission. Enhanced IQE due to the high crystal quality would be combined with strain-relaxed material for improved dopant incorporation.

Achieving this requires solving a number of challenges, with the bottom-up growth of AlGa<sub>N</sub> materials difficult due to the low mobility of Al species. Core-shell structures have traditionally required MOVPE growth, whereas most reports of AlGa<sub>N</sub> nanostructure growth have relied on MBE, using UV-absorbing GaN pedestals as nucleation seeds. Controlling the AlGa<sub>N</sub> alloy composition and dopant incorporation across the various crystal facets is an additional challenge. Furthermore, most lighting applications require a large number of parallel-driven nanorods and need a 3D contacting architecture. Any filling materials need to be non-absorbing, which becomes more challenging for emission further into the UV, as does achieving sufficient heat extraction and conductivity. Whilst the maturity of UV LEDs lags behind visible LEDs, they are sufficiently well-developed to be commercially available. 3D nanoscale LEDs will need to demonstrate unequivocally that their advantages can justify their more complex creation to have a chance to compete.

Alternatively, nanostructuring could be directed simply at improving IQE or LEE in planar devices. However, recovering a planar surface from nanostructured material requires carefully controlled coalescence to ensure a net reduction of extended defects and complete surface recovery to step-flow growth since AlGa<sub>N</sub> QWs are sensitive to any underlying roughness. A further challenge will be to simultaneously optimize both IQE and LEE as the ideal pattern for one is likely to compromise the other. One way of disentangling the effects is to improve LEE by employing nanostructuring after growing the active layers. Again, the benefits must outweigh the increased complexity of fabrication.

### 14.3. Advances in science and technology to meet challenges

To fully realize the potential benefits of nanostructuring for Al(Ga)<sub>N</sub> UV-emitters, various advances are needed. These include further steps towards achieving defect-free, bottom-up growth of AlGa<sub>N</sub> nanowires with controlled size, spacing and height, without relying on GaN seeding. As well as improving MBE approaches in this respect, a key advance will be expansion out to MOVPE, which will also allow easier scale-up. Further work should build on the use of polarization and strain relaxation to enhance doping. Hybrid approaches may



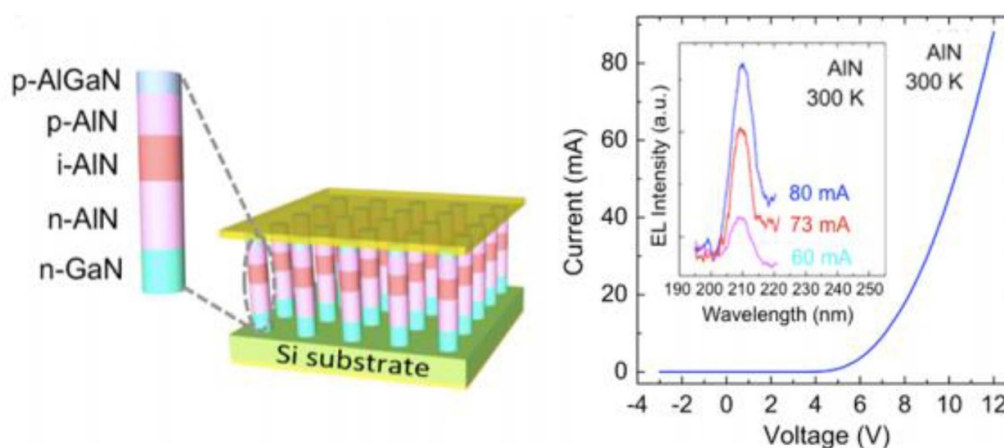


**Figure 23.** Electrical and electroluminescence results from an AlN nanowire LED. Reprinted by permission from Springer Nature Customer Service Centre GmbH: Science Reports [154] (2015).

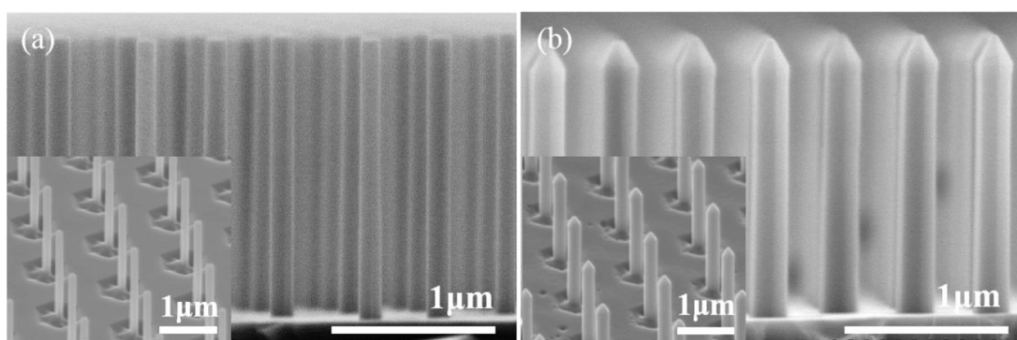


**Figure 24.** Cross-section SEM images of AlN nanorod arrays (a) after etching and (b) after subsequent MOVPE regrowth. Reprinted with permission from [156]. Copyright (2018) American Chemical Society.

be significant, for example building on the idea of the lateral re-growth of AlGaIn on etched AlN nanorods reported by Coulon *et al* ([156], figure 24). In this case, advances are required to increase the parameter space to grow high-quality non-polar material and improve precursor efficiency. Device designs and process flows optimized for performance and manufacture are required taking into account the specific vulnerabilities of electrical leakage and thermal management, where nanopatterned layers are to be used to create planar templates with reduced dislocation densities or for device structures, it is important to be able to balance dislocation bending with dislocation creation during coalescence of the neighbouring growth fronts. A deep understanding of the dislocation reduction process is required to achieve the best material quality for optimal LEE, additionally without having to resort to long growth runs.

Exploiting gratings or photonic crystal effects could help master the specific challenges in UV emitters but require the development of reliable techniques to manufacture the small nanostructure periodicities and the low edge roughnesses needed for the ultrashort wavelengths. Use of electron beam lithography is unlikely to be scalable, so large-area nanopatterning techniques such as nanoimprint and displacement Talbot lithography will likely become significant [157, 158].

Use of flip-chip processing to minimize optical absorption and improve thermal efficiency can be beneficially combined with use of nanopatterned material or arrays of nanowires grown on large area Si for commercial scale-up. Other promising directions are extending nano-patterning to substrates beyond sapphire or growing Al(Ga)N on layered transition metal dichalcogenides, such as MoS<sub>2</sub>, on sapphire with a view to overcoming challenges associated with lattice and thermal expansion mismatches [149].

Effort should be applied to further exploit plasmonic effects as they have been shown to be effective in enhancing light emission. Advances in modelling and fabrication are required to optimize the positions of metal nanoparticles to enhance TE-emission and LEE, even to positions within the active regions themselves. Whilst Al is typically used in the UV, advantage could be obtained by using other non-oxidizing materials such as Rh.

There will also be challenges to overcome for advanced characterization methods, such as mapping of dopant incorporation in core-shell nanorods, perhaps using optical signatures to aid their rapid development. Developments with techniques such as cathodoluminescence and atom probe tomography for nanopatterned UV materials will accelerate progress.



#### 14.4. Concluding remarks

There are a number of reports that have signalled the promise of nanostructuring to potentially solve longstanding issues in planar UV emitters. Whilst the field is in an early stage, it has accelerated at a phenomenal rate and it will not be a surprise if many of the challenges are surmounted in the next few years. Particular game changers would be: the successful bottom-up growth of regular arrays of non-absorbing and dislocation-free AlGaIn nanostructures, a detailed understanding of the effect of polarity and strain on enhanced Mg incorporation for different AlGaIn compositions, the convergence on an optimized 3D device architecture, and a routine capab-

ility to pattern materials with sub-100 nm resolution. Following that, the question will be whether nanostructured materials can be made in the multi-wafer growth reactors for commercial manufacture with sufficient yield to challenge conventional planar devices. This may be the toughest challenge of them all.

#### Acknowledgements

The authors wish to acknowledge funding from the Engineering and Physical Sciences Research Council (EPSRC), UK, Grant No. EP/M015181/1, 'Manufacturing of nano-engineered III-nitride semiconductors'.

## 15. Simulation of UV-light emitting diodes and lasers

Bernd Witzigmann<sup>1</sup>, Friedhard Römer<sup>1</sup> and Yuh-Renn Wu<sup>2</sup>

<sup>1</sup> University of Kassel

<sup>2</sup> National Taiwan University

### 15.1. Status

Optoelectronic device simulation is a multi-scale, multi-physics task. Optical, electronic, and thermal properties, and their interaction govern the characteristics. Nano-scale regions require ideally atomistic methods, but electrical contacts, thermal reservoirs or optical resonators are often on the macroscopic scale. For lasers and LEDs in the III-nitride system, numerical simulations are routinely done nowadays as a guideline to design the device specifications, which starts from the epitaxial layers for optimum waveguiding and carrier injection (see figure 25), and carrier-photon interaction, up to the chip processing for placement of contacts, or light outcouplers (such as facet coatings or anti-reflection structures). A comprehensive, but probably still incomplete overview of the large variety of numerical codes can be found in [159], and the main approaches are as follows. The most widely used models are based on the drift-diffusion currents in combination with continuity equations for electrons and holes, and the electrostatic potential being evaluated by a Poisson equation. This coupled nonlinear system can be discretized in up to three dimensions, and solved efficiently with a Newton type iterative method. Besides the current-voltage characteristics, one can study local current densities, recombination rates or carrier mobilities. For quantized regions, a single particle Schrödinger equation can be coupled to this system, also with decent convergence behaviour. Recent works on solving Schrödinger equations with the localization landscape theory to obtain the effective quantum potential provide an efficient tool to combine the semi-classical theory with quantum effects [160]. For non-equilibrium carrier transport, the Monte-Carlo method has been applied to LEDs, solving the semi-classical Boltzmann equation. While including non-equilibrium transport, it requires massive computational resources, and lacks a consistent inclusion of quantum effects. A full non-equilibrium quantum mechanical simulation has been realized with the non-equilibrium Green's function method, however again with large computational cost, and no model for non-radiative recombination [161].

The optical part requires numerical methods for solving Maxwell's equations, such as finite element, finite difference methods or ray tracing approaches. Here, the challenge is to include the interaction between the electromagnetics and the electronics, which occurs via stimulated and spontaneous emission, or absorption.

For application to device design and analysis, active research on the models, equation frameworks and material parameters goes along with the advancement of material synthesis and technology capabilities. This is currently the case

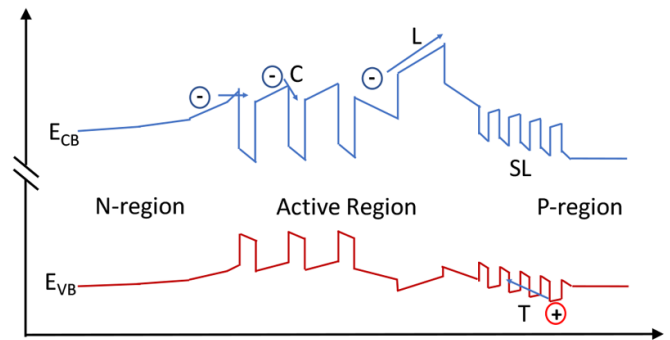


**Figure 25.** Schematic of conduction and valence band in a UV-LED. Carrier injection is influenced by tunnelling (T), capture (C) and leakage (L). On the p-side, a superlattice (SL) supports dopant activation in AlGaIn alloys. The active region consists of three quantum wells, alloy fluctuations will modulate the band edges, but are not shown for clarity here.

for III-nitride based light lasers and LEDs emitting at ultraviolet wavelengths. For their InGaIn based counterparts, simulations, in combination with numerous experiments, have contributed significantly to pushing the electro-optical efficiencies and wavelength coverage in the visible close to optimum values. As example, numerical simulations of the quantum confined Stark effect have clarified the impact of polarization charges at interfaces. Also, the characteristics of devices on semi- and non-polar crystal orientations have been studied in great detail by microscopic simulations. With this knowledge, the potential performance gains compared to polar devices could be studied. The efficiency droop has been studied using various models, which have helped identifying the role of leakage currents and Auger recombination [162].

### 15.2. Current and future challenges

Experimental data for III-nitride based UV LEDs currently exhibit low quantum efficiencies, high operation voltages and low optical extraction efficiencies. UV light emitters in the III-nitride system differ from their counterparts emitting in the visible range mostly by the extensive use of AlGaIn and AlN layers. This introduces alloy fluctuations in the entire device, and a different set of impurities and defects. The peculiarities of AlGaIn with high aluminium mole fractions have not been studied in detail, and the existing models calculating the laser or LED performance have not been tested to large extent. The major challenge for the simulation models will be to quantitatively explain the efficiency characteristics, and come up with proposals for high performance laser and LED structures. For strain, continuum models might not be able to represent the local strain due to alloy fluctuations properly. Impurity modelling in III-nitrides is another challenging field, as these materials show high luminescence in the presence of defects. Most of the AlGaIn related studies have been done for high electron mobility transistors, and while models for bulk and interface impurities are available in drift-diffusion based simulations, it is not clear how valid they are for UV light emitters. For silicon devices, the simulation of the process technology has resulted

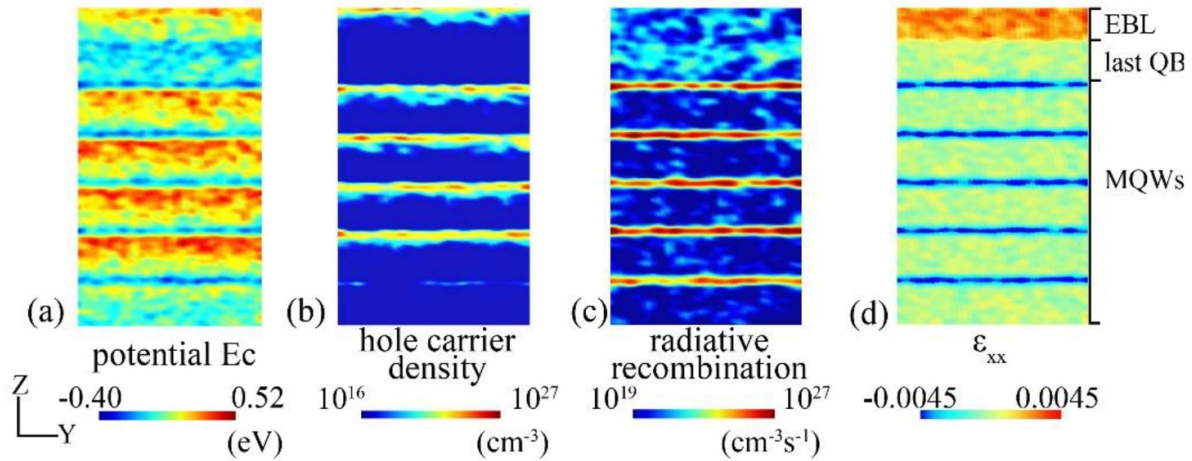


**Figure 26.** (a) Calculated fluctuated potential  $E_c$  of UVC-LEDs by considering the random alloy fluctuation in EBL, QBs, QWs, and even the injection layer. (b), (c) Hole density and radiative recombination, which is clearly affected by random alloy fluctuation. (d) Calculated strain  $\epsilon_{xx}$  in the QW. Due to the fluctuated composition and local strain relaxation, the compressive strain of QW has been relaxed at the interface, which may not be good for TE emission [164].

in a more accurate representation of the structural properties of the devices as input to the device simulation [163]. LED and laser simulation in the III-nitride system would benefit greatly from a process simulation, but is far from being established.

### 15.3. Advances in science and technology to meet challenges

AlGa<sub>N</sub> crystallizes in the anisotropic wurtzite lattice and is a direct semiconductor for all compositions. Calibrated sets of parameters for modelling the electronic band structure and the influence of strain with the kp-Schrödinger method exist [164]. The luminescence polarization changes from perpendicular to parallel to the c-lattice direction with increasing aluminium content. In thin film structures grown along the c-lattice direction TM-polarized radiation dominates above 5.2 eV. AlGa<sub>N</sub> exhibits spontaneous and piezoelectric polarization in the c-direction leading to sheet charges at hetero interfaces. The growth conditions of AlGa<sub>N</sub> material lead to alloy fluctuations. Ternary AlGa<sub>N</sub> layers build not only the active region, but also the carrier injection regions. The influence of local fluctuation on UVCLEDs has been analysed in [164] with 3D Poisson, drift-diffusion and localized landscape model [160] to account the effect of quantum potential. Figure 26 shows the cross section view of band profile, hole density, radiative recombination, and strain distribution. The preliminary results show that IQE is strongly affected by disorder as the blue LEDs. The poor hole injection due to low activated dopant and weaker blocking ability of the EBL caused by the fluctuating potentials may lead to strong droop effect. Furthermore, as shown in figures 26(b) and (d), Carriers are less confined in the QW and extend into the QBs due to the alloy potential fluctuations. The hole wave function extension into the QBs will enhance TM emission as shown from a k.p simulation of wave-functions admixture, which should then lead to poor light extraction. These preliminary results show that future simulation model should take this effect into account

for the whole structure, which leads an even higher computation burden if a full atomistic model is applied.

Carrier injection in principle suffers from the low hole mobility in p-doped AlGa<sub>N</sub> alloys, and the high ionization energy in excess of 0.5 eV for Mg acceptor atoms. Superlattices made of alternating thin layers with different band gap have been devised for enhancing the hole density and injection. Carriers in the superlattice are subject to quantization and minibands evolve due to the periodicity. The minibands and the polarization induced potential reduce the ionization energy and thus increase the hole density. The modelling and design of superlattices requires a quantum mechanical approach. Miniband dispersion relations have been calculated with the Kronig–Penney model [166]. The non-equilibrium Green's function method enables superlattice transport modelling.

### 15.4. Concluding remarks

While the basic equations for carrier transport and electromagnetics have been established, accurate material parameters and the impact of impurities still need improvement for UV light emitters. Parameters can be determined either by experiment or by *ab initio* simulations. A close collaboration between the communities in materials characterization and materials theory is beneficial in order to verify parameters and establish a general understanding of the device physics. *Ab initio* simulations for determining material and model parameters have given many valuable data for the device simulation community, such as Auger coefficients for GaN [167], or dopant activation in AlGa<sub>N</sub>. In the future, advanced methods beyond pure bulk computations will help understanding interfaces and quantum wells. In the field of materials characterization, techniques such as atomic probe tomography can resolve the structural and recombination properties of the device on an atomic level [168]. This will lead to much improved understanding of the optoelectronic properties.

## 16. Reliability of UV LEDs

Carlo De Santi<sup>1</sup>, Matteo Meneghini<sup>1</sup>, Johannes Glaab<sup>2</sup>, Jan Ruschel<sup>2</sup> and Sven Einfeldt<sup>2</sup>

<sup>1</sup> University of Padova

<sup>2</sup> Ferdinand-Braun-Institut, Leibniz-Institut für Höchstfrequenzte

### 16.1. Status

In order to enable a wide market acceptance of UV LEDs, these devices need to be stable over typically several thousand hours of operation. For the time being, the lifetime of UV LEDs cannot yet keep up with their visible counterparts. Nevertheless UVB and near UVC LEDs with L70 lifetimes (time until 70% of the initial optical power is reached) in the order of 10 000 h have been demonstrated on commercially available devices. On the other hand the lifetime of state-of-the-art deep UVC LEDs with emission below 250 nm is still short [135]. Usually, during constant current operation, several degradation effects can be observed in parallel, including (i) a reduction in optical power, which is rapid within the first hundred hours and slower for longer operation times (see figure 27(a)); (ii) a variation of the operating voltage (see figure 27(b) for voltages >4 V); (iii) an increase in the leakage current (see figure 27(b) for voltages <4 V); (iv) changes in the spectral purity [169]; (v) catastrophic failure (devices suddenly stop working) [170]. Furthermore, it was found that typically the degradation is accelerated by the operation current [171, 172] (figure 27(a)) and temperature [171].

So far, the main focus of most of the degradation studies has been on semiconductor issues of the UV LED chip. Here, the discussed possible physical causes of the degradation include:

- (i) The generation of defects driven by current and temperature; such defects form deep levels and behave as centres for non-radiative Shockley–Read–Hall recombination. For example, the degradation was correlated to an increased density of midgap states in 308 nm UVB LEDs [173].
- (ii) The migration of defects through the heterostructure [174]. Some authors reported on the migration of hydrogen [175] (see figures 28(b) and (c)) or aluminium [176]. Dislocations or V-pits and the electric field were proposed to enhance the migration.
- (iii) The pile-up of charges at heterointerfaces due to the generation and/or diffusion of defects that can affect the injection or escape efficiency of charge carriers [177].
- (iv) Changes in the charge distribution within the doped regions due to activation/compensation processes [135, 178].

### 16.2. Current and future challenges

To narrow down critical issues in the fabrication chain and to localize the degradation effects in the device are important aspects of current and future research on the degradation of UV LEDs. Therefore, empirical studies of the impact of heterostructure design (e.g. design of the electron blocking layer), epitaxial growth (e.g. variation of substrates), chip

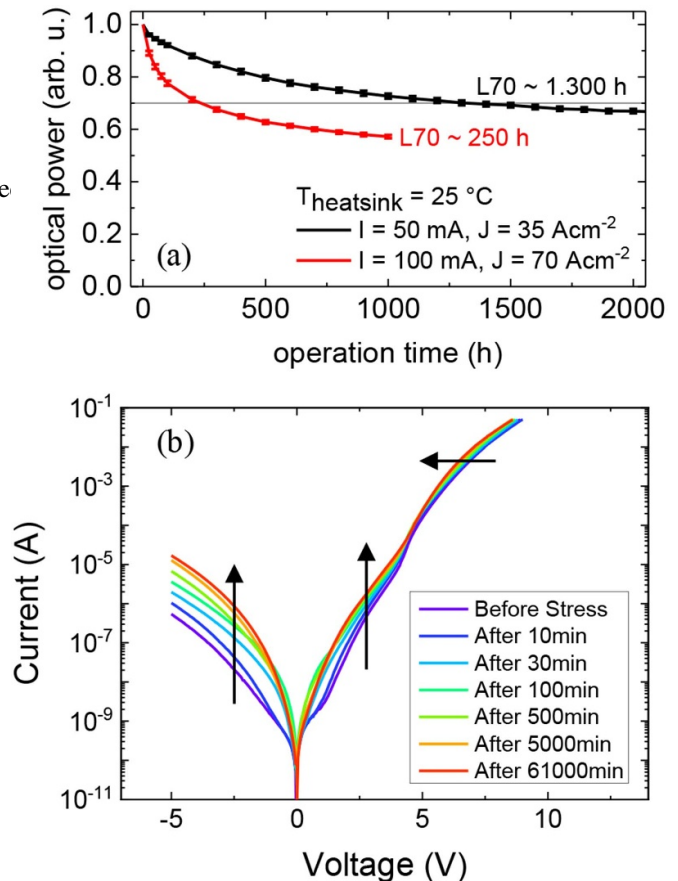


**Figure 27.** (a) Optical power (normalized to the value at 0 h) as a function of operation time of UVB LEDs operated at 50 mA and 100 mA, respectively, and 25 °C. The L70 values indicate the time at which the optical power of the LEDs reached 70% of its initial value. (b) Current-voltage characteristics of UVB LEDs measured after different operation times over 1000 h of operation at 100 mA and 20 °C.

design (e.g. different insulator materials) and of chip fabrication and mounting on degradation are ongoing with the goal of enhancing device lifetimes.

Another essential aspect is to analyse the degradation mechanisms and stress-induced changes in the devices in order to understand the physics behind. Here the identification and localization of defects causing deep levels in the semiconductor are the key issue (see section 5). Important techniques to study the density and the energy of these levels are the capacitance and optical deep level transient spectroscopy (C-DLTS and O-DLTS, see figure 28(a)), deep level optical spectroscopy, photocurrent spectroscopy and analysis of the low frequency noise. The structure of emerging defects, their changes and motion can be studied by techniques as transmission electron microscopy, secondary ion mass spectrometry (SIMS), cathodoluminescence, or electron beam induced current.

Considering the future use of UV LEDs, new aspects might be important. For example for applications which require the LED wavelength to stay in a certain spectral window, operation-induced parasitic emission bands lowering the spectral purity might be unacceptable, even if other electro-optical



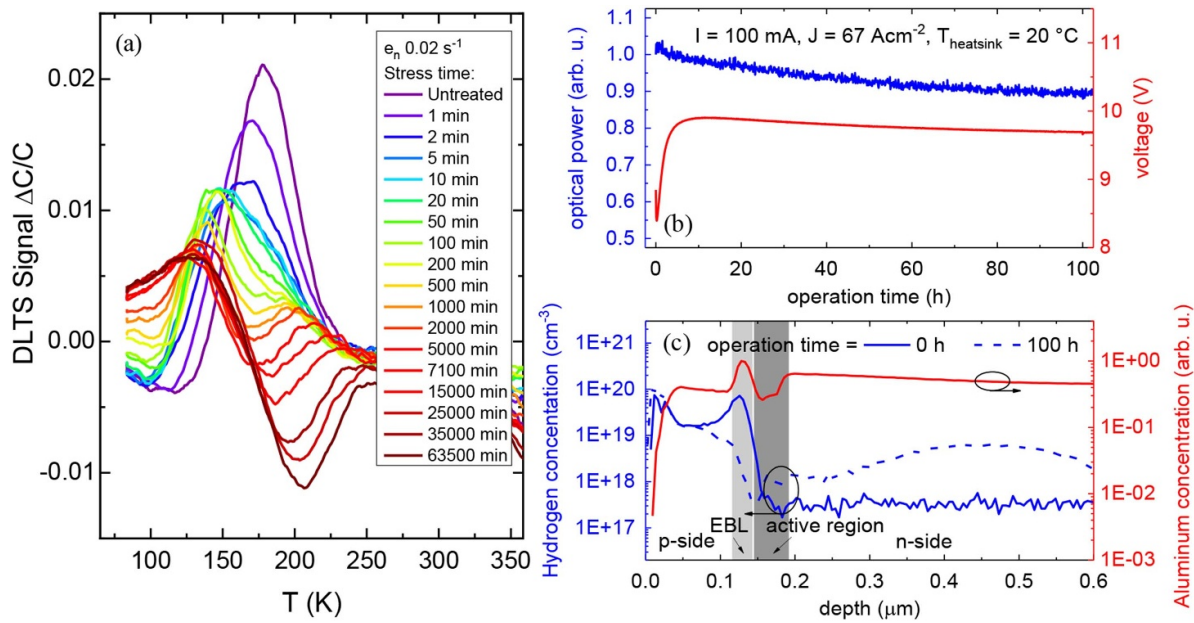


**Figure 28.** (a) Variation in C-DLTS signal in a 308 nm LED stressed at 100 mA. (b) Optical power and drive voltage as a function of operation time of one InAlGaN-based UVB LED operated at 100 mA and 20 °C. (c) Corresponding depth profiles of the LEDs shown in (b) of the H-concentration (blue curves) at 0 h and 100 h of operation as determined by SIMS. The Al concentration profile (red curve, normalized to the max. value) is for the calibration of the depth.

parameters stay constant. Also, it is worth studying approaches to make the devices less sensitive to temperature or to switching. Certain applications may require studying the influence of the environmental gas or of ionizing radiation. For the use of UV LEDs in a harsh environment, packaging issues will be critical. Therefore, the impact of the UV radiation and the large amount of generated heat on the stability of encapsulation materials and optical reflectors used in the package have to be considered. Recently, a photon-induced generation of point defects that takes place even without any applied bias was reported for GaN-based devices [179] and could turn out to be relevant also in AlGaIn-based UV LEDs.

Future UV LEDs may make use of new device concepts such as tunnel junctions (see section 17) or polarization p-type doping which could result in unforeseen reliability issues.

### 16.3. Advances in science and technology to meet challenges

To improve device reliability, advances in clarifying the nature of the relevant defects and in understanding how they form and change during device operation are needed. Despite first studies showing that the defects form deep level acceptors [173], only little is known about the defect structure, i.e. whether it is an isolated vacancy or impurity, a complex of point defects and whether dislocations are involved. The charge state and the density of the defects are unknown as well. Therefore, spatially resolved measurement techniques, particularly luminescence studies, are needed at different stages of the degradation process. As the generation or activation of defects requires the supply of energy [175], hot carriers could be involved [172]. The generation of hot carriers in blue LEDs has already been

verified and attributed to Auger recombination by Iveland *et al* [180]. A similar study on UV LEDs is missing.

Moreover, additional work is needed to reduce the initial concentration of point defects and to suppress their migration, which could for instance be achieved by specific epitaxy techniques or conditions and by optimizing post-growth processes such as the activation of p-type conductivity. The introduction of additional layers into the heterostructure acting as migration barriers could be of interest as well.

Degradation could possibly be reduced through specific device concepts. For example the temperature and current density could be lowered and made more uniform by increasing the size of the active area. Additionally, an enhanced hole injection efficiency could reduce the excess of electrons with respect to holes in the active region, which may trigger the formation of defects if Auger recombination is involved.

Finally, it is mandatory to develop and improve the mathematical models that describe the performance of UV LEDs [135, 172, 181]. For example, De Santi *et al* proposed a simple model for the temperature dependence of the emission spectrum of UVB LEDs [181]. Such models can be used for the analysis of the variation in performance at increasing stress time, and can eventually be extended to predict the LED lifetimes under different operation conditions.

### 16.4. Concluding remarks

Before LEDs become competitive in the market of UV light sources, the origin of their degradation should be understood to improve their lifetime. The reduction in optical power in current UV LEDs is most likely dominated by a generation



of deep-level acceptor states in the active region of the semiconductor heterostructure, which form non-radiative recombination centres. This process may be connected with a migration of point defects within the junction. Further studies are needed to understand the involved physical mechanisms. Both an empirical optimization of the device reliability and an analysis of the involved physical processes are required.

#### *Acknowledgements*

The authors would like to thank all colleagues at the University of Padova, at the Ferdinand-Braun-Institut and at the Technis-

che Universität Berlin for their contributions in the study. This work was partially supported by the German Federal Ministry of Education and Research (BMBF) through the consortia project ‘Advanced UV for Life’ and the Deutsche Forschungsgemeinschaft through the Collaborative Research Center ‘Semiconductor NanoPhotonics’. At the University of Padova, this work was supported in part by the INTERNET OF THINGS: SVILUPPI METODOLOGICI, TECNOLOGICI E APPLICATIVI project, co-founded (2018–2022) by the Italian Ministry of Education, Universities and Research (MIUR) under the aegis of the ‘Fondo per il finanziamento dei dipartimenti universitari di eccellenza’ initiative (Law 232/2016).

## 17. Tunnel junction-based UV LEDs

Siddharth Rajan and Yuewei Zhang

The Ohio State University, Columbus, OH

### 17.1. Status

The major factors limiting UV LED efficiency are the poor light extraction efficiency and low carrier injection efficiency. Both of them are closely related to the low p-type AlGaIn conductivity and high p-type contact resistance. Heavily doped p-GaN layers typically grown on top of p-AlGaIn to enable hole injection lead to significant absorption losses, and poor light extraction efficiency. Alternate strategies involving p-type metal contacts to p-AlGaIn [4] lead to significant improvement in the light extraction efficiency, but cause high electrical losses due to substantial increase in the operation voltage. Therefore, simultaneous improvement in the electrical efficiency and light extraction efficiency is intrinsically limited for the conventional device structures, and has remained a major challenge for the UV LED community. Tunnel-injected UV LED structures can enable non-equilibrium hole injection through transparent AlGaIn layers, and enable better light extraction, thus simultaneously enabling low absorption and electrical loss.

Realizing efficient tunnel junctions (TJs) becomes more challenging as the bandgap of the semiconductor is increased. Recent work [182–184] has shown that efficient interband tunnelling hole injection is feasible using tunnel junction structures where the spontaneous and piezoelectric polarization charges are used to create extreme electric fields [185]. These polarization sheet charges can create band-bending across nanometre-scale lengths, thereby reducing the tunnelling barrier and increasing tunnelling probability (figure 29(a)). This, and other innovations in semiconductor heterostructure design [186] have enabled high tunnelling conductivity to be achieved for bandgaps as high as 5.4 eV, with demonstrations of ultra violet LEDs for wavelengths as low as 257 nm (figure 29(b)) in planar films [187], and 242 nm in nanowires [188]. The availability of such tunnel junctions is especially important for shorter wavelength (high Al-content films) since the thermally activated hole concentration decreases dramatically with increasing Al content in the p-AlGaIn layer.

Interband tunnel junctions have the potential to enable ultra violet LEDs with power density and efficiency greatly exceeding state-of-art devices today. They could enable more efficient light extraction strategies for AlGaIn-based UV LEDs by taking advantage of the transparent top and bottom n-AlGaIn contacts, and the use of UV-reflective n-type contacts. Furthermore, the low sheet resistance of n-AlGaIn could enable new light extraction strategies, similar to those used for visible LEDs. Finally, electrically injected lasers have been a long-standing challenge [189]. While lasing at wavelength as short as 271.8 nm under pulsed current was recently demonstrated [190], the devices showed high threshold current and poor emission power due to the deficit in hole injection.

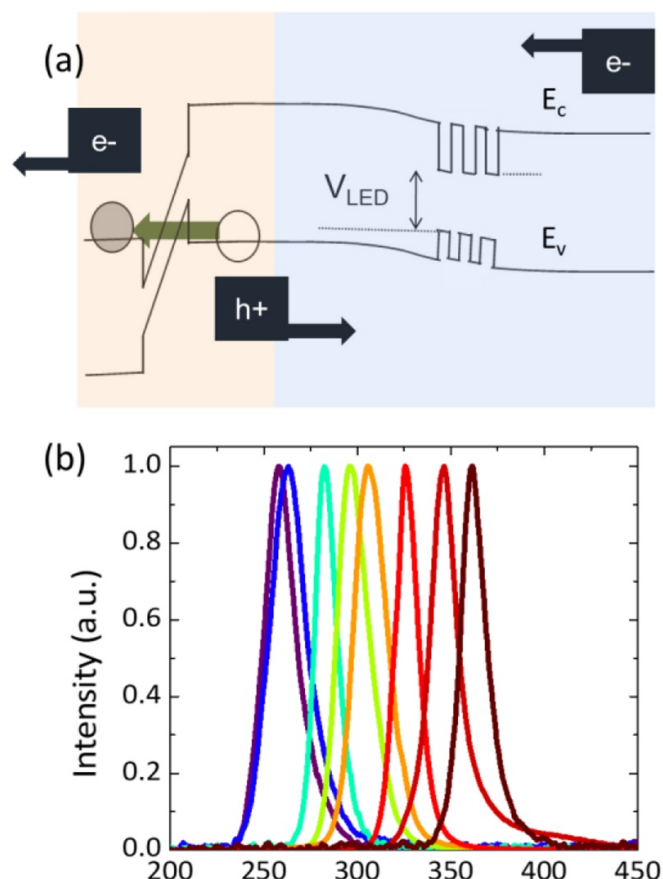


**Figure 29.** (a) Schematic energy band diagram of a tunnel-injected UV LED structure under forward bias. (b) Summary of the emission spectra achieved in tunnel-injected UV LEDs. Reprinted with permission from [187]. Copyright (2018), AIP Publishing LLC.

There are several potential applications for tunnel junctions in such devices, since they could enable efficient hole injection as well as a much thinner p-AlGaIn layer, thereby lowering p-type conduction resistance, and reducing free carrier losses. However, each of these areas require a concerted effort to improve understanding of growth physics, transport, doping, and optical characteristics.

### 17.2. Current and future challenges

Even though tunnelling hole injection has been demonstrated to be feasible, several challenges remain to be addressed before we can realize the potential of tunnel-injected UV LEDs. While metalorganic vapour phase epitaxy (MOVPE) is the most technologically mature growth technique for UV LEDs, it brings some unique challenges for the growth and fabrication of tunnel-injected UV LED structures. The existence of hydrogen atoms in the MOVPE chamber leads to passivation of the Mg acceptors. The n-type top contact layer in the tunnel-injected UV LED structure impedes hydrogen diffusion, making it difficult to achieve Mg activation. To circumvent this problem, lateral Mg activation from etched sidewalls was developed for MOVPE-grown tunnel-injected blue LEDs [191]. However, these tunnel junction based visible LEDs have

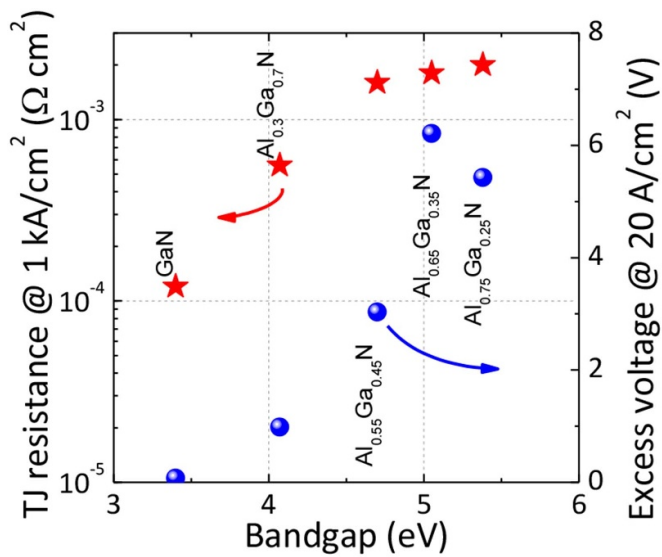


**Figure 30.** Summary of AlGaIn tunnel junction (TJ) resistance and the excess voltage drop measured for tunnel-injected UV LEDs. Reprinted with permission from [187]. Copyright (2018), AIP Publishing LLC.

shown higher turn-on voltage and differential resistance when compared to standard LEDs with metal ohmic contacts.

Another challenge comes with the growth of the tunnel junction layer using MOVPE. The large difference in the growth temperature between AlGaIn and the thin InGaIn layer adopted in the tunnel junction structure could lead to decomposition and intermixing of the InGaIn layer, resulting in poor tunnel junction performance. In comparison, molecular beam epitaxy (MBE) growth does not require p-AlGaIn activation after growth, and provides much lower growth temperature difference between AlGaIn and InGaIn layers. However, recent work [192] demonstrates promising results from all-MOVPE based LEDs that could suggest a future pathway for UV emitters based on tunnel injection.

Low tunnel junction resistance values below  $2 \times 10^{-3} \Omega \text{ cm}^2$  have been achieved for ultra-wide bandgap AlGaIn with Al content up to 70%. However, a substantial increase in the excess voltage drop is observed as the AlGaIn bandgap increases in the tunnel junction structure as shown in figure 30. Even though polarization engineering has been utilized to shrink the tunnel barrier through the insertion of an ultra-thin InGaIn layer between p+ and n+-AlGaIn layers, the large conduction band and valence band offsets at the heterointerfaces lead to extended depletion barriers for interband tunnelling [186]. Increasing the Al content in the AlGaIn layers leads to further increase in depletion barriers and reduced tunnelling probability. Therefore, a detailed understanding of the mechanisms in the tunnel junction layer is necessary to reduce the excess voltage drop. Furthermore, although tunnelling injection potentially reduces internal light absorption loss, there remains a severe limitation on the light extraction efficiency due to the lack of good encapsulants and reflective metals in the UV wavelength range.

### 17.3. Advances in science and technology to meet challenges

To fully exploit the advantages of tunnel-injected UV LEDs, fundamental scientific and engineering studies related to growth science, carrier transport, and optics are needed. One promising solution could be a hybrid growth method employing both MOVPE and MBE growth techniques. The epitaxial nucleation, thick n-AlGaIn bottom contact layer and the active region can be grown using MOVPE, while growth of the tunnel junction layer and the n-AlGaIn top contact layer can be done using MBE to exploit the high doping concentrations and the sharp heterointerfaces. This method would combine the high internal quantum efficiency of MOVPE-grown active regions with high electrical injection efficiency of the tunnel junctions grown by MBE. Alternately, further investigation of MOVPE-based tunnel junction design and growth, and study of p-AlGaIn activation could lead to solutions that take advantage of the relative maturity and performance of MOVPE growth.

In either case, it is critical to develop a better understanding of interband and intra-band tunnelling phenomena so that future designs can minimize voltage and resistance loss in tunnel-injected UV LEDs. For example, the introduction of high density polarization charges to reduce the depletion barrier was shown to reduce resistance due to conduction and valence band mismatch in p-AlGaIn/InGaIn/n-AlGaIn tunnel junction structures [186]. Background compensating charges, such as unintentional impurities or native defects, were found to be responsible for the extended depletion barriers in the tunnel junction layer. Therefore, growth optimization to reduce the compensating charge density could be critical for highly efficient interband tunnel junctions. Further improvement in the tunnelling probability could be achieved by exploring the doping limit in AlGaIn layers and by shrinking the interband tunnelling barrier.

The tunnel-injected UV LED structure minimizes the internal light absorption loss, making it possible to substantially improve the light extraction efficiency. Due to the high photon energy emitted from the UV LEDs, it is challenging to find transparent encapsulation materials with long operation lifetime. The tunnel-injected UV LED structure does provide flexibility to explore novel designs for light extraction and device packaging that are free from the widely used packaging materials. For example, tunnel junctions could allow for introduction of high reflectivity metal contact layers and specifically designed mesa structures to enable enhanced light extraction efficiency for both TE and TM polarized light.

### 17.4. Concluding remarks

Tunnel-injected UV LEDs employing interband tunnel junctions for non-equilibrium hole injection hold great promise for high performance UV emitters. AlGaIn tunnel junctions

have been demonstrated for emission in AlGaIn-based LEDs in wavelengths down to the UVC spectrum. While tunnel-injected UV LEDs emitting across the UV spectrum have been demonstrated, several opportunities still exist for improving the performance of the tunnel junctions, understanding the fundamental semiconductor physics in these structures, and for enhancing light extraction efficiency. A better understanding of these aspects could enable disruptive advances in solid

state ultraviolet sources, and have significant impact on downstream applications.

#### *Acknowledgements*

We acknowledge funding from the National Science Foundation (Nos. ECCS-1408416 and PFI AIR-TT 1640700) and the OSU TCO Accelerator Award.



## 18. E-beam pumped emitters

Thomas Wunderer

Palo Alto Research Center, Inc., Palo Alto, CA

### 18.1. Status

As we have seen in the previous sections, the challenges of realizing useful p-type doping in the ultra-wide bandgap AlGaIn materials limit the performance of UV emitters. Using high-energy electron beam excitation as an alternative pump strategy for the generation of electron-hole pairs can circumvent many of the issues encountered in conventional p-n-junction configurations. When using e-beam excitation, electron-hole pairs are created through a sequence of scattering events within the semiconductor material that obviate the need for p-type doping. Thus, resistive electrical losses from contact and sheet resistances become negligible. Also, efficient and homogeneous carrier injection can be achieved even with a wide active zone. There is no need for an electron blocking layer or other means to address the asymmetry in the electrical properties between electrons and holes that influence the effectiveness of carrier injection. Furthermore, high light extraction efficiency can be realized, with low optical absorption materials within the entire device heterostructure, because no low bandgap materials are needed to improve the electrical properties. All of these aspects make electron beam excitation an attractive platform technology, in particular for emitters in the mid-UV where p-type doping otherwise limits device performance.

An e-beam pumped AlGaIn chip producing spontaneous emission in the mid-UV was reported by Oto *et al* in 2010 [193]. Although their claimed optical output power efficiency may have been obscured by x-ray radiation, the proof-of-concept was clearly demonstrated. Other teams followed showing pure optical output powers as high as 230 mW at  $\lambda = 246$  nm [194, 195] and demonstrated the feasibility of implementing a compact form factor [196]. Record high optical intra-chip powers of about 10 W at 246 nm were shown with liquid-nitrogen cooled chips [197]. E-beam pumped spontaneous emitter sources compare favourably with state-of-the-art efficiencies from conventional UV-LEDs (see figure 31), and can deliver high optical output powers at the same time.

Using e-beam excitation for lasers is also particularly intriguing for the same reasons discussed above. Despite the fact that laser emission in the deep-UV has still to be demonstrated, longer-wavelength III-N lasers reveal the great benefits of this compelling platform technology (figure 32) [198–201].

### 18.2. Current and future challenges

E-beam pumped light emitters based on semiconductor materials share some common aspects with conventional LED manufacturing, including epitaxial growth and device fabrication processes. Various device design features follow

identical optimization schemes as known for LED development. These involve improving the well-known efficiency contributions through optimization of material quality, heterostructure design and device architecture. The key difference to consider between e-beam pumped light emitters and p/n-junction devices is how electrons and holes are created and injected into the active zone for photon generation.

E-beam pumping involves the bombardment of the target sample with high energy electrons (i.e. 5–30 keV) through which electron-hole pairs are generated in an extended volume that is dependent on the pump spot diameter and the chosen electron energy as well as the target materials. This process has an intrinsic energy efficiency limit of about 1/3. The carriers subsequently diffuse into the QWs where they recombine with the generation of photons. Proper electrical grounding removes net excess charge. Excess heating and possible hazards from soft x-ray generation require careful design and mounting schemes.

The operation of the electron beam requires a vacuum enclosure, dictating materials and manufacturing choices that are compatible with the mechanical, optical, electrical, and thermal needs.

Challenges for laser operation are not only related to the semiconductor gain chip, but are also convoluted with the actual e-beam properties. Both vertical and edge type laser configurations are feasible. Whereas it is straight-forward to realize a circular e-beam pump spot, as is convenient for vertical emitters, the short gain length makes essential the need for highly reflective mirrors. However, as known for electrically driven devices, epitaxial III-nitride DBRs are challenging to fabricate. Dielectric DBRs on the other hand might fulfil the optical requirements, but their robustness against extreme e-beam bombardment might be compromised. Also, in the case of vertical lasers, substrate removal might be required to minimize absorption losses in the optical cavity. Edge emitting laser configurations are easier to fabricate. However, realizing a narrow and long continuous e-beam excitation spot is non-trivial, and its precise alignment with respect to the resonator is important.

### 18.3. Advances in science and technology to meet challenges

In recent years, much progress has been made to develop high quality AlN substrates and templates that provide the base for the growth of the device heterostructures. The structural material quality of today's UV emitters has approached a satisfying level with radiative efficiencies exceeding 90% for the best materials. These advancements have also allowed the successful demonstration of low threshold optically pumped lasers all the way down to emission wavelength of 237 nm. Challenges related to efficient carrier injection even at high carrier densities as seen in conventional p/n-junction devices are addressed by means of e-beam pumping. Light extraction is one of the factors that still limits UV emitter performance today, especially for wavelength shorter than 240 nm. This is where light polarization switches from TE to TM and photons are

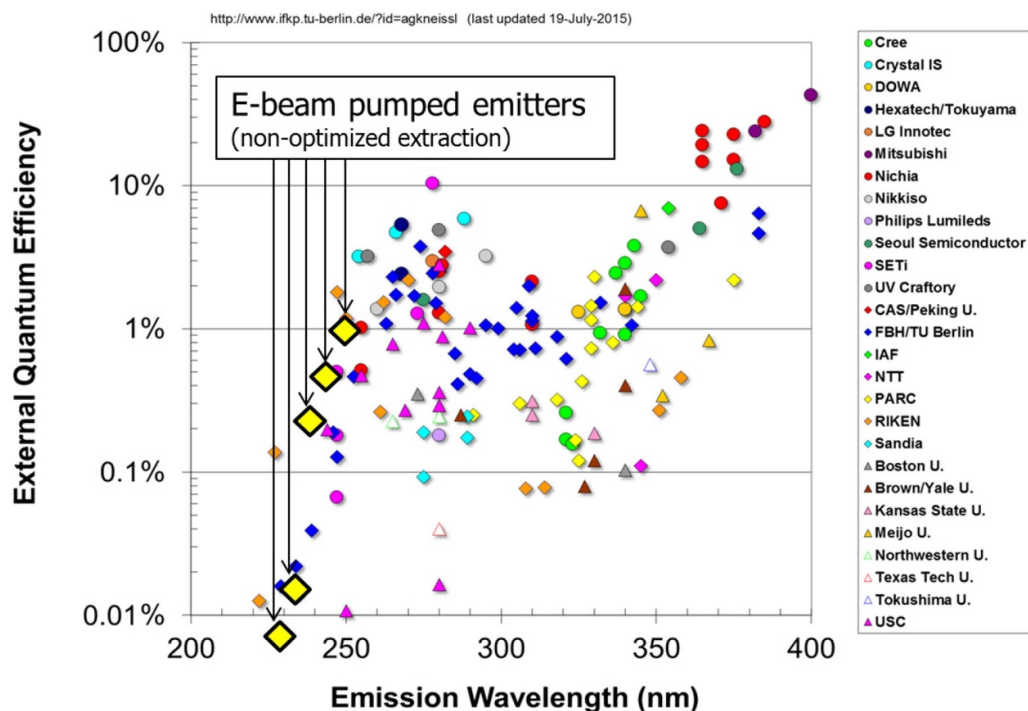


**Figure 31.** Comparison of e-beam pumped spontaneous emission device efficiencies with state-of-the art conventional LED performance. Collection of LED performance from M Kneissl at <http://www.ifkp.tu-berlin.de/?id=agkneissl>.

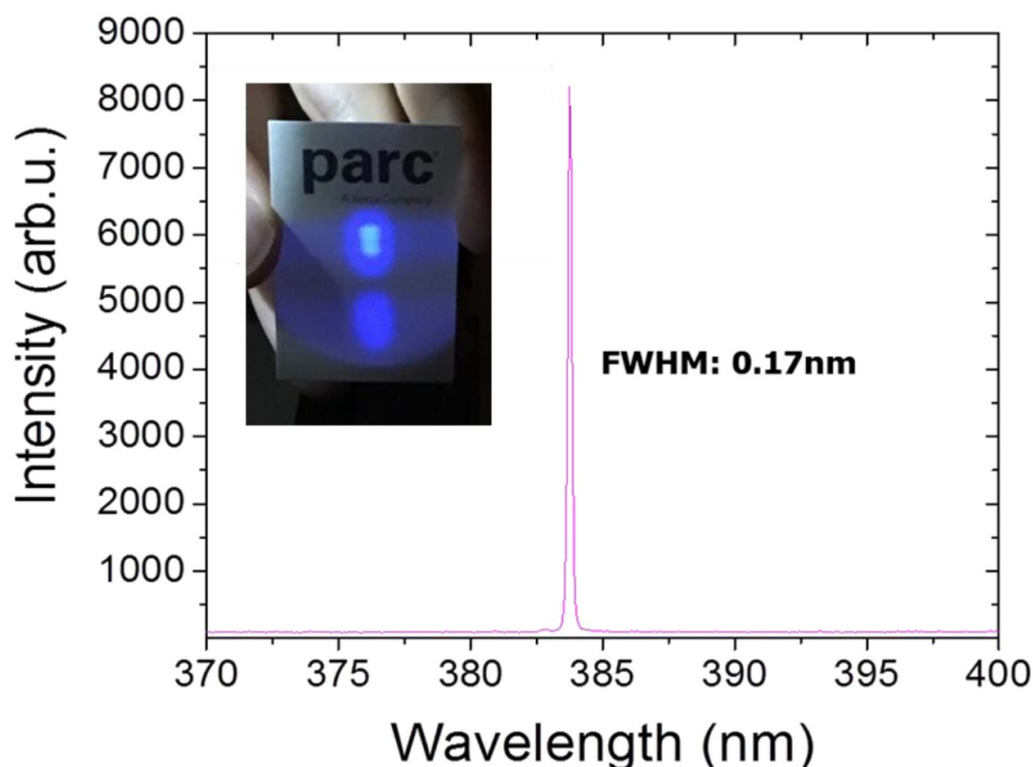


**Figure 32.** Laser spectrum from electron beam pumped GaN-based edge type laser. Inset: Far-field pattern of the laser emission made visible by focusing onto a fluorescing screen. The spot with lower intensity originates from reflections of the light on the wafer.

trapped within the chip. Structuring the chip surface and relying on scattering effects have showed promise for enhanced light extraction. However, the effective useable active area is

compromised. An alternative approach to overcome the challenges of photon extraction is to fabricate devices on non- or semipolar AlN crystal orientations. For example, first MQW

heterostructures grown on (2–201) AlN revealed very promising results [202] and further advances could enable efficient sub-240 nm emitters.

With respect to e-beam pumped edge type lasers further development of a compact line-shaped e-beam pump spot with high power density could significantly improve laser device performance. A longer excited resonator length can provide more gain per photon roundtrip and consequently reduce the laser threshold. Also implementing mirror concepts and laser cavities (for vertical emitting lasers) that do not degrade with high-energy electron bombardment would be of interest. For example, an e-beam pumped surface emitting laser with external cavity (VECSEL) could provide high optical output power with excellent beam properties and would circumvent the issues discussed above.

Further advances on thermal management and implementation of ultra-compact components, including the electron gun, vacuum housing, beam shaping, and drive electronics are greatly desired. It is believed that these technical challenges can be mastered and that the final

product could be as compact as a conventional light bulb.

#### 18.4. Concluding remarks

Electron-beam pumping of semiconductor materials can be considered an enabling alternative excitation strategy for UV optical emitters. High pump powers of up to 100 Watts and high pump-power densities (e.g.  $\sim 1 \text{ MW cm}^{-2}$ ) are accessible to achieve laser operation in both edge type and vertical emitting laser configurations. Especially for the ultra-wide bandgap AlGaIn materials e-beam excitation is particularly appealing, as no p-type doping is required in the device heterostructure. As a result, device efficiencies of e-beam pumped spontaneous UV emitters have been shown to meet or exceed state-of-the-art performance levels from conventional LEDs, while delivering high optical output powers. Further advances in miniaturization of various device components will realize a platform technology for compact and efficient emitter systems that can access a wide range of emission wavelengths.

## 19. UV laser diodes

Tim Wernicke<sup>1</sup> and Michael Kneissl<sup>1,2</sup>

<sup>1</sup> Technische Universität Berlin, Institute of Solid State Physics

<sup>2</sup> Ferdinand-Braun-Institut, Leibniz Institut für Höchstfrequenztechnik

### 19.1. Status

Although AlGaIn-based ultraviolet light emitting diodes (UV-LEDs) with emission wavelength as short as 211 nm have been realized with emitters covering the entire composition range (see section 12) the situation is quite different for current-injection UV laser diodes (LDs). Due to the greater complexity and increased requirements commercially available UV laser diodes are limited to emission wavelengths above 370 nm [203] and the shortest emission wavelength for a current-injection LD was for a long time 326 nm [203]. However recently edge emitting laser diodes emitting in the UVC at 271.8 nm [190], and UVB spectral region at 298 nm [204] were demonstrated. As shown in figure 33, lasers emitting below 370 nm exhibit an increase in threshold current density with shorter emission wavelength [205]. Laser emitting around 400 nm exhibit threshold current densities of 1–2 kA cm<sup>-2</sup>, while the thresholds of lasers emitting below 340 nm exceed 15 kA cm<sup>-2</sup> and can be only operated under pulsed current conditions [203]. The AlGaIn quantum well (QW) based current-injection lasers in the UVB and UVC wavelength region exhibit a laser threshold of 41.2 kA cm<sup>-2</sup> [204], 25 kA cm<sup>-2</sup> [190], and 19.6 kA cm<sup>-2</sup> [206].

Optically pumped lasing from AlGaIn heterostructures with emission wavelengths from 310 nm down to 237 nm [21, 121, 207, 208] has been demonstrated and over the past decade the threshold power densities have been significantly reduced and are now reaching <10 kW cm<sup>-2</sup> for AlGaIn multiple quantum well (MQW) structures grown on low defect density bulk AlN substrates [21]. Investigations of the optical gain in such AlGaIn MQW heterostructures show a high material gain [207], moderate optical waveguide losses even in the presence of Mg-doped layers [209], and fairly large confinement factors [207]. Advanced laser concepts such as vertical cavity surface emitting lasers (VCSELs) [209], distributed feedback (DFB) [211], and tapered lasers are currently being explored for emitters in the wavelength range from 400 nm to 369 nm. For emitters in the UVB and UVC spectral range research activities are predominantly focused on edge-emitting lasers due to significant challenges in materials development (e.g. Mg-doping of AlGaIn alloys) and device fabrication technologies (e.g. ohmic contacts).

### 19.2. Current and future challenges

The challenges for UV lasers are tremendous but depend strongly on the emission wavelength and composition. In the spectral range above 370 nm, low threshold density GaN-based laser diodes operating in continuous-wave mode with

long lifetimes are already commercially available. Lasers emitting at shorter wavelength require AlGaIn or InAlGaIn active regions and confinement heterostructures leading to increasing tensile strain with increasing aluminium mole fraction when grown on low defect density bulk GaN substrates [203]. In order to avoid the formation of cracks in the laser heterostructure the development of special strain relief techniques is required. Furthermore, the performance characteristic of these lasers also degrades much faster due to the increased operating voltages and currents leading to Joule heating as well as the higher defect densities in these materials. For UVB lasers one of the biggest challenges is the lack of high quality AlGaIn substrates with a lattice constant corresponding to the medium AlGaIn composition range. For example, growth on bulk AlN substrates is not ideal since the strong compressive strain in the AlGaIn quantum well heterostructures leads to relaxation and defect formation during growth [213] and consequently a degradation of the optical properties. This might be the main reason for higher lasing threshold of the demonstrated UVB laser diode in comparison for UVC laser diodes grown on bulk AlN [190, 204]. On the upside, highly conductive n-AlGaIn layers and low resistance Ohmic n-contacts have been demonstrated for emitters in this aluminium alloy composition range as also described in sections 6 and 7. Furthermore, due to the only moderately higher Mg acceptor ionization energies, low resistivity Mg-doped p-AlGaIn layers are also easier to realize [207]. UVC lasers with high structural quality can be realized on low defect density bulk AlN [21, 190, 207, 208]. Since these high aluminium mole fraction AlGaIn heterostructures can be grown pseudomorphically strained on bulk AlN [213], they exhibit excellent optical properties as described in the previous paragraph. However, efficient carrier injection and confinement as well as low resistivity p-AlGaIn cladding layers with an aluminium content exceeding 70% pose very difficult challenges for the realization of AlGaIn QW lasers emitting in the UVC. As described in section 7, the ionization energy for Mg acceptors in AlGaIn alloys steadily increases with the aluminium content leading to very low room temperature conductivities. Here polarization doped p-AlGaIn layers [214] without Mg employed in all UVB and UVC laser diodes so far [190, 204] allow moderate voltages of 13.8 V at the threshold current density of 25 kA cm<sup>-2</sup> [190].

Finally, designing current injection structures that allow high current density operation [190, 204] is a crucial challenge to achieve lasing and find a suitable way for optimizing the structures.

### 19.3. Advances in science and technology to meet challenges

For laser diodes in the UVA spectral range emitting below 370 nm recent research developments including reducing point defects in AlGaIn alloys (section 5), improved doping schemes (section 7) as well as low resistance Ohmic contacts to AlGaIn layers (section 6) should lead to a reduction in operation voltages, cw operation, and improved laser diode lifetimes. As is often the case, laser diode technologies will



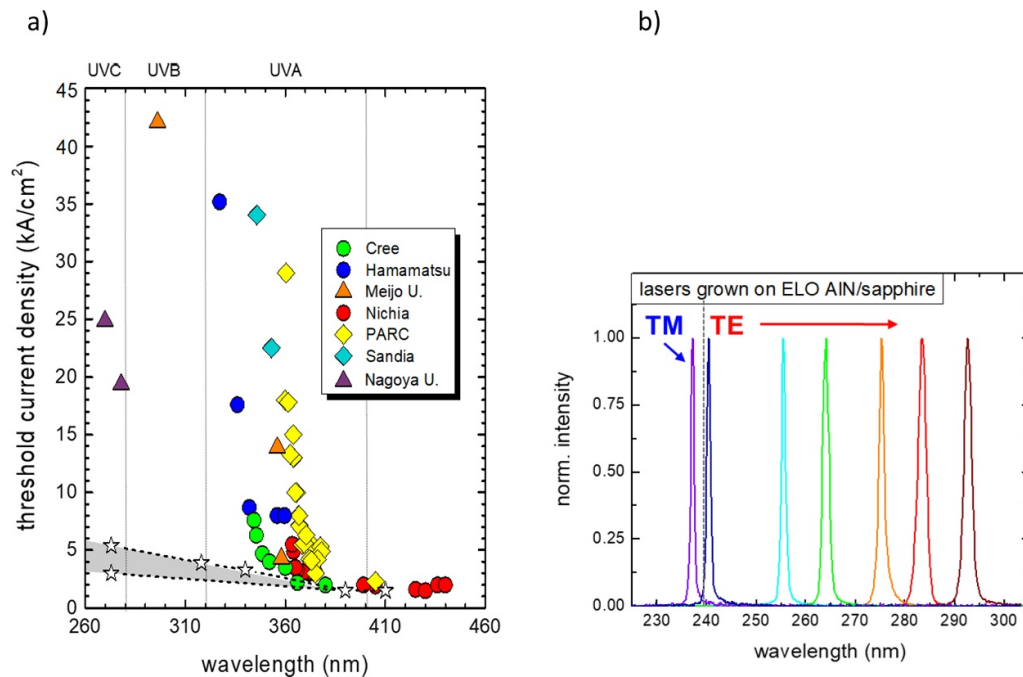


**Figure 33.** (a) Previously published threshold current densities of current injection laser diodes [190] with data added from [190, 204, 206]. (b) Spectra of optically pumped lasers in the range of 237 nm to 292 nm. Reproduced from [207]. CC BY 4.0.

also profit from the progress made in the development of UV-LEDs (section 9). However, the root causes for the strong increase in threshold current density at shorter wavelengths is not yet well-understood. Since the increased strain in the AlGaIn layers is certainly playing a role different approaches for the growth of low defect density AlGaIn heterostructures are critical. This could be either achieved by strain relaxation which, however, needs to be attained without introducing additional threading dislocations or by realizing low defect density AlGaIn templates allowing for the coherent growth of a laser diode heterostructure with AlGaIn cladding layers exceeding an Al mole fraction of 30%. Another option is the incorporation of InAlN cladding layers for which n- and p-doping was successfully demonstrated [212] and which can be grown lattice-matched onto low defect density bulk GaN substrates. For lasers in the UVB spectral range the creation of high quality heterostructures by using metamorphic AlGaIn buffer layers that promote strain relaxation (see section 10 and [121, 204]) are effective to reduce the TDD. In the longer term  $\text{Al}_{0.5}\text{Ga}_{0.5}\text{N}$  quasi substrates grown, e.g. by hydride vapour phase epitaxy (HVPE), could provide near lattice-matched templates with low threading dislocation densities, smooth surfaces and vertical current-injection through a conducting substrate.

Now, shortly after the first realization of UVC laser diodes it is not clear which factors contribute to the lasing threshold. However, carrier injection and optical confinement under the condition that the diode can sustain high current densities to reach the threshold are probably the most crucial contributions. Part of this is optimizing the polarization doping for efficient hole injection transport [214].

Novel concepts, especially tunnel junctions will also be investigated as these would allow the incorporation of low resistance Si-doped AlGaIn cladding layers on both sides of the active region with only a thin Mg-doped tunnel heterojunction for hole injection. Here the key challenge is to minimize the excess voltage drop at the AlGaIn tunnel-junction, e.g. by using low-bandgap interlayers (see section 17). The best growth technologies for deep UV tunnel-junction laser diodes either by MOVPE or hybrid MOVPE/MBE as well as the optimum design for a low optical loss of the lasing mode at the tunnel-heterojunction are currently being investigated. Another approach for carrier injection that is currently investigated is the pumping by a high energy electron beam with acceleration voltages of 5–10 kV (see section 18). Using this approach, electron-hole pairs are excited in the laser heterostructure through e-beam irradiation and thus completely avoiding all problems connected to Mg-doping and current-injection. However, such a device requires a very different laser heterostructure design as well as a detailed understanding of the carrier dynamics in order to efficiently collect the charge carriers in the AlGaIn quantum wells. Another concern is the long term stability under high density electron beam irradiation as well as the effects of Joule heating, since only 1/3 of the energy is converted to generate electron-hole pairs and the rest is dissipated via various other channels.

Advanced laser concepts will be a topic of intense research as soon as technological building blocks are present and they will be first realized in the UVA region. For DFB, DBR and tapered lasers the technological prerequisites exist and advances will be achieved by optimizing the fabrication technology. Future breakthroughs for VCSELs in the UVA region

will be achieved by improving the fabrication of high reflectivity mirrors, e.g. based electro chemical etching [210], and reducing the optical losses in p-contact layers. An extension towards shorter emission wavelength will then be possible by improved epitaxial growth and fabrication technology in combination with tunnel junctions or e-beam pumping.








#### 19.4. Concluding remarks

Laser diodes emitting in the UV spectral range have so far proven to be a much bigger challenge than UV LEDs. For the recent realization of deep UV current-injection laser diodes significant advances in material quality and device fabrication were required. With the recent improvements in materials growth (e.g. bulk AlN substrates, polarization doping, minimizing point defects) and fabrication technologies (e.g. Ohmic contact formation) initiated by the development of deep UV-LEDs significant reduction of the lasing threshold of UVB and UVC laser diodes can be expected.

#### Acknowledgements

We gratefully acknowledge support by the German Research Foundation (DFG) within the Collaborative Research Center ‘Semiconductor Nanophotonics’ (CRC 787).

#### ORCID iDs

Carlo De Santi  <https://orcid.org/0000-0001-6064-077X>  
 Johannes Glaab  <https://orcid.org/0000-0002-9252-8368>  
 Robert Martin  <https://orcid.org/0000-0002-6119-764X>  
 Frank Mehnke  <https://orcid.org/0000-0001-5406-0832>  
 Peter J Parbrook  <https://orcid.org/0000-0003-3287-512X>  
 Jan Ruschel  <https://orcid.org/0000-0001-6914-0958>  
 Biplab Sarkar  <https://orcid.org/0000-0003-0074-0626>  
 Leo J Schowalter  <https://orcid.org/0000-0002-4854-8521>  
 Philip Shields  <https://orcid.org/0000-0003-0517-132X>  
 Luca Sulmoni  <https://orcid.org/0000-0002-5341-7032>  
 Tim Wernicke  <https://orcid.org/0000-0002-5472-8166>  
 Yuh-Renn Wu  <https://orcid.org/0000-0002-1457-3681>  
 Yuewei Zhang  <https://orcid.org/0000-0002-4192-1442>

#### References

- [1] Khan A, Balakrishnan K and Katona T 2008 Ultraviolet light-emitting diodes based on group three nitrides *Nat. Photon.* **2** 77
- [2] Kneissl M, Seong T-Y, Han J and Amano H 2019 The emergence and prospects of deep ultraviolet light emitting diode technologies *Nat. Photon.* **13** 233
- [3] Kneissl M and Rass J 2016 *III-Nitride Ultraviolet Emitters—Technology and Applications* (Berlin: Springer) (<https://doi.org/10.1007/978-3-319-24100-5>)
- [4] Takano T, Mino T, Sakai J, Noguchi N, Tsubaki K and Hirayama H 2017 Deep-ultraviolet light-emitting diodes with external quantum efficiency higher than 20% at 275 nm achieved by improving light-extraction efficiency *Appl. Phys. Express* **10** 031002
- [5] Choi R 2017 Current status and future works of high-power deep UV LED *Proc. SPIE* **10104** 101041N
- [6] Innatek L G 2017 LG Innatek unveils the world’s first ‘100 mW’ UV-C LED ([http://cps.lginnoteck.com/en/itk\\_news/lg-innoteck-unveils-worlds-first-100mw-uv-c-led/](http://cps.lginnoteck.com/en/itk_news/lg-innoteck-unveils-worlds-first-100mw-uv-c-led/))
- [7] Nagai S, Yamada K, Hirano A, Ippommatsu M, Ito M, Morishima N, Aosaki K, Honda Y, Amano H and Akasaki I 2016 Development of highly durable deep-ultraviolet AlGaIn-based LED multichip array with hemispherical encapsulated structures using a selected resin through a detailed feasibility study *Japan. J. Appl. Phys.* **55** 082101
- [8] Ban K, Yamamoto J, Takeda K, Ide K, Iwaya M, Takeuchi T, Kamiyama S, Akasaki I and Amano H 2011 Internal quantum efficiency of whole-composition-range AlGaIn multiquantum wells *Appl. Phys. Express* **4** 052101
- [9] Reentilä O, Brunner F, Knauer A, Mogilatenko A, Neumann W, Protzmann H, Heuken M, Kneissl M, Weyers M and Tränkle G 2008 Effect of the AlN nucleation layer growth on AlN material quality *J. Cryst. Growth* **310** 4932
- [10] Kueller V *et al* 2012 Modulated epitaxial lateral overgrowth of AlN for efficient UV LEDs *IEEE Photonics Technol. Lett.* **24** 1603
- [11] Kneissl M *et al* 2011 Advances in group III-nitride-based deep UV light-emitting diode technology *Semicond. Sci. Technol.* **26** 014036
- [12] Mohn S *et al* 2016 Polarity control in group-III nitrides beyond pragmatism *Phys. Rev. Appl.* **5** 054004
- [13] Zeimer U *et al* 2015 Spatial inhomogeneities in Al<sub>x</sub>Ga<sub>1-x</sub>N quantum wells induced by the surface morphology of AlN/sapphire templates *Semicond. Sci. Technol.* **30** 114008
- [14] Miyake H, Lin C-H, Tokoro K and Hiramatsu K 2016 Preparation of high-quality AlN on sapphire by high-temperature face-to-face annealing *J. Cryst. Growth* **456** 155–9
- [15] Susilo N *et al* 2018 AlGaIn-based deep UV LEDs grown on sputtered and high temperature annealed AlN/sapphire *Appl. Phys. Lett.* **112** 041110
- [16] Manley P, Walde S, Hagedorn S, Hammerschmidt M, Burger S and Becker C 2020 Nanopatterned sapphire substrates in deep-UV LEDs: is there an optical benefit? *Opt. Express* **28** 3619–35
- [17] Hagedorn S *et al* 2020 Improving AlN crystal quality and strain management on nanopatterned sapphire substrates by high-temperature annealing for UVC light-emitting diodes *Phys. Status Solidi a* **217** 1900796
- [18] Hagedorn S *et al* 2020 Status and prospects of AlN templates on sapphire for ultraviolet light-emitting diodes *Phys. Status Solidi a* **217** 1901022
- [19] Epelbaum B M, Bickermann M and Winnacker A 2002 Seeded PVT growth of aluminum nitride on silicon carbide *Silicon Carbide and Related Materials* ed P Bergman and E Janzen (Zurich: TransTech Publications) pp 983–6
- [20] Schlessler R and Sitar Z 2002 Growth of bulk AlN crystals by vaporization of aluminum in a nitrogen atmosphere *J. Cryst. Growth* **234** 2–3
- [21] Kirste R, Guo Q, Dycus J H, Franke A, Mita S, Sarkar B, Reddy P, LeBeau J M, Collazo R and Sitar Z 2018 6 kW/cm<sup>2</sup> UVC laser threshold in optically pumped lasers achieved by controlling point defect formation *Appl. Phys. Express* **11** 082101
- [22] Shi Y, Xie Z Y, Liu L H, Liu B, Edgar J H and Kuball M 2001 Influence of buffer layer and 6H-SiC substrate polarity on the nucleation of AlN grown by the sublimation sandwich technique *J. Cryst. Growth* **233** 177–86
- [23] Krishnan B, Iwaya M, Kamiyama S, Amano H, Akasaki I, Takagi T and Noro T 2004 Study on the seeded growth of AlN bulk crystals by sublimation *Japan. J. Appl. Phys.* **43** 7448

- [24] Bryan I *et al* 2018 Doping and compensation in Al-rich AlGa<sub>N</sub> grown on single crystal AlN and sapphire by MOCVD *Appl. Phys. Lett.* **112** 062102
- [25] Bryan I, Bryan Z, Mita S, Rice A, Hussey L, Shelton C, Tweedie J, Maria J-P, Collazo R and Sitar Z 2016 The role of surface kinetics on composition and quality of AlGa<sub>N</sub> *J. Cryst. Growth* **451** 65–71
- [26] Wunderer T *et al* 2012 Optically pumped UV lasers grown on bulk AlN substrates *Phys. Status Solidi c* **9** 3–4
- [27] Kneissl M, Yang Z, Teepe M, Knollenberg C, Schmidt O, Kiesel P, Johnson N M, Schujman S and Schowalter L J 2007 Ultraviolet semiconductor laser diodes on bulk AlN *J. Appl. Phys.* **101** 123103–5
- [28] Bickermann M *et al* 2010 UV transparent single-crystalline bulk AlN substrates *Phys. Status Solidi c* **7** 1
- [29] Alden D *et al* 2018 Point-defect nature of the ultraviolet absorption band in AlN *Phys. Rev. Appl.* **9** 054036
- [30] Reddy P, Kaess F, Tweedie J, Kirste R, Mita S, Collazo R and Sitar Z 2017 Defect quasi Fermi level control-based CN reduction in GaN: evidence for the role of minority carriers *Appl. Phys. Lett.* **111** 152101
- [31] Collazo R, Mita S, Xie J, Rice A, Tweedie J, Dalmau R and Sitar Z 2011 Progress on n-type doping of AlGa<sub>N</sub> alloys on AlN single crystal substrates for UV optoelectronic applications *Phys. Status Solidi c* **8** 2031–3
- [32] Schulz T, Irmscher K, Albrecht M, Hartmann C, Wollweber J and Fornari R 2007 n-type conductivity in sublimation-grown AlN bulk crystals *Phys. Status Solidi Rapid Res. Lett.* **1** 147–9
- [33] Reddy P, Washiyama S, Kaess F, Kirste R, Mita S, Collazo R and Sitar Z 2017 Point defect reduction in MOCVD (Al)Ga<sub>N</sub> by chemical potential control and a comprehensive model of C incorporation in GaN *J. Appl. Phys.* **122** 245702
- [34] Kohno T, Sudo Y, Yamaguchi M, Mitsui K, Kudo H, Okagawa H and Yamada Y 2012 Internal quantum efficiency and nonradiative recombination rate in InGa<sub>N</sub>-based near-ultraviolet light-emitting diodes *Japan. J. Appl. Phys.* **51** 072102
- [35] Iwata Y, Banal R, Ichikawa S, Funato M and Kawakami Y 2015 Emission mechanisms in Al-rich AlGa<sub>N</sub>/AlN quantum wells assessed by excitation power dependent photoluminescence spectroscopy *J. Appl. Phys.* **117** 075701
- [36] Kojima K, Ohtomo T, Ikemura K, Yamazaki Y, Saito M, Ikeda H, Fujito K and Chichibu S F 2016 Determination of absolute value of quantum efficiency of radiation in high quality Ga<sub>N</sub> single crystals using an integrating sphere *J. Appl. Phys.* **120** 015704
- [37] Kawakami Y, Inoue K, Kaneta A, Okamoto K and Funato M 2015 Quantification of the internal quantum efficiency in Ga<sub>N</sub> via analysis of the heat generated by non-radiative recombination processes *J. Appl. Phys.* **117** 105702
- [38] Yamaguchi A, Kawakami K, Shimizu N, Takahashi Y, Kobayashi G, Nakano T, Sakai S, Kanitani Y and Tomiya S 2018 A novel method to measure absolute internal quantum efficiency in III-nitride semiconductors by simultaneous photo-acoustic and photoluminescence spectroscopy *IEICE Trans. Electron.* **E101–C** 527–31
- [39] Kaneta A, Okamoto K, Kawakami Y, Fujita S, Marutsuki G, Narukawa Y and Mukai T 2002 Spatial and temporal luminescence dynamics in an In<sub>x</sub>Ga<sub>1-x</sub>N single quantum well probed by near-field optical microscopy *Appl. Phys. Lett.* **81** 4353
- [40] Kawakami Y, Kaneta A, Hashiya A and Funato M 2016 Impact of radiative and nonradiative recombination processes on the efficiency-droop phenomenon in In<sub>x</sub>Ga<sub>1-x</sub>N single quantum wells studied by scanning near-field optical microscopy *Phys. Rev. Appl.* **6** 044018
- [41] Marcinkevičius S, Jain R, Shatalov M, Yang J, Shur M and Gaska R 2014 High spectral uniformity of AlGa<sub>N</sub> with a high Al content evidenced by scanning near-field photoluminescence spectroscopy *Appl. Phys. Lett.* **105** 241108
- [42] Ishii R, Funato M and Kawakami Y 2018 Development of a deep-ultraviolet scanning nearfield optical microscope for nanospectroscopic characterizations of Al<sub>x</sub>Ga<sub>1-x</sub>N (x: 0-1) active layers *Int. Workshop on Nitride Semiconductors*, Kanazawa, Japan pp CR12–1
- [43] Ishii R, Funato M and Kawakami Y 2019 Pushing the limits of deep-ultraviolet scanning near-field optical microscopy *APL Photon.* **4** 070801
- [44] Hangleiter A, Jin Z, Gerhard M, Kalincev D, Langer T, Bremers H, Rossow U, Koch M, Bonn M and Turchinovich D 2015 Efficient formation of excitons in a dense electron-hole plasma at room temperature *Phys. Rev. B* **92** 241305(R)
- [45] Ichikawa S, Funato M and Kawakami Y 2018 Dominant nonradiative recombination paths and their activation processes in Al<sub>x</sub>Ga<sub>1-x</sub>N-related materials *Phys. Rev. Appl.* **10** 064027
- [46] Reshchikov M A and Morkoç H 2005 Luminescence properties of defects in Ga<sub>N</sub> *J. Appl. Phys.* **97** 061301
- [47] Lyons J L, Janotti A and Van de Walle C G 2014 Effects of carbon on the electrical and optical properties of InN, GaN, and AlN *Phys. Rev. B* **89** 035204
- [48] Harris J S, Baker J N, Gaddy B E, Bryan I, Bryan Z, Mirrieles K J, Reddy P, Collazo R, Sitar Z and Irving D L 2018 *Appl. Phys. Lett.* **112** 152101
- [49] Kinoshita T, Obata T, Yanagi H and Inoue S 2013 *Appl. Phys. Lett.* **102** 012105
- [50] Li J, Oder T N, Nakarmi M L, Lin J Y and Jiang H X 2002 *Appl. Phys. Lett.* **80** 1210
- [51] Hartmann C, Wollweber J, Sintonen S, Dittmar A, Kirste L, Kollowa S, Irmscher K and Bickermann M 2016 *Cryst. Eng. Comm.* **18** 3488
- [52] Bryan Z, Bryan I, Xie J Q, Mita S, Sitar Z and Collazo R 2015 High internal quantum efficiency in AlGa<sub>N</sub> multiple quantum wells grown on bulk AlN substrates *Appl. Phys. Lett.* **106** 142107
- [53] Murotani H, Akase D, Anai K, Yamada Y, Miyake H and Hiramatsu K 2012 Dependence of internal quantum efficiency on doping region and Si concentration in Al-rich AlGa<sub>N</sub> quantum wells *Appl. Phys. Lett.* **101** 042110
- [54] Bryan Z *et al* 2014 *Appl. Phys. Lett.* **105** 222101
- [55] Reddy P *et al* 2016 *J. Appl. Phys.* **120** 185704
- [56] Alberi K and Scarpulla M A 2016 *Sci Rep* **6** 27954
- [57] Ruvimov S, Liliental-Weber Z, Washburn J, Qiao D, Lau S S and Chu P K 1998 *Appl. Phys. Lett.* **73** 2582
- [58] Daele B V, Tendeloo G V, Ruythooren W, Derluyn J, Leys M R and Germain M 2005 *Appl. Phys. Lett.* **87** 061905
- [59] Van de Walle C G, Stampfl C, Neugebauer J, McCluskey M D and Johnson N M 1999 *MRS Int. J. Nitride Semicond. Res.* **4** 890
- [60] Motayed A, Bathe R, Wood M C, Diouf O S, Vispute R D and Mohammad S N 2002 *J. Appl. Phys.* **93** 1087
- [61] Wang L, Mohammed F M and Adesida I 2007 *J. Appl. Phys.* **101** 013702
- [62] Miller M A, Koo B H, Bogart K H A and Mohny S E 2008 *J. Electron. Mater.* **37** 564
- [63] Mehnke F, Sulmoni L, Guttman M, Wernicke T and Kneissl M 2019 Influence of light absorption on the performance characteristics of UV LEDs with emission between 239 nm and 217 nm *Appl. Phys. Express* **12** 012008
- [64] Nagata N, Senga T, Iwaya M, Takeuchi T, Kamiyama S and Akasaki I 2016 *Phys. Status Solidi c* **14** 1600243



- [65] Mehnke F, Wernicke T, Pingel H, Kuhn C, Reich C, Kueller V, Knauer A, Lapeyrate M, Weyers M and Kneissl M 2013 *Appl. Phys. Lett.* **103** 212109
- [66] Narukawa Y, Ichikawa M, Sanga D, Sano M and Mukai K 2010 *J. Phys. D: Appl. Phys.* **43** 354002
- [67] Cao X A, Piao H, LeBoeuf S F, Li J, Lin J Y and Jiang H X 2006 *Appl. Phys. Lett.* **89** 082109
- [68] Lapeyrate M, Muhin A, Einfeldt S, Zeimer U, Mogilatenko A, Weyers M and Kneissl M 2013 *Semicond. Sci. Technol.* **28** 125015
- [69] Miller M A, Mohney S E, Nikiforov A, Cargill III G S and Bogart K H A 2006 *Appl. Phys. Lett.* **89** 132114
- [70] Miller M A and Mohney S E 2007 *Appl. Phys. Lett.* **91** 012103
- [71] France R, Xu T, Chen P, Chandrasekaran R and Moustakas T 2007 *Appl. Phys. Lett.* **90** 062115
- [72] Mori K, Takeda K, Kusafuka T, Iwaya M, Takeuchi T, Kamiyama S, Akasaki I and Amano H 2016 *Japan. J. Appl. Phys.* **55** 05FL03
- [73] Pampili P and Parbrook P J 2017 *Mater. Sci. Semicond. Process.* **62** 180
- [74] Mehnke F, Trinh X T, Pingel H, Wernicke T, Janzén E, Son N T and Kneissl M 2016 *J. Appl. Phys.* **120** 145702
- [75] Sarkar B *et al* 2018 *ECS Trans.* **86** 25
- [76] Washiyama S *et al* 2020 *J. Appl. Phys.* **127** 105702
- [77] Blasco R, Ajay A, Robin E, Bougerol C, Lorentz K, Alves L C, Mouton I, Amichi L, Grenier A and Monroy E 2019 *J. Phys. D: Appl. Phys.* **52** 125101
- [78] Gordon L, Lyons J L, Janotti A and Van de Walle C G 2014 *Phys. Rev. B* **89** 085204
- [79] Sarkar B *et al* 2017 *Appl. Phys. Lett.* **111** 032109
- [80] Chen Y, Wu H, Han E, Yue G, Chen Z, Wu Z, Wang G and Jiang H 2015 *Appl. Phys. Lett.* **106** 162102
- [81] Ebata K, Nishinaka J, Taniyasu Y and Kumakura K 2018 *Japan. J. Appl. Phys.* **57** 04FH09
- [82] Dalmau R and Moody B 2018 *ECS Trans.* **86** 31
- [83] Uesugi K, Hayashi Y, Shojiki K and Miyake H 2019 *Appl. Phys. Express* **12** 065501
- [84] Breckenridge M H *et al* 2020 Shallow Si donor in ion-implanted homoepitaxial AlN *Appl. Phys. Lett.* **116** 172103
- [85] Zhang M and Li X 2017 Structural and electronic properties of wurtzite  $B_xAl_{1-x}N$  from first-principles calculations *Phys. Status Solidi b* **254** 1600749
- [86] Shen J-X, Wickramaratne D and Van de Walle C G 2017 Band bowing and the direct-to-indirect crossover in random BAlN alloys *Phys. Rev. Mater.* **1** 065001
- [87] Abid M *et al* 2012 Distributed Bragg reflectors based on diluted boron-based BAlN alloys for deep ultraviolet optoelectronic applications *Appl. Phys. Lett.* **100** 051101
- [88] Liu K, Sun H, AlQatari F, Guo W, Liu X, Li J, Torres Castaneda C G and Li X 2017 Wurtzite BAlN and BGaN alloys for heterointerface polarization engineering *Appl. Phys. Lett.* **111** 222106
- [89] Ravindran V, Boucherit M, Soltani A, Gautier S, Moudakir T, Dickerson J, Voss P L, Di Forte-Poisson M-A, De Jaeger J-C and Ougazzaden A 2012 Dual-purpose BGaN layers on performance of nitride-based high electron mobility transistors *Appl. Phys. Lett.* **100** 243503
- [90] Kimura T and Matsuoka T 2007 Calculation of phase separation in Wurtzite  $In_{1-x-y-z}Ga_xAl_yB_zN$  *Japan. J. Appl. Phys.* **46** L574
- [91] Teles L, Furthmüller J, Scolfaro L, Tabata A, Leite J, Bechstedt F, Frey T, As D and Lischka K 2002 Phase separation and gap bowing in zinc-blende InGaN, InAlN, BGaN, and BAlN alloy layers *Physica E* **13** 1086
- [92] Sun H *et al* 2018 Revealing microstructure and dislocation behavior in BAlN/AlGaN heterostructures *Appl. Phys. Express* **11** 011001
- [93] Li X *et al* 2015 BAlN thin layers for deep UV applications *Phys. Status Solidi a* **212** 745
- [94] Gunning B P, Moseley M W, Koleske D D, Allerman A A and Lee S R 2017 Phase degradation in  $B_xGa_{1-x}N$  films grown at low temperature by metalorganic vapor phase epitaxy *J. Cryst. Growth* **464** 190
- [95] Park S-H and Ahn D 2016 Effect of boron incorporation on light emission characteristics of UV BAlGaN/AlN quantum well structures *Appl. Phys. Express* **9** 021001
- [96] Rettig O *et al* 2018 Investigation of boron containing AlN and AlGaN layers grown by MOVPE *Phys. Status Solidi b* **255** 1700510
- [97] Sundaram S *et al* 2016 Single-crystal nanopyrnidal BGaN by nanoselective area growth on AlN/Si(111) and GaN templates *Nanotechnology* **27** 115602
- [98] Akasaka T and Makimoto T 2006 Flow-rate modulation epitaxy of wurtzite AlBN *Appl. Phys. Lett.* **88** 041902
- [99] Li X *et al* 2015 MOVPE grown periodic AlN/BAlN heterostructure with high boron content *J. Cryst. Growth* **414** 119
- [100] Muramoto Y, Kimura M and Nouda S 2014 *Semicond. Sci. Technol.* **29** 084004
- [101] Yole Développement 2018 UV LEDs: technology, manufacturing and applications trends ([www.yole.fr/UVLED\\_StatusIndustry.aspx](http://www.yole.fr/UVLED_StatusIndustry.aspx))
- [102] Akasaki I and Amano H 1994 *J. Electrochem. Soc.* **141** 2266
- [103] Han J, Crawford M H, Shul R J, Figiel J J, Banas M, Zhang L, Song Y K, Zhou H and Nurmikko A V 1998 *Appl. Phys. Lett.* **73** 1688
- [104] Mukai T and Nakamura S 1999 *Japan. J. Appl. Phys.* **38** 5737
- [105] Wang T, Liu Y H, Lee Y B, Ao J P, Bai J and Sakai S 2002 *Appl. Phys. Lett.* **81** 2508
- [106] Nishida T, Saito H and Kobayashi N 2001 *Appl. Phys. Lett.* **79** 711
- [107] Chichibu S F, Uedono A, Kojima K, Ikeda H, Fujito K, Takashima S, Edo M, Ueno K and Ishibashi S 2018 *J. Appl. Phys.* **123** 161413
- [108] Kojima K, Nagasawa Y, Hirano A, Ipponmatsu M, Honda Y, Amano H, Akasaki I and Chichibu S F 2019 *Appl. Phys. Lett.* **114** 011102
- [109] Pampili P, Zublialevich V Z, Maaskant P, Akhter M, Corbett B and Parbrook P J 2019 *Japan. J. Appl. Phys.* **58** SCCB33
- [110] LG Innatek, LED Catalog 2018 (<http://104.215.62.75/wp-content/uploads/2018/03/LG-Innatek-UV-LED-Catalog-Jan-2018.pdf>)
- [111] Kuhn C *et al* 2018 *J. Phys. D: Appl. Phys.* **51** 415101
- [112] Kawase Y, Ikeda S, Sakuragi Y, Yasue S, Iwayama S, Iwaya M, Takeuchi T, Kamiyama S, Akasaki I and Miyake H 2019 *Japan. J. Appl. Phys.* **58** SC1052
- [113] Enslin J *et al* 2017 Metamorphic  $Al_{0.5}Ga_{0.5}N:Si$  on AlN/sapphire for the growth of UVB LEDs *J. Cryst. Growth* **464** 185
- [114] Kaneda M, Pernot C, Nagasawa Y, Hirano A, Ipponmatsu M, Honda Y, Amano H and Akasaki I 2017 Uneven AlGaN multiple quantum well for deep-ultraviolet LEDs grown on macrosteps and impact on electroluminescence spectral output *Japan. J. Appl. Phys.* **56** 061002
- [115] Won J-Y, Kim D-H, Kang D, Sung J-S, Kim D-S, Kim S-K and Seong T-Y 2017 *Phys. Status Solidi a* **214** 1600789
- [116] Susilo N, Enslin J, Sulmoni L, Guttmann M, Zeimer U, Wernicke T, Weyers M and Kneissl M 2017 *Phys. Status Solidi a* **215** 1700643
- [117] Khan M A, Maeda N, Jo M, Akamatsu Y, Tanabe R, Yamada Y and Hirayama H 2019 *J. Mater. Chem. C* **7** 143
- [118] Allerman A A, Crawford M H, Lee S R and Clark B G 2014 *J. Crystal Growth* **388** 76



- [119] Kolbe T, Mehnke F, Guttman M, Kuhn C, Rass J, Wernicke T and Kneissl M 2013 *Appl. Phys. Lett.* **103** 031109
- [120] Cho H K, Krüger O, Küllberg A, Rass J, Zeimer U, Kolbe T, Knauer A, Einfeldt S, Weyers M and Kneissl M 2017 *Semicond. Sci. Technol.* **32** 12LT01
- [121] Zhang Y, Allerman A A, Krishnamoorthy S, Akyol F, Moseley M W, Armstrong A M and Rajan S 2016 *Appl. Phys. Express* **9** 052102
- [122] Nagasawa Y and Hirano A 2018 A review of AlGaIn-based deep-ultraviolet light-emitting diodes on sapphire *Appl. Sci.* **8** 1264
- [123] Ichikawa M, Fujioka A, Kosugi T, Endo S, Sagawa H, Tamaki H, Mukai T, Uomoto M and Shimatsu T 2016 High-output-power deep ultraviolet light-emitting diode assembly using direct bonding *Appl. Phys. Express* **9** 072101
- [124] Shatalov M *et al* 2014 High power AlGaIn ultraviolet light emitters *Semicond. Sci. Technol.* **29** 084007
- [125] Grandusky J R, Chen J F, Gibb S R, Mendrick M C, Moe C G, Rodak L, Garrett G A, Wraback M and Schowalter L J 2013 270 nm 2014 Pseudomorphic ultraviolet light-emitting diodes with over 60 mW continuous wave output power *Appl. Phys. Express* **6** 032101
- [126] Inoue S, Naoki T, Kinoshita T, Obata T and Yanagi H 2015 Light extraction enhancement of 265 nm deep-ultraviolet light-emitting diodes with over 90 mW output power via an AlN hybrid nanostructure *Appl. Phys. Lett.* **106** 131104
- [127] Yamada K, Furusawa Y, Nagai S, Hirano A, Ippommatsu M, Aosaki K, Morishima N, Amano H and Akasaki I 2015 Development of underfilling and encapsulation for deep-ultraviolet LEDs *Appl. Phys. Express* **8** 012101
- [128] Taniyasu Y and Kasu M 2010 Surface 210 nm light emission from an AlN p-n junction light-emitting diode enhanced by A-plane growth orientation *Appl. Phys. Lett.* **96** 221110
- [129] Moe C G, Sugiyama S, Kasai J, Gradusky J R and Schowalter L 2018 AlGaIn light-emitting diodes on AlN substrates emitting at 230 nm *Phys. Status Solidi a* **215** 1700660
- [130] Hirayama H, Fujikawa S, Noguchi N, Norimatsu J, Takano T, Tsubaki K and Kamata N 2009 222–282 nm AlGaIn and InAlGaIn-based deep-UV LEDs fabricated on high-quality AlN on sapphire *Phys. Status Solidi a* **206** 1176
- [131] Hirayama H, Tsukada Y, Maeda T and Kamata N 2010 Marked enhancement in the efficiency of deep-ultraviolet AlGaIn light-emitting diodes by using a multiquantum-barrier electron blocking layer *Appl. Phys. Express* **3** 031002
- [132] Liu D *et al* 2018 229 nm UV LEDs on aluminum nitride single crystal substrates using p-type silicon for increased hole injection *Appl. Phys. Lett.* **112** 081101
- [133] Liu D *et al* 2018 226 nm AlGaIn/AlN UV LEDs using p-type Si for hole injection and UV reflection *Appl. Phys. Lett.* **113** 011111
- [134] Mehnke F *et al* 2014 Efficient charge carrier injection into sub-250 nm AlGaIn multiple quantum well light emitting diodes *Appl. Phys. Lett.* **105** 051113
- [135] Yoshikawa A, Hasegawa R, Morishita T, Nagase K, Yamada S, Grandusky J, Mann J, Miller A and Schowalter L 2020 Improved efficiency and long lifetime UVC LEDs with wavelengths between 230 and 237 nm *Appl. Phys. Express* **13** 022001
- [136] (<https://www.optanled.com/products/optan-235-nm>)
- [137] Banal R G, Funato M and Kawakami Y 2009 Optical anisotropy in [0001]-oriented  $\text{Al}_x\text{Ga}_{1-x}\text{N}/\text{AlN}$  quantum wells ( $x > 0.69$ ) *Phys. Rev. B* **79** 121308(R)
- [138] Reich C *et al* 2015 Strongly transverse-electric-polarized emission from deep ultraviolet AlGaIn quantum well light emitting diodes *Appl. Phys. Lett.* **107** 142101
- [139] Bickermann M, Epelbaum B M, Filip O, Helmann P, Feneberg M, Nagata S and Winnacker A 2010 Deep-UV transparent bulk single-crystalline AlN substrates *Phys. Status Solidi c* **7** 1743
- [140] Glaab J, Ruschel J, Mehnke F, Lapeyrade M, Guttman M, Wernicke T, Weyers M, Einfeldt S and Kneissl M 2018 Degradation behavior of AlGaIn-based 233 nm deep-ultraviolet light emitting diodes *Semicond. Sci. Technol.* **33** 095017
- [141] Kashima Y *et al* 2018 *Appl. Phys. Express* **11** 012101
- [142] Guttman M, Mehnke F, Belde B, Wolf F, Reich C, Sulmoni L, Wernicke T and Kneissl M 2019 *Japan. J. Appl. Phys.* **58** SCCB20
- [143] Shatalov M *et al* 2012 *Appl. Phys. Express* **5** 082101
- [144] Jo M, Maeda N and Hirayama H 2016 *Appl. Phys. Express* **9** 012102
- [145] Cho H K, Ostermay I, Zeimer U, Enslin J, Wernicke T, Einfeldt S, Weyers M and Kneissl M 2017 *IEEE Photon. Technol. Lett.* **29** 2222
- [146] Maeda N, Yun J, Jo M and Hirayama H 2018 *Japan. J. Appl. Phys.* **57** 04FH08
- [147] Zhang L, Xu F, Wang J, He C, Guo W, Wang M and Shen B 2016 *Sci. Rep.* **6** 35934
- [148] Inoue S, Tamari N and Taniguchi M 2017 150 mW deep-ultraviolet light-emitting diodes with large area AlN nanophotonic light extraction structure emitting at 265 nm *Appl. Phys. Lett.* **110** 141106
- [149] Alias M S *et al* 2018 Review of nanophotonics approaches using nanostructures and nanofabrication for III-nitrides ultraviolet-photonics devices *J. Nanophoton.* **12** 043508
- [150] Conroy M, Zubialevich V Z, Li H, Petkov N, Holmes J D and Parbrook P J 2015 Epitaxial lateral overgrowth of AlN on self-assembled patterned nanorods *J. Mater. Chem. C* **3** 431–7
- [151] Dong P *et al* 2013 282-nm AlGaIn-based deep ultraviolet light-emitting diodes with improved performance on nano-patterned sapphire substrates *Appl. Phys. Lett.* **102** 241113
- [152] Hagedorn S, Knauer A, Mogilatenko A, Richter E and Weyers M 2016 AlN growth on nano-patterned sapphire: a route for cost efficient pseudo substrates for deep UV LEDs *Phys. Status Solidi a* **213** 3178
- [153] Dai J *et al* 2017 Fabrication of AlGaIn nanorods with different Al compositions for emission enhancement in UV range *Nanotechnology* **28** 385205
- [154] Zhao S *et al* 2015 Aluminum nitride nanowire light emitting diodes: breaking the fundamental bottleneck of deep ultraviolet light sources *Sci. Rep.* **5** 8332
- [155] Yin J *et al* 2014 Surface plasmon enhanced hot exciton emission in deep UV-emitting AlGaIn multiple quantum wells *Adv. Opt. Mater.* **2** 451–8
- [156] Coulon P-M, Kusch G, Martin R W and Shields P A 2018 Deep UV emission from highly ordered AlGaIn/AlN core-shell nanorods *ACS Appl. Mater. Interfaces* **10** 33441–9
- [157] Coulon P-M *et al* 2019 Displacement Talbot Lithography for nano-engineering of III-nitride materials *Microsyst. Nanoeng.* **5** 52
- [158] Coulon P-M *et al* 2017 Optical properties and resonant cavity modes in axial InGaIn/GaN nanotube microcavities *Opt. Express* **25** 28246–57
- [159] ([www.nusod.org/inst/software.html](http://www.nusod.org/inst/software.html))
- [160] Li C, Piccardo M, Lu L S, Mayboroda S, Martinelli L, Weisbuch C, Filoche M and Wu Y R 2017 Localization landscape theory of disorder in semiconductors III: application to transport and radiative recombination in light emitting diodes *Phys. Rev. B* **95** 144206

- [161] Shedbalkar A, Andreev Z and Witzigmann B 2015 Simulation of an indium gallium nitride quantum well light-emitting diode with the non-equilibrium Green's function method *Phys. Status Solidi b* **1**–6 [158](#)
- [162] Römer F and Witzigmann B 2014 Effect of Auger recombination and leakage on the droop in InGaN/GaN quantum well LEDs *Opt. Express* **22** [1440–52](#)
- [163] Selberherr S 1984 *Analysis and Simulation of Semiconductor Devices* (Berlin: Springer) (<https://doi.org/10.1007/978-3-7091-8752-4>)
- [164] Chen H, Speck J, Weisbuch C and Wu Y R 2018 Three dimensional simulation on the transport and quantum efficiency of UVC-LEDs with random alloy fluctuations *Appl. Phys. Lett.* **113** [153504](#)
- [165] Vurgaftman I and Meyer J R 2003 Band parameters for nitrogen-containing semiconductors *J. Appl. Phys.* **94** [3675–96](#)
- [166] Duboz J-Y 2014 GaN/AlGaIn superlattices for p contacts in LEDs *Semicond. Sci. Technol.* **29** [035017](#)
- [167] Kioupakis E, Rinke P, Delaney K T and Van de Walle C G 2011 Indirect Auger recombination as a cause of efficiency droop in nitride light-emitting diodes *Appl. Phys. Lett.* **98** [161107](#)
- [168] Humphreys C J *et al* 2017 The atomic structure of polar and non-polar InGaN quantum wells and the green gap problem *Ultramicroscopy* **176** [93–98](#)
- [169] Pinos A, Marcinkevičius S, Yang J, Gaska R, Shatalov M and Shur M S 2010 Optical studies of degradation of AlGaIn quantum well based deep ultraviolet light emitting diodes *J. Appl. Phys.* **108** [93113](#)
- [170] Shatalov M, Gong Z, Gaevski M, Wu S, Sun W, Adivarahan V and Asif Khan M 2006 Reliability of AlGaIn-based deep UV LEDs on sapphire *Proc. SPIE* **6134** [61340P](#)
- [171] Gong Z, Gaevski M, Adivarahan V, Sun W, Shatalov M and Asif Khan M 2006 Optical power degradation mechanisms in AlGaIn-based 280nm deep ultraviolet light emitting diodes on sapphire *Appl. Phys. Lett.* **88** [121106](#)
- [172] Ruschel J, Glaab J, Beidoun B, Lobo Ploch N, Rass J, Kolbe T, Knauer A, Weyers M, Einfeldt S and Kneissl M 2019 Current-induced degradation and lifetime prediction of 310 nm ultraviolet light-emitting diodes *Photon. Res.* **7** [B36–40](#)
- [173] Monti D *et al* 2017 Defect-related degradation of AlGaIn-Based UV-B LEDs *IEEE Trans. Electron. Dev.* **64** [200–5](#)
- [174] Sawyer S, Rumyantsev S L and Shur M S 2008 Degradation of AlGaIn-based ultraviolet light emitting diodes *Solid-State Electron.* **52** [968–72](#)
- [175] Glaab J *et al* 2019 Degradation of (In)AlGaIn-based UVB LEDs and migration of hydrogen *IEEE Photon. Techn. Lett.* **31** [529–32](#)
- [176] Pinos A, Marcinkevičius S, Yang J, Bilenko Y, Shatalov M, Gaska R and Shur M S 2009 Aging of AlGaIn quantum well light emitting diode studied by scanning near-field optical spectroscopy *Appl. Phys. Lett.* **95** [181914](#)
- [177] Monti D *et al* 2019 High-current stress of UV-B (In)AlGaIn-based LEDs: defect-generation and diffusion processes *IEEE Trans. Electron. Dev.* **66** [3387](#)
- [178] Moe C G *et al* 2010 Current-induced degradation of high performance deep ultraviolet light emitting diodes *Appl. Phys. Lett.* **96** [213512](#)
- [179] De Santi C, Caria A, Renso N, Dogmus E, Zegaoui M, Medjdoub F, Meneghesso G, Zanoni E and Meneghini M 2018 Evidence of optically-induced degradation in gallium nitride optoelectronic devices *Appl. Phys. Exp.* **11** [111002](#)
- [180] Iveland J, Martinelli L, Peretti J, Speck J S and Weisbuch C 2013 Direct measurement of auger electrons emitted from a semiconductor light-emitting diode under electrical injection: identification of the dominant mechanism for efficiency droop *Phys. Rev. Lett.* **110** [177406](#)
- [181] De Santi C *et al* 2017 Recombination mechanisms and thermal droop in AlGaIn-based UV-B LEDs *Photonics Res.* **5** [A44–51](#)
- [182] Krishnamoorthy S, Akyol F, Park P S and Rajan S 2013 Low resistance GaN/InGaIn/GaN tunnel junctions *Appl. Phys. Lett.* **102** [113503](#)
- [183] Zhang Y, Krishnamoorthy S, Johnson J M, Akyol F, Allerman A, Moseley M W, Armstrong A, Hwang J and Rajan S 2015 Interband tunneling for hole injection in III-nitride ultraviolet emitters *Appl. Phys. Lett.* **106** [141103](#)
- [184] Akyol F, Krishnamoorthy S, Zhang Y and Rajan S 2015 GaIn-based three-junction cascaded light-emitting diode with low-resistance InGaIn tunnel junctions *Appl. Phys. Express* **8** [082103](#)
- [185] Grundmann M J and Mishra U K 2007 Multi-color light emitting diode using polarization-induced tunnel junctions *Phys. Status Solidi c* **4** [2830](#)
- [186] Zhang Y, Krishnamoorthy S, Akyol F, Allerman A A, Moseley M W, Armstrong A M and Rajan S 2016 Design and demonstration of ultra-wide bandgap AlGaIn tunnel junctions *Appl. Phys. Lett.* **109** [121102](#)
- [187] Zhang Y *et al* 2018 Tunnel-injected sub 290 nm ultra-violet light emitting diodes with 2.8% external quantum efficiency *Appl. Phys. Lett.* **112** [071107](#)
- [188] Zhao S, Sadaf S M, Vanka S, Wang Y, Rashid R and Mi Z 2016 Sub-milliwatt AlGaIn nanowire tunnel junction deep ultraviolet light emitting diodes on silicon operating at 242 nm *Appl. Phys. Lett.* **109** [201106](#)
- [189] Taketomi H, Aoki Y, Takagi Y, Sugiyama A, Kuwabara M and Yoshida H 2016 Over 1 W record-peak-power operation of a 338 nm AlGaIn multiple-quantum-well laser diode on a GaIn substrate *Japan. J. Appl. Phys.* **55** [05FJ05](#)
- [190] Zhang Z, Kushimoto M, Sakai T, Sugiyama N, Schowalter L J, Sasaoka C and Amano H 2019 A 271.8 nm deep-ultraviolet laser diode for room temperature operation *Appl. Phys. Express* **12** [124003](#)
- [191] Kuwano Y, Kaga M, Morita T, Yamashita K, Yagi K, Iwaya M, Takeuchi T, Kamiyama S and Akasaki I 2013 Lateral hydrogen diffusion at p-GaIn layers in nitride-based light emitting diodes with tunnel junctions *Japan. J. Appl. Phys.* **52** [08JK12](#)
- [192] Kuhn C, Sulmoni L, Guttmann M, Glaab J, Susilo N, Wernicke T, Weyers M and Kneissl M 2019 MOVPE-grown AlGaIn-based tunnel heterojunctions enabling fully transparent UVC LEDs *Photon. Res.* **7** [B7](#)
- [193] Oto T, Banal R G, Kataoka K, Funato M and Kawakami Y 2010 100mW deep-ultraviolet emission from aluminium-nitride-based quantum wells pumped by an electron beam *Nat. Photonics* **4** [767](#)
- [194] Tabataba-Vakili F, Wunderer T, Kneissl M, Yang Z, Teepe M, Batres M, Feneberg M, Vancil B and Johnson N M 2016 Dominance of radiative recombination from electron-beam-pumped deep-UV AlGaIn multi-quantum-well heterostructures *Appl. Phys. Lett.* **109** [181105](#)
- [195] Ivanov S V, Jmerik V N, Nechaev D V, Kozlovsky V I and Tiberi M D 2015 E-beam pumped mid-UV sources based on MBE-grown AlGaIn MQW *Phys. Status Solidi a* **212** [1011–6](#)
- [196] Matsumoto T, Iwayama S, Saito T, Kawakami Y, Kubo F and Amano H 2012 Handheld deep ultraviolet emission device based on aluminum nitride quantum wells and graphene nanoneedle field emitters *Opt. Express* **20** [24320–9](#)
- [197] Wunderer T 2016 Invited talk at E-MRS Meeting Warsaw, Poland

- [198] Kozlovsky V I *et al* 1997 Electron beam pumped MQW InGaN/GaN laser *MRS Internet J. Nitride Semicond. Res.* **2** 38
- [199] Gamov N A, Zhdanova E V, Zverev M M, Peregudov D V, Studenov V B, Mazalov A V, Kureshov V A, Sabitov D R, Padalitsa A A and Marmalyuk A A 2015 Pulsed electron-beam-pumped laser based on AlGaIn/InGaIn/GaN quantum-well heterostructure *Quantum Electron.* **45** 601–3
- [200] Hayashi T, Kawase Y, Nagata N, Senga T, Iwayama S, Iwaya M, Takeuchi T, Kamiyama S, Akasaki I and Matsumoto T 2017 Demonstration of electron beam laser excitation in the UV range using a GaN/AlGaIn multiquantum well active layer *Sci Rep* **7** 2944
- [201] Wunderer T, Jeschke J, Yang Z, Teepe M, Batres M, Vancil B and Johnson N 2017 Resonator-length dependence of electron-beam-pumped UV-A GaN-based lasers *IEEE Photon. Tech. Lett.* **29** 1344
- [202] Wunderer T, Yang Z, Feneberg M, Batres M, Teepe M and Johnson N 2017 Structural and optical characterization of AlGaIn multiple quantum wells grown on semipolar (20-21) bulk AlN substrate *Appl. Phys. Lett.* **111** 111101
- [203] Yoshida H 2018 *Encyclopedia of Modern Optics* 2nd edn vol 2 eds B D Guenther and D G Steel (New York: Academic) p 271
- [204] Sato K *et al* 2020 *Appl. Phys. Express* **13** 031004
- [205] Kneissl M, Kolbe T, Schlegel J, Stellmach J, Chua C, Yang Z, Knauer A, Weyers M and Johnson N M 2011 AlGaIn-based ultraviolet lasers—applications and materials challenges *OSA Technical Digest JtuB1* ([https://doi.org/10.1364/CLEO\\_AT.2011.JTuB1](https://doi.org/10.1364/CLEO_AT.2011.JTuB1))
- [206] Sakai T, Kushimoto M, Zhang Z, Sugiyama N, Schowalter L J, Honda Y, Sasaoka C and Amano H 2020 *Appl. Phys. Lett.* **116** 122101
- [207] Martens M 2018 Optical gain and modal loss in AlGaIn based deep UV lasers *Dissertation* TU Berlin (<https://doi.org/10.14279/depositonce-7512>)
- [208] Wunderer T, Northrup J E and Johnson N M 2016 AlGaIn-based ultraviolet laser diodes *III-Nitride Ultraviolet Emitters* vol 227 eds M Kneissl and J Rass (Berlin: Springer) (<https://doi.org/10.1007/978-3-319-24100-5>)
- [209] Martens M, Kuhn C, Simoneit T, Hagedorn S, Knauer A, Wernicke T, Weyers M and Kneissl M 2017 *Appl. Phys. Lett.* **110** 081103
- [210] Park Y J *et al* 2019 *Proc. SPIE* **10938** 109380A
- [211] Kang J-H, Wenzel H, Hoffmann V, Freier E, Sulmoni L, Unger R-S, Einfeldt S, Wernicke T and Kneissl M 2018 *IEEE Photonics Technol. Lett.* **30** 231
- [212] Taniyasu Y, Carlin J-F, Castiglia A, Butté R and Grandjean N 2012 *Appl. Phys. Lett.* **101** 082113
- [213] Kuhn C, Simoneit T, Martens M, Markurt T, Enslin J, Mehnke F, Bellmann K, Schulz T, Albrecht M, Wernicke T and Kneissl M 2018 MOVPE growth of smooth and homogeneous Al<sub>0.8</sub>Ga<sub>0.2</sub>N:Si superlattices UVC laser cladding layers *Phys. Status Solidi a* **215** 1800005
- [214] Simon J, Protasenko V, Lian C, Xing H and Jena D 2010 *Science* **327** 60
- [215] Bergmann M A, Enslin J, Yapparov R, Hjort F, Wickman B, Marcinkevičius S, Wernicke T, Kneissl M and Haglund Å 2020 *Appl. Phys. Lett.* **116** 121101
- [216] Khan M A, Matsuura E, Kashima Y and Hirayama H 2019 *Phys. Status Solidi a* **216** 1900185